広島大学学位請求論文

Frictional properties of materials along subduction plate boundaries and implications for the 2011 Tohoku-oki earthquake

（沈み込み帯プレート境界物質の摩擦特性：
東北地方太平洋沖地震発生機構の解明に向けて）

2015 年
広島大学大学院理学研究科
地球惑星システム学専攻

澤井　みち代

目次

1. 主論文

   Frictional properties of materials along subduction plate boundaries and implications for the 2011 Tohoku-oki earthquake

   （沈み込み帯プレート境界物質の摩擦特性：東北地方太平洋沖地震発生機構の解明に向けて）

   Michiyo Sawai（澤井みち代）

2. 公表論文

   (1) Sawai, M., Hirose, T. and Kameda, J., 2014. Frictional properties of incoming pelagic sediments at the Japan Trench: implications for large slip at a shallow plate boundary during the 2011 Tohoku earthquake. Earth, Planets and Space, 66(1), 1-8, DOI 10.1186/1880-5981-66-65.

   (2) Sawai, M., Katayama, I. Hamada, A., Maeda, M. and Nakashima, S., 2013. Dehydration kinetics of antigorite using in situ high-temperature infrared microspectroscopy. Physics and Chemistry of Minerals 40, 319–330, DOI 10.1007/s00269-013-0573-9.

   (3) Sawai, M., Shimamoto, T. and Togo, T., 2012. Reduction in BET surface area of Nojima fault gouge with seismic slip and its implication for the fracture energy of earthquakes. Journal of Structural Geology 38, 117-138. doi: 10.1016/j.jsg.2012.01.002.

主論文

Contents

要旨

2011 年 3 月 11 日に東北地方太平洋沖地震（Mw 9.0）（以下，東北地震）が発生し，甚大な被害をもたらした．さらに，東北地震前に東北日本で 20 km より浅部においてスロー地震が発生したことが報告されている（Kato et al., 2012; Ito et al., 2013）．このように，東北沖の沈み込み帯では，Mw 7~8 の地震をおこすアスペリティと呼ばれる領域と非地震性すべりをおこる領域が混在していると考えられている．そこで本博士論文研究では，東北沖ではなぜこのように多様な地震活動がおこるのかを理解するために，当地域の沈み込みプレート境界に存在すると予想される岩石の低速～高速すべり摩擦特性を調べた．実験には，沈み込み帯浅部を代表する物質として掘削コアで得られた粘土鉱物に富む堆積物を，深部に存在する岩石として低温・高圧下で形成された藍閃石片岩を用いた．東北地震では浅部プレート境界にて約 50 m に達する大きな変位がおこっており，高速摩擦実験は浅部プレート境界の地震時のすべり運動を再現するためにおこなった．また，地震発生初期の深部プレート境界断層運動を再現する低速摩擦実験は，東北沖の多様な地震活動を理解することを目的として，深部の高圧・熱水条件下でおこなった．下記に主な 3 つの研究結果を示す．

1．日本海溝に沈み込む遠洋性堆積物の地震時摩擦特性とプレート境界浅部の巨大すべり

東北沖地震では，大きくはすべらないと考えられていた海溝軸付近で約 50 m に達する大規模なすべりが発生し（例えば Fujiwara et al., 2011），この大きなすべりが巨大津波を引き起こした．本研究では，太平洋プレート上の 2 種類の遠洋性堆積物（DSDP, Leg 56, Site 436, Core 38 and 40）を用いてこの巨大すべりを再現する高速摩擦実験をおこなった．用いた堆積物は，2012 年東北地方太平洋沖地震調査掘削（JFAST）で報告された東北沖プレート境界物質に類似しており，将来プレート境界を構成する物質であるといえる．実験は高知コア研究所の回転式高速摩擦試験機を使用して，150 μm~1 m/s の速度下でおこなった．その結果，摩擦係数が幅広い速度領域で 0.2 以下と極めて小さいこと，さらに，地震性高速すべり時の破壊エネルギーは他の断層物質と比較して数桁小さいことが初

めて明らかになった．このように浅部プレート境界に沿って破壊すべりが進展しやすいことが，大きな断層変位がおこった理由と考えられる．また得られた摩擦係数は，JFAST でおこなわれた摩擦熱を検出する温度測定から見積もられた摩擦係数（0.08; Fulton et al., 2013）ともよく一致する．

2．東北沖プレート境界断層の摩擦特性とスロー地震

東北日本では深さ 20 km 以下の浅い領域においてスロー地震が起こっており，その震源が東北地震の大きなすべり域をはじめ，地震発生域と一部重なることから，海溝型巨大地震との関係も含め注目されている．東北地震直後に日本海溝でおこなわれた JFAST 航海で強く剪断されたプレート境界物質が回収され，地震時にその近傍がすべった可能性が示唆されている．本研究では，浅部プレート境界断層の性質を理解するため，このプレート境界物質が沈み込み，徐々に温度が上昇していくに従って，摩擦特性がどのように変化するのかを検証した．実験にはオランダ・ユトレヒト大学設置の回転式剪断試験機を使用し，有効圧 50 MPa，間隙水圧 50 MPa，温度 20~200ºC，すべり速度 0.3~100 μm/s の条件で，断層すべりの安定性を示すパラメータ(*a*-*b*)の温度・すべり速度依存性を調べた．その結果，浅部プレート境界の温度条件（20-50℃）では，すべり速度が上昇するにつれて(*a*-*b*)が負から正へと増えていくことがわかった．低温条件下で速度が上がるにつれ安定的な挙動を示そうとするこの傾向は，断層すべりが徐々に速度を増しながら伝播する際のバリアになり，それがスロー地震上限になりうる可能性を示唆する．また，スロー地震は，(*a*-*b*)が非常に 0 に近い負の領域で起こると考えられている．実験の結果，50-100ºC の温度条件で(*a*-*b*)が 0 に近い負の値をとることが明らかになり，150ºC 以上では安定的な挙動（*a*-*b*>*0*）を示した．東北沖沈み込み帯の温度構造から，スロー地震の下限はおよそ 150ºC だと考えられており，本実験結果はこの観測結果とよい一致を示している．

3．東北地震震源域に分布すると考えられる藍閃石片岩の低速摩擦挙動と地震発生及びスロー地震

東北沖沈み込み帯で発生する多様な地震活動と東北地震の発生機構を理解するためには，深部の高圧・熱水条件下でプレート境界断層の摩擦特性を調べる

必要がある．そこで本研究では，低温・高圧型沈み込み帯の地震発生域に広く分布すると考えられる藍閃石片岩の粉砕物（断層模擬ガウジ）を用いて，25~200 MPa の有効圧，25~200 MPa の間隙水圧，22~400ºC の温度，0.1~100 μm/s のすべり速度条件下で摩擦実験をおこなった．実験にはユトレヒト大学の回転式剪断試験機を使用した．実験の結果，藍閃石片岩は温度 100-300ºC の間では摩擦の速度依存性パラメータ(*a*-*b*)が負となり（200ºC で最低値），地震を引き起こす性質を持つことが明らかになった．東北地震の震源域温度が約 160ºC 程度と推測されていることから（Kimura et al., 2012），藍閃石片岩の摩擦特性は震源核形成に起因しうると考えられる．また，(*a*-*b*)が正の温度条件においても，有効圧が小さくなるにつれて(*a*-*b*)が負に遷移する傾向が確認された．このことは，間隙水圧が上昇すると，(*a*-*b*)が正から負に変化する点でスロー地震が発生する条件が現れることを示唆している．東北沈み込み帯のプレート境界浅部の堆積岩，及び深部の藍閃石片岩の摩擦特性（上記 2 & 3）からプレート境界全体を捉えると，低有効応力（高間隙水圧）条件下の摩擦特性分布を考えることによって，現在の東北日本前弧域で発生するスロー地震の分布をうまく説明できることがわかった．

Abstract

The 2011 off the Pacific coast of Tohoku Earthquake (Mw 9.0) (called as "the 2011 Tohoku-oki earthquake") nucleated at 24 km depth along the plate boundary and produced huge slip (~50 m) on the shallow part of the megathrust fault (e.g., Fujiwara et al., 2011), resulting in destructive tsunamis. Moreover, episodic tremor and slow slip events occurred just before the 2011 Tohoku-oki earthquake on a shallow portion (less than 20 km depth) in the Tohoku subduction zone (Ito et al., 2013). Frictional property of rocks composed of a subducting oceanic plate is one of factors for controlling the diverse slip behavior from aseismic to seismogenic slip at the Japan Trench. However, friction data of the rocks to model such subduction earthquakes are quite limited. In this these, I report the results of an experimental study aimed at determining the frictional properties of sediments and metamorphic rock that are representative materials along the plate boundary fault in the Tohoku subduction zone at slow to high slip velocities under various fluid pressure and temperature conditions. Research outcomes are outlined below.

1. Coseismic frictional behavior of incoming pelagic sediments to the Japan Trench: Relationship to large slip during the 2011 Tohoku-oki earthquake

The 2011 Tohoku-oki earthquake produced a very large slip on the shallow part of a plate boundary fault that resulted in destructive tsunamis. The frictional property of sediments around the fault, particularly at coseismic slip velocities, may significantly contribute to large slip along such faults. Hence, I have investigated the frictional properties of incoming pelagic sediments that will subduct beneath the Tohoku region (Deep Sea Drilling Project (DSDP), Leg56, Site 436, Core 38 and 40), in order to understand the rupture processes that can cause large slip in the shallow parts of subduction zones. Core 38 is diatom-rich clayey sediment, while Core 40 contains mainly smectite which could correspond to black-colored sheared clay in the plate boundary fault zone recovered during Integrated Ocean Drilling Program (IODP) Expedition 343. Experiments are performed at slip velocities of 2.5 x 10^{-4} to 1.3 m/s,

normal stresses of 0.8 to 2.0 MPa and slip displacement of ~16 m under brine saturated conditions, using a rotary-shear friction apparatus at Kochi Core Center. Steady-state friction coefficient of clayey sediment at the base of the sedimentary section on the Pacific Plate is remarkably low ($\mu < 0.2$) over a wide range of slip velocities (0.25 mm/s to 1.3 m/s), and extremely low fracture energy during slip weakening, as compared with previous experiments of disaggregated sediments under coseismic slip conditions. My experimental results suggest that smectite-rich pelagic sediment, possibly source material of the current plate boundary fault zone, is energetically very easy for earthquake ruptures to propagate at shallow portion of the Tohoku subduction zone, leading to large slip near the trench.

2. Depth limits of slow slip events at the Japan Trench based on the frictional property of plate-boundary material under in-situ conditions

Episodic tremor and slow slip occurred just before the 2011 Tohoku-oki earthquake on a shallow portion in the Tohoku subduction zone (Ito et al., 2013). To understand the generation mechanisms of the slow slip events based on frictional property of the plate boundary fault, friction experiments were performed on smectite-rich pelagic sediments retrieved from the plate boundary fault during IODP Expedition 343 using a rotary shear apparatus at Utrecht University. The sediments were disaggregated and simulated gouges were then sheared at temperatures of 20-200^{o}C, an effective normal stress of 50 MPa and a pore fluid pressure of 50 MPa. I conducted velocity-stepping sequences (0.3 to 100 μm/s) and determined the rate and state friction parameter (*a*-*b*) as it is one of the primary factors controlling the slip stability. In particular, I investigated how the parameter (*a*-*b*) changes with temperature and slip velocity. At low temperatures of 20^{o}C, the values of parameter (*a*-*b*) are negative at low velocities, while those becomes positive values as increasing velocity to 100 μm/s. This frictional property may inhibit further slip acceleration even if the slip commences, and could thus represent the upper limit of slow slip events at the shallow portion of the plate boundary. At temperatures of 50-100^{o}C the gouges show nearly neutral or slightly negative values of (*a*-*b*), while at temperature of >150^{o}C those exhibit

positive values of (*a-b*) under almost all velocity conditions tested. Slow slip events are considered to generate under the conditions where (*a-b*) value is negative and close to zero, particularly at lower slip velocities. The conditions met at temperatures of 50-100^{o}C in the experiments, that is consistent with temperature conditions where the slow slip events occurs along the plate boundary. Thus, the frictional properties of the pelagic sediments explain well the observed distributions of slow slip events along the plate boundary fault in the Tohoku subduction zone.

3. Frictional properties of blueschist at hypocentral conditions: implications for the nucleation mechanism of the earthquakes and slow slip events

Diverse slip behavior including large coseismic rupture (e.g. devastating earthquakes such as the 2011 Tohoku-oki earthquake), micro-seismicity and aseismic creep (e.g. slow earthquakes) were observed in the Tohoku subduction zone. Despite considerable research, the mechanisms of the slip behavior, particularly slow earthquakes, are still not well understood. It is crucial to understand the frictional behavior of the material that is expected to be present around hypocenters in the Tohoku subduction zone, under hypocentral conditions of confining pressure, fluid pressure and temperature. Here I study on frictional property of blueschist at temperatures of 22-400^{o}C, effective normal stresses of 25-200 MPa and pore fluid pressures of 25-200 MPa, using a rotary shear apparatus at Utrecht University. I particularly investigated the effect of temperature and effective pressure on the rate and state friction parameter (*a-b*) by conducting velocity-stepping experiments with velocity range from 0.1 to 100 μm/s. At 22^{o}C, the gouges show a positive *(a-b)* values which decrease to become negative with increasing temperature. At 200^{o}C, the behavior is velocity weakening and shows negative *(a-b)* values. In some cases the samples exhibit stick-slip behavior. At 300^{o}C, slip is velocity weakening (negative *(a-b)* value) at low pressure but strengthening at high pressure, showing larger *(a-b)* values than at 200 ^{o}C. The samples show unstable stick-slips under some conditions. *(a-b)* values slightly decrease at 400^{o}C. There is also effective normal stress dependence: *(a-b)* values are negative at low effective pressure and increase to positive with increasing effective normal stress except those at 200^{o}C

which remain negative under almost all pressure conditions. My results suggest that earthquakes can nucleate in blueschist at depths within a temperature range of 100-300^{o}C or/and low effective pressure. The temperature of the Tohoku earthquake hypocenter is reported to be about 160^{o}C, which is in agreement with my experimental results. According to my experimental results on the sediments and blueschist, frictional properties under low effective normal stress are necessary to explain the observed diverse slip behavior along the Tohoku plate boundary.

Chapter 1

Introduction

1.1 General motivation

Subduction megathrust earthquakes generate when unstable slip is nucleated in the seismogenic zone, and sometimes result in tsunami. The 2011 off the Pacific coast of Tohoku Earthquake (Mw 9.0) (called as “the 2011 Tohoku-oki earthquake”), which hit on 11 March 2011, and subsequent tsunami must be still fresh in our memory (e.g. Ide et al., 2011; Ozawa et al., 2011; Simons et al., 2011). Other examples are the 1960 Chili earthquake which was the largest event ever recorded (Mw 9.5) (Plafker and Savage, 1970), or the Sumatra Mw 9.1 earthquake and associated tsunami of December 2004 (e.g. Lay et al., 2005). Moreover slow earthquakes (e.g. slow slip events; low frequency earthquakes) occur near upper and lower limit of seismogenic zone, such as the Japan Trench (Obara et al., 2004a; Asano et al., 2008), the Nankai Trough (Obara et al., 2004b; Ito and Obara, 2006b), the Cascadia (Rogers and Dragert, 2003), and Costa Rica (Brown et al., 2005). Particularly, episodic tremor and slow slip events occurred just before the 2011 Tohoku-oki earthquake on the shallow portion in the Tohoku subduction zone. Thus understanding the generation mechanisms of megathrust earthquakes, including the large slip during the earthquake resulting in destructive tsunami, and slow slip events is critical to understanding the diverse seismic activities in the subduction zone.

Numerous studies have been tackled to these topics in the view point of various fields, e.g. by experimental studies, simulation or geodesy. Recently, the scientific drilling initiatives, such as Japan Trench Fast Drilling Project (JFAST) or the Nankai Trough Seismogenic Zone Experiment (NanTroSEIZE), are also conducted. The drilled core samples and other information from them are receiving a lot of attention.

To understand both subduction megthrust earthquakes and slow slip events, the frictional property of rocks composed of a subducting oceanic crust is one of important factors for controlling the various slip behavior from aseismic to seismogenic slip (e.g.

Scholz, 1998). Many previous studies have focused on the frictional behavior of fault rocks to understand the stability of frictional sliding. However, friction data of the rocks to model such subduction earthquakes and slow slip events are quite limited. Almost all experiments have been conducted under limited experimental conditions (e.g. limit of temperature, pressure, and shear displacements) and few experiments have been performed on realistic materials under relevant in-situ conditions. In this thesis, I report the experimental results done for determining the frictional behavior of materials expected to present in the Tohoku subduction zone under in-situ P-T conditions, addressing low sliding velocities relevant to earthquake nucleation and slow slip events and high slip velocities associated with the rupture propagation during the earthquakes.

1.2 Aims of this thesis

The main goal of my PhD project is to understand the diverse seismic activities at the Japan Trench including the 2011 Tohoku-oki earthquake based on frictional properties of rocks existed at the Tohoku subduction zone. I report the results of an experimental study aimed at determining the mechanical properties of (1) sediments that are collected at the Japan Trench by the Deep Sea Drilling Project (DSDP) and Integrated Ocean Drilling Program (IODP) and (2) metamorphic rocks that are exhumed possibly from the depth of hypocenter area of major earthquakes at the Tohoku subduction at low to high slip velocities under various fluid pressure and temperature conditions. I believe that the properties at low to intermediate slip rates potentially control the initiation processes of diverse slip behavior in the Japan Trench (e.g., seismic and aseismic slip behaviors), whereas frictional properties at high slip rates are essential to understand the rupture propagation toward the shallow part of subduction zone, leading to the megathrust earthquake and subsequent tsunami generation.

Chapter 2

Frictional properties of incoming pelagic sediments at the Japan Trench: implications for large slip at a shallow plate boundary during the 2011 Tohoku earthquake

This chapter was published as: Sawai, M., Hirose, T. and Kameda, J., 2014. Frictional properties of incoming pelagic sediments at the Japan Trench: implications for large slip at a shallow plate boundary during the 2011 Tohoku earthquake. Earth, Planets and Space, 66(1), 1-8, DOI 10.1186/1880-5981-66-65.

Reprinted with permission from Springer.

Abstract

The 2011 Tohoku earthquake (Mw 9.0) produced a very large slip on the shallow part of a megathrust fault that resulted in destructive tsunamis. Although multiple causes of such large slip at shallow depths are to be expected, the frictional property of sediments around the fault, particularly at coseismic slip velocities, may significantly contribute to large slip along such faults. I have thus investigated the frictional properties of incoming pelagic sediments that will subduct along the plate boundary fault at the Tohoku subduction zone, in order to understand the rupture processes that can cause large slip in the shallow parts of subduction zones. My experimental results on clayey sediment at the base of the sedimentary section on the Pacific Plate yield a low friction coefficient of <0.2 over a wide range of slip velocities (0.25 mm/s to 1.3 m/s), and extremely low fracture energy during slip weakening, as compared with previous experiments of disaggregated sediments under coseismic slip conditions. Integrated Ocean Drilling Program (IODP) Expedition 343 confirmed that the clay-rich sediment investigated here is identical to those in the plate boundary fault zone, which ruptured and generated the Tohoku earthquake. The present results suggest that smectite-rich pelagic sediment not only accommodates cumulative plate motion over interseismic periods but also

energetically facilitates the propagation of earthquake rupture towards the shallow part of the Tohoku subduction zone.

2.1 Introduction

An unexpectedly large coseismic slip at a shallow plate interface was produced by the 2011 Tohoku earthquake, and it extended near the trench (e.g., Fujiwara et al. 2011; Ide et al. 2011; Ito et al. 2011; Ozawa et al. 2011; Mitsui et al. 2012). Frictional properties of a fault, particularly at coseismic slip velocities, are a key control on whether an earthquake rupture can propagate up-dip through subduction forearcs (e.g., Faulkner et al. 2011). Recently, the active slip zone of the Tohoku earthquake was successfully sampled by the Integrated Ocean Drilling Program (IODP) Expedition 343 (Chester et al. 2013; Fulton et al. 2013). The fault zone is highly localized and consists of clay-rich material with a scaly fabric (Chester et al. 2013). The clay-rich materials in the fault zone exhibit very low friction not only at coseismic slip velocities (*ca*. m/s) but also at low slip velocities (*ca*. μm/s) (Hirose et al. 2013; Ujiie et al. 2013). These studies have proposed that this frictional property of the fault zone potentially facilitated the shallow and large slip during the Tohoku earthquake. However, it is also possible that the measured very low friction of the plate boundary fault resulted from the large slip (>50 m) during the Tohoku earthquake, and the frictional property of the fault *prior to* the earthquake is poorly known.

In this study, I investigate the frictional properties of incoming pelagic sediments at the Tohoku subduction zone that were collected from the outer rise of the Pacific Plate by Leg 56 of the Deep Sea Drilling Project (DSDP; Figure 1). In particular, I focus on the clay-rich sediment at the base of the sedimentary section of the Pacific Plate, which is a potential section to be the plate boundary fault confirmed by Expedition 343 (Chester et al. 2013). I consider this clay-rich sediment as an analog of the material along the plate boundary fault prior to the Tohoku earthquake. Thus, the results of my friction experiment of this sediment at coseismic slip conditions provide information on the frictional property of the plate boundary fault during the Tohoku earthquake. Based

on the frictional property of the pelagic sediments, I discuss a possible mechanism of the large slip along the shallow plate boundary during the Tohoku earthquake.

2.2 Experimental methods

I used pelagic sediments deposited on the Pacific Plate collected from Site 436 of DSDP Leg 56 (Core 38 at 358 mbsf and Core 40 at 376.8 mbsf) for my friction experiments (Figure 1b). The core sites are located *ca*. 260 km northeast of Site C0019 drilled during IODP Expedition 343 (Figure 1a). Core 38 is composed mainly of diatomaceous amorphous silica (approximately 69 wt.%) with some clays, quartz, and plagioclase, whereas Core 40 is dominated by clay minerals (approximately 85 wt.%) with minor quartz, amorphous silica, and plagioclase. The clay in both samples is mainly smectite, with minor illite and kaolinite, as quantitatively identified by X-ray diffraction (XRD) analysis (Figure 2). Based on the mineralogy and lithology of that region, the smectite-rich Core 40 sediment appears to be identical to the material in the plate boundary fault zone observed at Site C0019 (Chester et al. 2013).

Friction experiments were conducted on disaggregated samples that are analogs of fault gouge, following the procedures of Mizoguchi et al. (2007). One gram of sample was placed between porous sandstone cylinders with diameters of 25 mm and porosity of approximately 18%. The sample was confined using a Teflon sleeve. The effect of Teflon friction on mechanical data was corrected by subtracting the intercept value obtained from a shear stress versus normal stress plot (Figure 3b,e), following Togo et al. (2011). The experiments were performed at constant slip velocities ranging from 0.25 mm/s to 1.3 m/s, constant normal stresses of 0.7 to 2.0 MPa, and with a nearly constant total displacement of approximately 16 m using a rotary shear friction apparatus (Shimamoto and Tsutsumi 1994; Hirose and Shimamoto 2005). Both the gouge sample and host rocks were saturated with brine in a vacuum chamber before the experiments. A high-velocity slip on the fault was obtained by keeping one specimen stationary while rotating the other at high speed using a servomotor. Equivalent slip velocity and displacement, which are used in this study to present experimental results, follow the definitions in Hirose and Shimamoto (2005). I also measured the temperature

increase by frictional heating in this simulated fault zone with a K-type thermocouple that was placed on a surface between the gouge zone and host rock on the stationary side.

2.3 Results

In both Cores 38 and 40 at a coseismic slip velocity of 1.3 m/s, typical slip weakening behavior appears at all normal stresses between 0.7 and 2.0 MPa. The friction coefficient (=measured shear stress / applied normal stress) rapidly increases with slip velocity to 1.3 m/s at the onset of sliding (hereafter referred to as the initial peak of friction) and subsequently decreases almost exponentially to below 0.2 with displacement over a characteristic slip weakening distance of 0.03 to 1.08 m (Figure 3a,d; Table 1). The slip weakening distance and steady-state values were calculated by fitting the entire data set from the peak friction to the end of runs with the empirical equation of Mizoguchi et al. (2007):

$$\mu(d) = \mu_{ss} + (\mu_p - \mu_{ss}) \exp\left[\ln(0.05) d / D_c\right]$$

where μ is the friction coefficient at displacement d, μ_p is the peak friction coefficient, μ_{ss} is the steady-state friction coefficient, and D_c is the slip-weakening distance defined as the displacement corresponding to the 95% reduction of ($\mu_p - \mu_{ss}$). The temperature in the fault zone at a slip velocity of 1.3 m/s and normal stress of 1.0 MPa increased to 150°C and 110°C after a displacement of approximately 16 m in Cores 38 and 40, respectively (Figure 3a,d). However, little temperature rise was observed during slip weakening.

Figure 3b,e shows the normal stress dependence of shear stress at the initial peak and steady-state stages (coseismic slip velocity = 1.3 m/s). The linear slope of the steady-state data shows low friction coefficients of 0.1 and 0.07 for Cores 38 and 40, respectively. Thus, shear stress is nearly independent of normal stress at this coseismic slip velocity. The slope of the initial peak data is quite different for the two samples, with the friction coefficient being 0.63 for Core 38 and 0.18 for Core 40. This difference

appears to reflect the friction coefficients at lower slip velocities. For Core 38, the friction coefficient at steady state shows a decrease from 0.52 to 0.09 over slip velocities ranging from 0.31 mm/s to 1.3 m/s. In contrast, Core 40 exhibits nearly constant friction values of 0.06 to 0.18 over more than 4 orders of magnitude change in slip velocity (Figure 3c,f).

Microstructures of the two core samples sheared at a normal stress of 1.0 MPa and a slip velocity of 1.3 m/s were compared under a scanning electron microscope (SEM). In Core 38, deformation features such as compaction and grain size reduction are developed within a 0.5-mm-thick zone on the rotation side (Figure 4a). No localized slip surfaces are evident in this zone. On the stationary side, diatoms still retain their original shape. These microstructures indicate that fracturing and subsequent shear-enhanced compaction are the dominant deformation processes taking place during the experiment. In contrast, Core 40 exhibits widely distributed oblique shear planes characterized by the preferential alignment of clay particles towards the rotation side of the host rock (Figure 4b). This texture is similar to the scaly fabric observed in the drilling core from the plate boundary fault collected by IODP Expedition 343 (Chester et al. 2013). The difference in deformation textures between Cores 38 and 40 might result from the differences in clay content, which have a strong effect on frictional behavior at low velocities.

2.4 Discussion

Figure 5 shows the steady-state friction of Cores 38 and 40 as a function of slip velocity, compared with the steady-state friction of the core samples recovered from the Japan Trench as well as the Nankai subduction zone. Apart from Core 40, the overall trend of the friction-velocity curve is consistent with other rock types (e.g., Di Toro et al. 2011). Core 40 characteristically exhibits low friction of 0.06 to 0.18 at slip velocities from 0.25 mm/s to 1.31 m/s. This relationship could reflect clay content and, in particular, smectite content, as the friction of smectite is relatively low for a clay mineral due to the low strength of its interlayer bond (Moore and Lockner 2004). A similar velocity dependence on the friction of clay-rich gouge with 60% to 70%

smectite has been reported by Ferri et al. (2011). The total clay content of Core 40 is estimated to be 85%, including a smectite content of 76%, whereas that of Core 38 and the Nankai samples ranges from 53% to 64% (Expedition 316 Scientists 2009a, b). It appears that at least 50% smectite is necessary to lower frictional strength, although the effect of the smectite fraction in gouge on friction depends strongly on slip velocity, normal stress, strain, fluid saturation conditions, and interlayer cations (e.g., Saffer and Marone 2003; Behnsen and Faulkner 2013). Smectites are abundant in sediments on subducting oceanic plates, and thus, further studies are needed to investigate the effect of smectite on frictional behavior and fault rheology under various conditions in the shallow parts of plate boundaries.

The frictional work on a fault plane during slip weakening is known as the fracture energy, and its magnitude indicates the ease with which a rupture may propagate (Tinti et al. 2005; Cocco et al. 2006). I calculated the fracture energy at coseismic slip velocity from the area under the shear stress versus displacement curve, as shown in the inset in Figure 6. I also roughly estimated the fracture energy of the plate boundary fault from the shear stress versus displacement curves reported in Ujiie et al. (2013), for comparison. The calculated values range between 0.001 and 0.121 MJ/m^2 in both Cores 38 and 40 (Table 1), and that in the plate boundary fault is approximately 0.2 MJ/m^2. These values are 2 orders of magnitude lower than for other gouges, apart from talc, which were deformed previously under nearly the same experimental conditions using similar rotary shear apparatuses (Mizoguchi et al. 2007; Brantut et al. 2008; Boutareaud et al. 2012; Sawai et al. 2012). Based on the microstructural observations and temperature data, the observed low fracture energy probably results from a shorter slip weakening distance. The shorter weakening distance is most likely due to pressurization of pore fluid by shear-enhanced compaction, and probably not by shear heating because almost no temperature rise takes place during slip weakening (Figure 3a). Ujiie and Tsutsumi (2010) and Faulkner et al. (2011) suggested the same mechanism of dynamic weakening at the onset of rapid slip. Although such fluid pressurization might commonly occur in gouge experiments at high slip velocities and large displacements, the lower fracture energy as compared with other gouge

samples is confirmed as a characteristic of incoming sediments as well as the plate boundary fault at the Japan Trench (Figure 6). A primary factor for lowering the fracture energy of those sediments is currently unclear and will be investigated in detail in future work.

The low fracture energy of the investigated sediments and the plate boundary fault suggests that when the incoming pelagic sediments subduct into the plate boundary at the Japan Trench, those can energetically facilitate earthquake ruptures to propagate to shallow depths in the Tohoku subduction zone, where smectite is present and has not been transformed to illite (Figure 6). However, there is a significant contrast in steady-state friction at low velocities in the two cores. Core 38 has a friction coefficient of approximately 0.5 at slip velocities of 0.31 mm/s to 0.13 m/s, whereas Core 40 is characterized by low friction of <0.2 over a velocity range from 0.25 mm/s to 1.31 m/s, which is much lower than the value predicted by Byerlee's law (Figure 5). Such a weak formation in a sedimentary sequence on the subducting Pacific Plate could become a potential site for a future plate boundary fault. In fact, this smectite-rich formation is identical to that in the plate boundary fault zone recognized by drilling in the Tohoku forearc during IODP Expedition 343 (Chester et al. 2013). The observed frictional properties of the smectite-rich pelagic sediment appear to be responsible for accommodating not only the cumulative plate motion over interseismic periods but also the coseismic slip during the Tohoku earthquake.

2.5 Conclusions

A series of rotary shear friction experiments was performed on the pelagic sediments entering the Japan Trench in order to understand the rupture processes that caused the large slip during the Tohoku earthquake. The main results of this study are as follows:

1. Incoming pelagic sediments on the Pacific Plate collected from Site 436 of DSDP Leg 56 (Cores 38 and 40) show slip weakening behavior at coseismic slip velocities. However, at low velocities, there is a significant difference in the friction coefficient between the two cores. The steady-state friction coefficient of

Core 38 has high values of approximately 0.5 at low velocities, but decreases to <0.1 as seismic slip velocity increases to 1.3 m/s. In contrast, the steady-state friction coefficient of Core 40 is remarkably low (<0.2) over a wide range of velocities (0.25 mm/s to 1.31 m/s).

2. SEM observations of the samples revealed different deformation processes in the fault zone. Core 40 is characterized by the preferred orientation of clay particles along distributed shear planes, resulting in the development of a scaly fabric, similar to that from the Tohoku plate boundary fault documented by IODP Expedition 343. In contrast, fracturing and subsequent shear-enhanced compaction appear to be the dominant deformation processes in Core 38. The difference in frictional properties between the two sediments can be attributed to a difference in smectite content that potentially controls deformation processes during fault zone shearing.
3. The specific fracture energy of the sediments during slip weakening at coseismic slip velocity ranges from 0.001 to 0.121 MJ/m^2. These values are lower by more than 2 orders of magnitude than those of previous experiments conducted under similar conditions on disaggregated sediments. These results suggest that the incoming pelagic sediments make it energetically easy for earthquake ruptures to propagate up-dip along the plate boundary and therefore led to the large near-trench slip during the Tohoku earthquake.

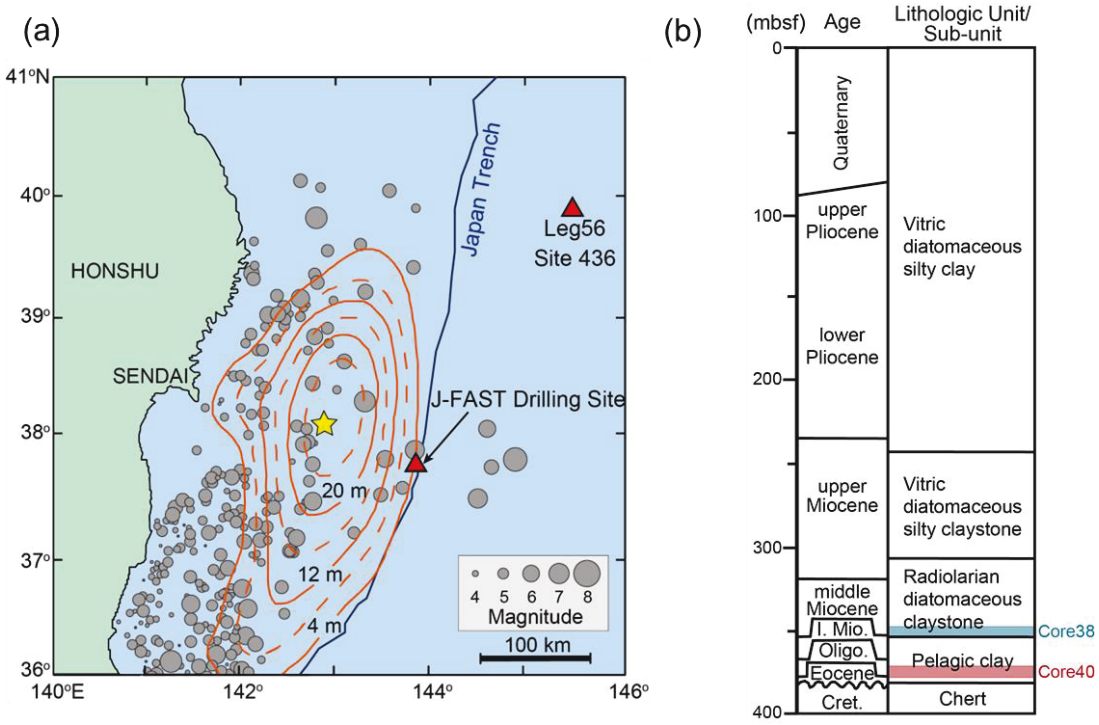

Figure 2.1 Locations of Site 436 and Site C0019 and lithologic zonation of DSDP Site 436. (a) Locations of Site 436 (DSDP Leg 56) and Site C0019 (IODP Expedition 343) (J-FAST) (red triangles). Orange contour lines at 4-m intervals show the coseismic slip displacement of the 2011 Tohoku earthquake off the Pacific coast of Japan, as compiled from Ozawa et al. (2011). The yellow star denotes the epicenter of the mainshock, and gray circles are the aftershocks and the largest foreshock. The blue line shows the Japan Trench. (b) Lithologic zonation of DSDP Site 436 (modified from Shipboard Scientific Party 1980). The drilling depth was 397.5 m below sea floor (mbsf) at this site. Core 38 (blue line) and Core 40 (red line) used in this study were recovered from 358 and 376.8 mbsf, respectively.

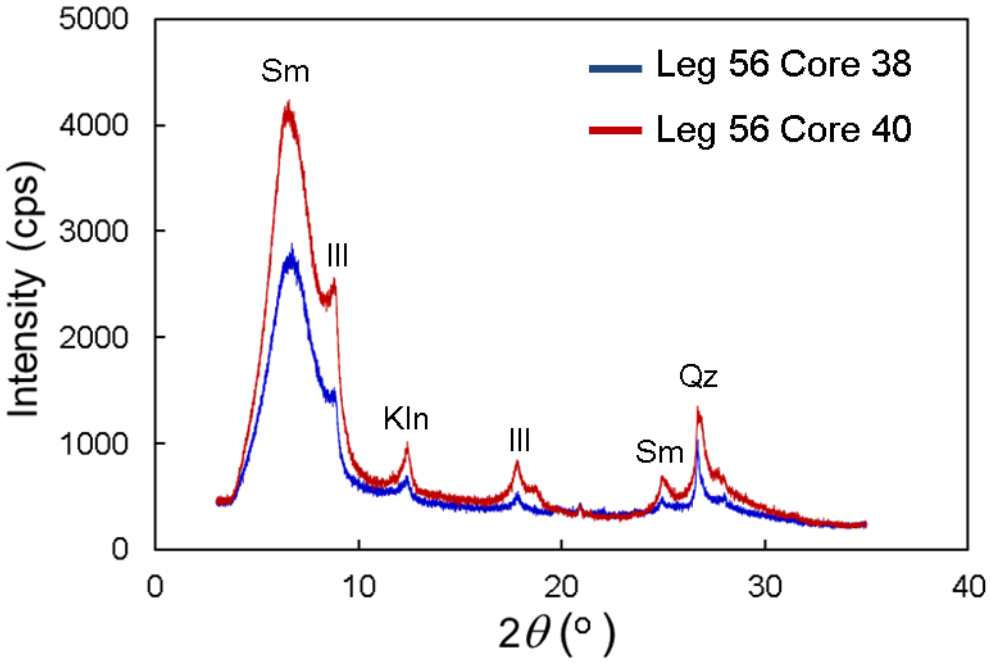

Figure 2.2 X-ray diffraction patterns of the pelagic sediments used for the experiments. Sm, smectite; Ill, illite; Kln, kaolinite; Qz, quartz.

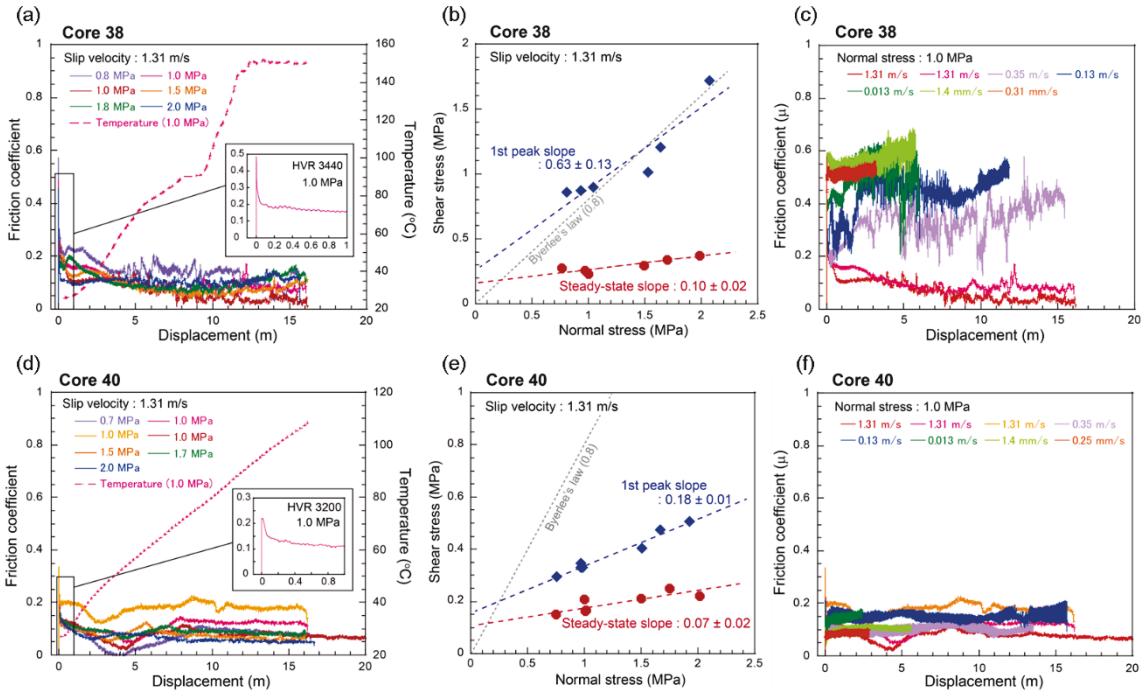

Figure 2.3 Frictional behavior of pelagic sediments sampled from Cores 38 and 40 of DSDP Site 436. (a, d) Friction coefficient versus displacement curves at a constant slip velocity of 1.3 m/s under normal stresses of 0.7 to 2.0 MPa. Temperature evolution of the fault zone during the run at a normal stress of 1.0 MPa is shown by the red dotted lines. Inserted plots show an enlarged view of the onset of the slip. (b, e) Measured shear stress plotted against applied normal stress at initial peak friction (blue diamonds) and steady-state friction (red circles). Intercepts have been interpreted as due to friction between the Teflon sleeve and the outer surface of the specimen. (c, f) Friction coefficient versus displacement curves at a constant normal stress of 1 MPa and different slip velocities of 0.25 mm/s to 1.3 m/s.

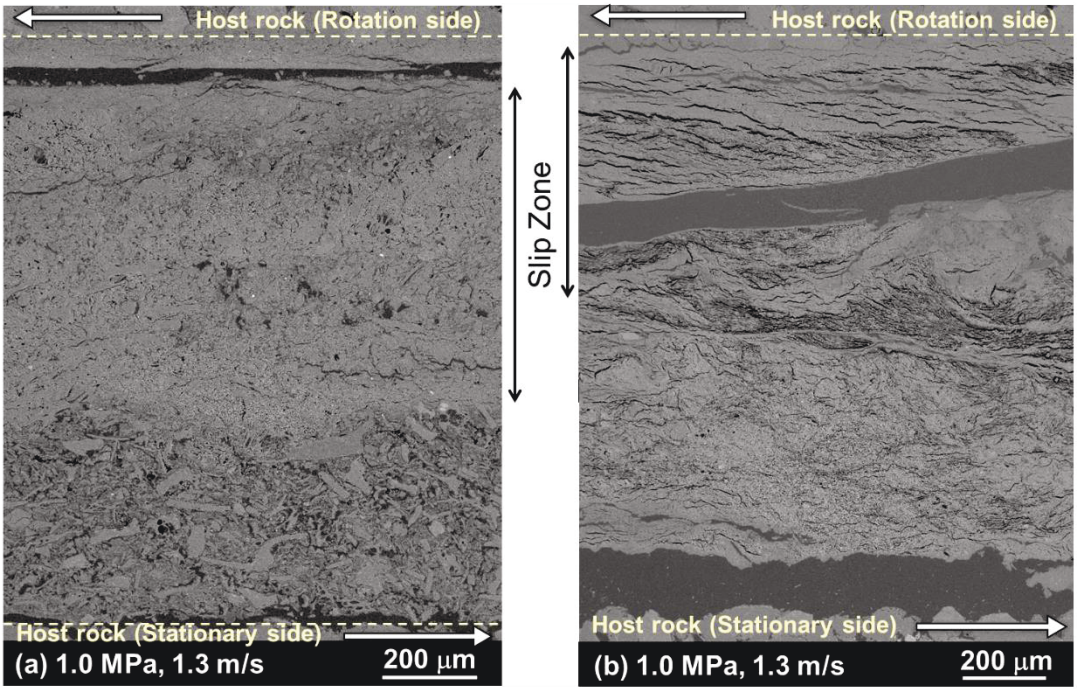

Figure 2.4 SEM photomicrographs of Cores 38 (a) and 40 (b). The two core samples were deformed at a normal stress of 1.0 MPa and slip velocity of 1.3 m/s (run numbers are HVR 3278 and 3265, respectively).

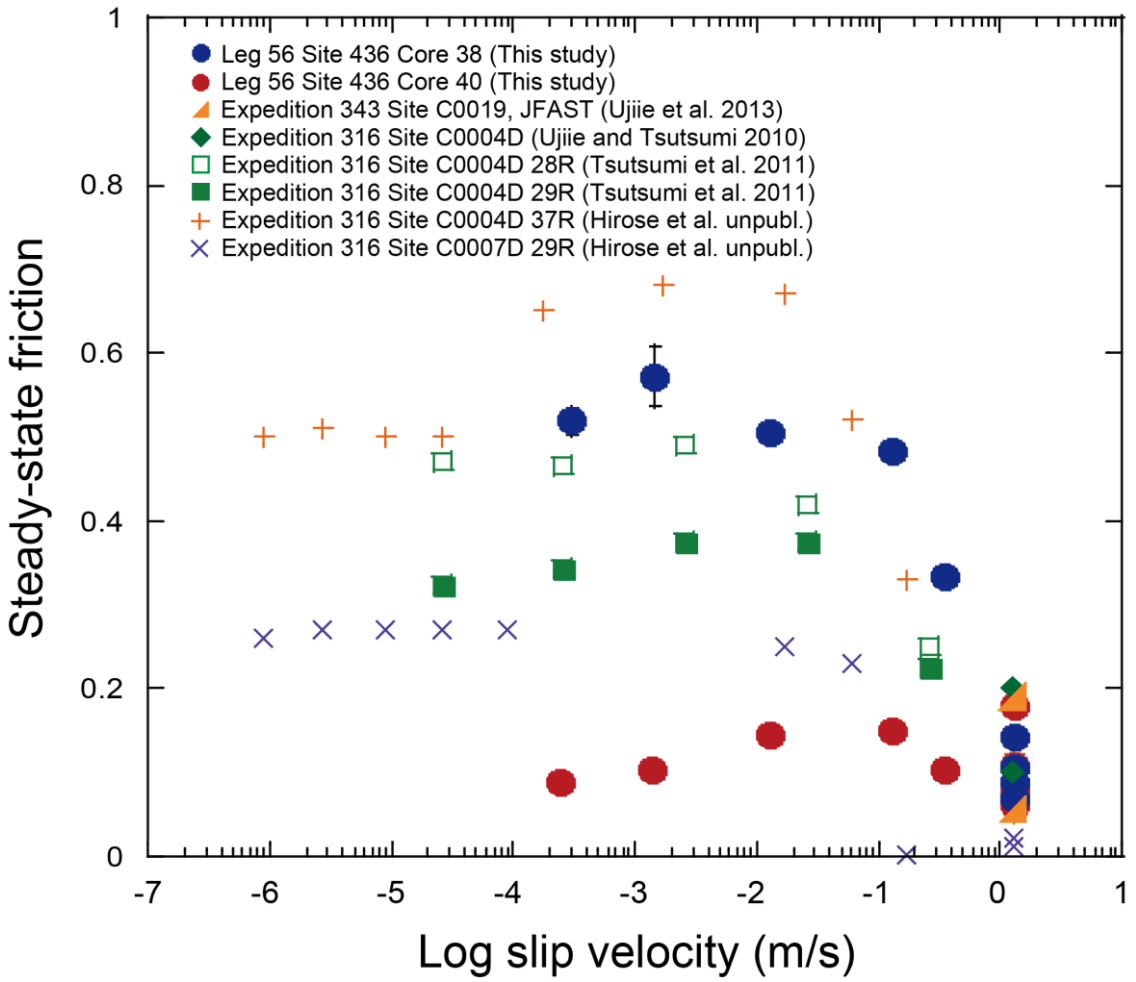

Figure 2.5 Steady-state friction coefficient plotted against the logarithm of slip velocity. Blue and red circles show the data determined in this study using samples from DSDP Site 436. Yellow triangles are the data obtained through rotary shear experiments on the plate boundary fault collected at the Japan Trench (Expedition 343; Site C0019), reported in Ujiie et al. (2013). Other symbols are experimental results obtained by rotary shear experiments on sediments that occur around faults in the Nankai Trough (Expedition 316; Sites C0004D and C0007D), from Ujiie and Tsutsumi (2010), Tsutsumi et al. (2011), and Hirose et al. (2008), shown for comparison.

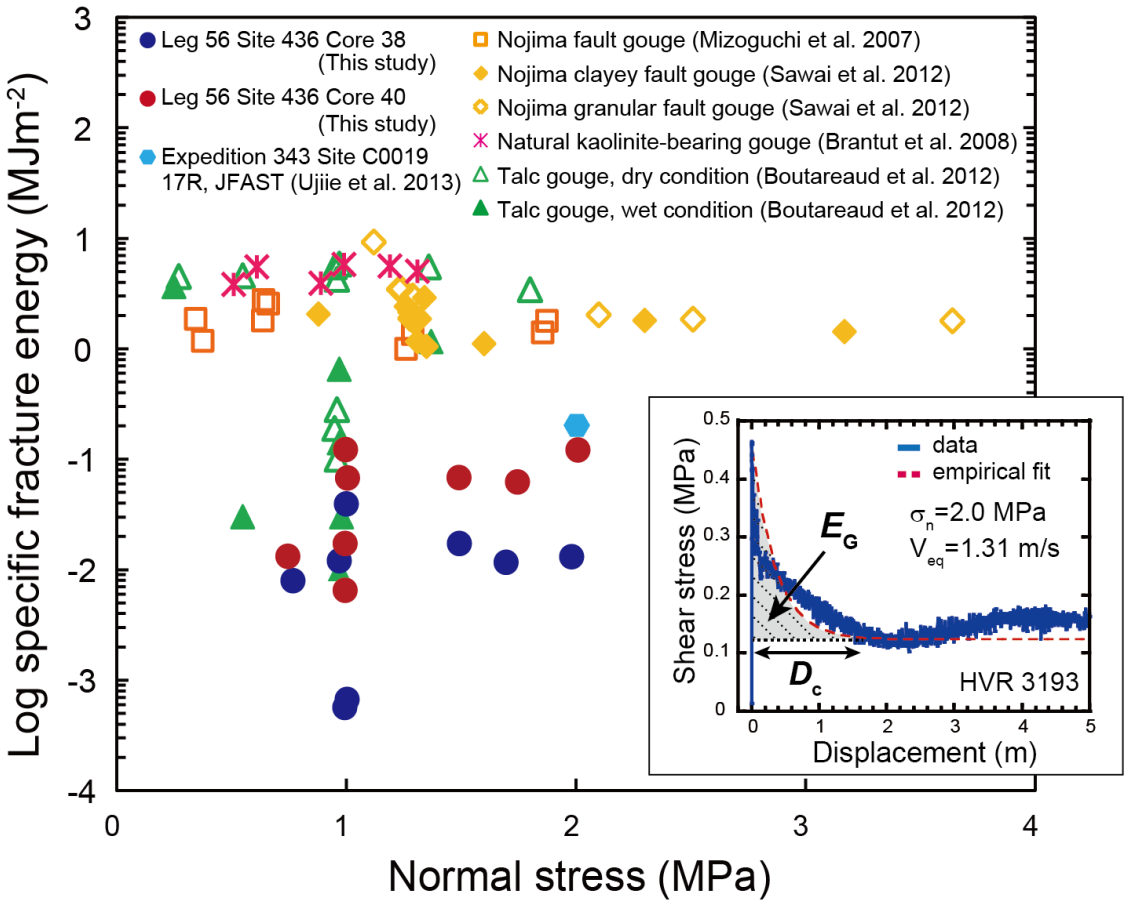

Figure 2.6 Logarithm of fracture energy (EG) plotted against normal stress. Fracture energy represents a part of the frictional work that occurs during slip weakening over a characteristic distance (Dc), which is defined by the shaded area under a shear stress versus displacement curve (inset). Dc was calculated by fitting data with an empirical exponential equation (Mizoguchi et al. 2007) (red dashed curve). Data for Cores 38 and 40 from Site 436 are shown as blue and red circles, respectively. Also shown are the fracture energy of the plate boundary fault from the Japan Trench (Ujiie et al. 2013), the Nojima fault gouge (Mizoguchi et al. 2007; Sawai et al. 2012), kaolinite-bearing gouge from the Median Tectonic Line (Brantut et al. 2008), and talc gouge (Boutareaud et al. 2012), as determined under similar experimental conditions to those of the present study.

Table 1 Summary of friction experiments on Cores 38 and 40 from DSDP Site 436

Experimental number	Normal stress (MPa)	Slip velocity (m/s)	Displacement (m)	μ_p	μ_{ss}	D_c (m)	Specific fracture energy (MJ/m^2)
Core 38							
HVR 3269	1.5	1.31	16.2	0.51	0.09 ± 0.001	0.08 ± 0.005	0.017
HVR 3270	2.0	1.31	15.7	0.72	0.11 ± 0.000	0.03 ± 0.001	0.013
HVR 3271	0.8	1.31	16.1	0.78	0.14 ± 0.001	0.05 ± 0.004	0.008
HVR 3272	1.7	1.31	16.0	0.59	0.11 ± 0.001	0.04 ± 0.003	0.012
HVR 3273	1.0	0.35	15.4	0.51	0.33 ± 0.001	0.01 ± 0.005	0.001
HVR 3274	1.0	0.13	11.8	0.49	0.45 ± 0.001	0.04 ± 0.031	0.001
HVR 3275	1.0	0.013	6.0	-	0.50 ± 0.066	-	-
HVR 3276	1.0	0.0014	5.8	-	0.57 ± 0.036	-	-
HVR 3277	1.0	0.00031	3.2	-	0.52 ± 0.015	-	-
HVR 3278	1.0	1.31	16.2	0.64	0.07 ± 0.001	0.21 ± 0.009	0.039
HVR 3440	1.0	1.31	16.0	0.68	0.10 ± 0.001	0.06 ± 0.003	0.012
Core 40							
HVR 3190	1.0	1.31	47.7	0.31	0.07 ± 0.000	0.84 ± 0.022	0.067
HVR 3192	1.5	1.31	16.1	0.20	0.08 ± 0.000	1.07 ± 0.042	0.068
HVR 3193	2.0	1.31	16.7	0.23	0.06 ± 0.000	1.08 ± 0.026	0.121
HVR 3194	1.0	0.13	15.7	0.22	0.15 ± 0.000	-	-
HVR 3195	1.0	0.013	2.4	0.20	0.14 ± 0.000	-	-
HVR 3196	1.0	0.014	5.6	0.11	0.10 ± 0.010	-	-
HVR 3197	1.0	0.35	13.5	0.24	0.10 ± 0.000	-	-
HVR 3199	1.0	0.00025	6.7	0.10	0.09 ± 0.008	-	-
HVR 3200	1.0	1.31	16.2	0.23	0.11 ± 0.000	0.41 ± 0.035	0.017
HVR 3206	0.7	1.31	16.5	0.30	0.07 ± 0.001	0.23 ± 0.019	0.013
HVR 3208	1.7	1.31	16.1	0.23	0.09 ± 0.000	0.73 ± 0.024	0.062
HVR 3265	1.0	1.31	16.2	0.35	0.18 ± 0.000	0.11 ± 0.011	0.006

Chapter 3

Depth limits of slow slip events at Tohoku subduction zone: Insights from friction experiments under in-situ conditions

Abstract

Episodic tremor and slow slip events have occurred on a shallow portion in the Tohoku subduction zone. To understand the generation mechanisms of the slow slip events based on frictional property of the plate boundary fault, I have conducted friction experiments on smectite-rich pelagic sediments retrieved from the plate-boundary thrust during IODP Expedition 343. The sediments were sheared at temperatures of 20-200^{o}C, an effective normal stress of 50 MPa and a pore fluid pressure of 50 MPa and slip velocities of 0.3 to 100 μm/s. At low temperatures of < 50^{o}C, the smectite-rich sediments mainly exhibit negative values of (*a*-*b*). However, the sediments show neutral to positive (*a*-*b*) values at temperatures of >100^{o}C. In addition, the value of parameter (*a*-*b*) depends significantly on slip velocities: at low temperature it increases from negative to positive with increasing slip velocities, whereas it tends to decrease with increasing slip velocities at temperatures higher than 100^{o}C. The downdip temperature limit of the slow slip events at Japan Trench seems to be in the range between 100 to 150^{o}C. The transition in (*a*-*b*) value from neutral to positive, occurs at the same temperature range. Hence, this could correspond to the observed downdip limit of the slow slip events. Furthermore, at the lowest temperature of 20^{o}C this transition also occurs, but with increasing slip velocity. This frictional property may inhibit further slip acceleration even if the slip commences, and could thus represent the upper limit of slow slip events at the shallow portion of the plate boundary.

3.1 Introduction

Subduction zone earthquakes are generated by megathrust faults and sometimes result in devastationg tsunamis. On the other hand various type of aseismic events (e.g. slow slip events and tremor) also occurred throughout subduction. Indeed slow slip

events was detected just before the 2011 Tohoku-oki earthquake and locations of those seismic and aseismic events seem to overlap each other (Kato et al., 2012; Ito et al., 2013)(Figure 3.1b). However why those different slip behavior occurs at nearly same pressure and temperature conditions is still unknown. The frictional properties of fault rocks is one of the important factors controlled the mechanical behavior of major fault. Integrated Ocean Drilling Program (IODP) Expedition 343 and 343T (Japan Trench Fast Drilling Project, JFAST) sailed in order to investigate the plate-boundary décollement at the Japan Trench and the active slip zone of the 2011 Tohoku-oki earthquake was successfully sampled at core site C0019 (Chester et al., 2012, 2013; Fulton et al., 2013) (Figure 3.1a). The fault zone is highly localized and consists of clay-rich material with a scaly fabric (Chester et al. 2013). Frictional behavior on this plate-boundary clay material was investigated under low slip velocity conditions by Ikari et al. (2015) and at coseismic slip velocity (~1m/s) by Ujiie et al. (2013), and Sawai et al. (2014) explored the frictional properties of incoming clay-rich pelagic sediments just prior to subduction which is a potential section to be the plate boundary fault (Deep Sea Drilling Project (DEDP) Leg 56, Site 436). These studies have revealed that the plate-boundary fault zone which composed by smectite-rich sediments is extremely weak and allow the rupture to propagate very easy. Clay minerals, smectite and illite in particular, have been well studied because the velocity strengthening and properties of stable sliding of clay-rich sediments have probably resulted in the lack of seismicity on the shallow portion at subduction zone (Logan and Rauenzahn, 1987; Saffer and Marone, 2003; Moore and Lockner, 2004; Ikari et al., 2007, 2009; Faulkner et al., 2011) at low temperature condition. Almost all clays and mixtures of clay and quartz exhibit velocity-strengthening behavior even when its friction levels are low (Logan and Rauenzahn, 1987; Ikari et al., 2009; Tembe et al., 2010). However the frictional properties of smectite show complex: velocity-weakening behavior at slow sliding velocity and low normal stress conditions (Saffer et al., 2001; Saffer and Marone, 2003). As it showed, systematic and detailed study on frictional constitutive properties, especially under in-situ conditions, is important to understand the stability of fault gouge. There is a high possibility that distributions of seismic and aseismic region is

thermally controlled and increasing temperature with depth should alter the mechanical properties of such clay minerals. Therefore to reveal the frictional properties of clay-rich sediments under elevating temperature is needed to understand the various seismic activities including the slow slip events at shallow portion.

I thus investigate the frictional properties of the smectite-rich sediment at various temperature conditions and discuss how its properties change with increasing temperature, i.e. with the plate subducting to the Japan Trench, based on its properties.

3.2 Experimental methods

3.2.1 Starting material

I used smectite-rich clay sediment for the friction experiments derived from the Japan Trench, cored during IODP Expedition 343, JFAST. This smectite-rich sediment at 822 mbsf is the plate-boundary décollement which identified in core 17 collected from Site C0019 (Chester et al., 2012, 2013; Kirkpatrick et al., 2014; Kameda et al., 2015). Core 17 I used is dominated by clay minerals (approximately 90 wt.%) with minor quartz and plagioclase (Kameda et al., 2015). The clay is mainly smectite, with minor illite and kaolinite, as quantitatively identified by X-ray diffraction (XRD) analysis. The smectite-rich sediment was crushed by hand and sieved at <125 μm in order to prepare simulated gouges for the experiments. I prepared the ring-shaped samples with inner and outer diameters of 22 and 28 mm before the experiments by pre-pressuring ~0.81 g of the simulated fault gouges mixed with ~0.05 g of distilled water, in order to reduce loss of sample material during the experiments. Pre-pressing was conducted at 50 MPa for 20 min at room temperature.

3.2.2 Friction experiments

Friction experiments on smectite-rich sediment were performed using the hydrothermal ring shear apparatus at Utrecht University (described in detail by Niemeijer et al., 2008 and den Hartog et al., 2012a) (Figure 3.2). The ring-shaped samples were contained between two roughened opposing superalloy pistons, which thickness prior to loading is ~1.7 mm (Figure 3.2). The gouge sample is kept in place by

inner and outer confining rings of stainless steel which were coated with Molykote spray to reduce wall friction. In this study, after loading the vessel into the Instron frame, an effective normal stress is applied before the distilled water was obtained into the pore fluid system because smectite-rich samples are very easy to go out of the original position through the tiny gap or opening. After applying a fluid pressure of ~10 MPa, then the furnace was switched on. Since the fluid pressure increased during heating, I withdrew water from the system to keep the desired fluid pressure (50 MPa). The system was subsequently left to equilibrate and then start to be rotated by a servo-controlled motor and gearbox. Smectite-rich sediment were deformed at temperatures (T) of 20–200°C, effective normal stresses (σ_n^{eff}) of 50 MPa, a fluid pressure (P_f) of 50 MPa and sliding velocities of 0.3-100 μm/s.

The velocity dependence of friction is described by the rate and state dependent friction (RSF) law (Dieterich, 1978, 1979; Ruina, 1983), which is written

$$\mu = \mu_0 + aln\left(\frac{V}{V_0}\right) + bln\left(\frac{V_0\theta}{D_c}\right) \tag{5.1}$$

$$\frac{d\theta}{dt} = 1 - \frac{V\theta}{D_c} \tag{5.2}$$

where μ is the instantaneous friction coefficient, μ_0 is a reference friction coefficient at a reference velocity V_0. θ is a state variable and D_c is a characteristic distance. a is a direct effect, which reflects an instantaneous response in μ resulting from a stepwise change in velocity. b represents the a decay in the friction to a new steady-state, called an evolutionary effect. The frictional stability are quantified using the parameter (a-b), which given by equation (5.1) and (5.2):

$$(a - b) = \frac{\Delta\mu_{ss}}{\Delta \ln(V/V_0)} \tag{5.3}$$

(e.g. Marone, 1998; Scholz, 1998). $\Delta\mu_{ss}$ is the change in steady-state friction coefficient when slip velocity changes from V_0 to V. A positive (a-b) value means that a slip accelerates friction increases and stable slip occurs, i.e. velocity-strengthening. And negative ones signify velocity-weakening. I performed velocity-stepping sequences to determine these rate and state parameter on the smectite-rich sediment and explored how this parameter changed with temperature and slip velocity.

3.3 Results

Table 3.1 lists each experiment and the corresponding experimental conditions. The samples were first deformed through an initial displacement of approximately 10 mm before the velocity-stepping. I have repeated the same velocity-stepping sequences four times to explore the effect of shear displacement. Friction coefficient (μ) as a function of displacement is shown in Figure 3.3. The average of friction at each temperature is μ = 0.3-0.4.

The velocity dependence of μ, described as (a-b), is shown in Figure 3.4, 3.5, and 3.6 which illustrate the effect of temperature, slip velocity and shear strain, respectively. At low temperatures of 20ºC, the simulated gouges exhibit negative values of (a-b) with a background friction coefficient of 0.38, except at the highest slip velocity of 0.03-0.1 mm/s. However, the gouges show neutral to positive values of (a-b) at temperatures of >50ºC with the same background friction coefficient as at lower temperatures. In addition, the value of parameter (a-b) depends significantly on slip velocities: at temperatures of 20ºC it increases from negative to positive with increasing slip velocities to 0.1 mm/s, whereas it tends to decrease with increasing slip velocity at temperatures higher than 150ºC. There is also the effect of shear strain at 20ºC, which the value of parameter (a-b) decrease with increasing the shear strain, although (a-b) values at other temperatures don't exhibit any clear dependence on shear strain.

The constitutive parameter a, b and D_c show various and complex behavior. These values are plotted against temperature in Figure 3.7. With increasing the temperature, the parameter a increases and b decrease, whereas D_c seems to be independent of temperature. For the slip velocity, the parameter a, b and D_c display

more complex behavior (Figure 3.8). The parameter *a* seems to increase with increasing (*a*-*b*) and decrease with decreasing (*a*-*b*): *a* decrease with increasing slip velocity at 20^{o}C, exhibit neutral approaching ~0.005 at 50-100^{o}C and decrease with decreasing slip velocity at 200^{o}C (Figure 3.8a, d, g, j, m). The values of *b* is generally constant although it shows a negative dependence on slip velocity at 20^{o}C (Figure 3.8b, e, h, k, n). D_c looks like it exhibit a small positive dependence, but not clear. Figure 3.9 shows the same friction parameter *a*, *b* and D_c plotted against shear strain. These values are insensitive to shear strain, except the values of b at 20^{o}C which show a positive dependence.

3.4 Discussion

3.4.1 Comparison with previous data

It is widely accepted that clay minerals including smectite mainly exhibit velocity-strengthening behavior. However my results revealed that smectite-rich clay sediment show velocity-weakening behavior under some set of temperature and slip velocity conditions. Saffer et al. (2001) and Saffer and Marone (2003) have reported that smectite under the room temperature exhibits velocity-weakening at low slip velocities (< 20 μm/s) and low normal stress (< 40MPa) conditions. In the present study, smectite-rich clay sediment also show velocity-weakening at post-step velocity < 30 μm/s under room temperature, which shows good agreements with previous studies (Figure 3.4, 3.5). In addition, I find that increasing temperature alter the frictional properties of smectite-rich sediment. Although the values of parameter (*a*-*b*) change from negative to positive with increasing slip velocity at room temperature as shown previously, that trend gradually disappears and become to be neutral with increasing temperature. Furthermore the opposite tendency appear more than 150^{o}C and the (a-b) values finally become positive under all velocity condition at 200^{o}C (Figure 3.5). I have not find any evidence yet, but it is probably due to the beginning of some reactions, such as dehydration. The positive (*a*-*b*) values at high temperature is likely to import that water resulting from the dehydration behaves as a pore fluid pressure and yields dilatant which generally causes the velocity-strengthening behavior.

Smectite-rich pelagic sediments retrieved from the plate-boundary thrust during IODP Expedition 343 is highly localized (Chester et al., 2012, 2013; Kirkpatrick et al., 2014). From the repeated velocity-step tests, I confirmed that there is a strain dependence at room temperature: the values of (*a*-*b*) decrease with increasing shear strain. Marone and Cox (1994) has reported the same results using gabbro. Moreover I extended the temperature condition to higher regimes and found that the parameter (*a*-*b*) is approximately independent at the temperature > 50^{o}C. Mechanisms of such complex frictional behavior are still unknown, so further works, such as microstructural observations, are clearly needed.

3.4.2 Frictional constitutive properties

Frictional constitutive parameter I investigated revealed the some relationship with the frictional behavior on fault. The values of (a-b) obtained in present study are attributable to the friction parameter *a* and/or *b.* Those values at the room temperature in this study show similar dependence on slip velocity to those reported by Ikari et al. (2009). With increasing slip velocity, the parameter *a* increase and *b* decrease. For the temperature, the velocity dependence of friction are especially attributed to the parameters *a* and *b*. The higher (*a*-*b*) is due to high values of *a* and in particular neutral or negative *b*. The values of *b* decrease with increasing temperature and approach to 0 at 200^{o}C. Scholz (2002) interpreted that the parameter *b* reflected the evolution of contact area with time and Saffer and Marone (2003) suggested that neat 0 values of *b* result from complete contact of clay gouge surfaces and not changing the real contact area after the velocity step. The contact area of smectite is likely to become to saturate with elevating temperature.

3.4.3 Implications for slow slip events at the Japan Trench

A number of studies have modeled slow earthquakes using elastic material, and friction laws as the boundary condition on the fault interface. Tse & Rice (1986) introduced this method into numerical modeling using a rate and state friction law. Based on this view, some studies used friction laws with a velocity cutoff, where

friction changes from velocity weakening to velocity strengthening and explain the mechanism of slow slip events (Kato, 2003; Shibazaki and Iio, 2003; Shibazaki and Shimamoto, 2007). The downdip temperature limit of the slow slip events at Japan Trench seems to be in the range between 100 to 150^{o}C (Figure 3.1b). The transition in (*a*-*b*) value from neutral to positive, particularly at lower slip velocities, occurs at the same temperature range in present results. Hence, this could correspond to the observed downdip limit of the slow slip events. Slow slip event occurs when (*a*-*b*) shows a very small negative value (e.g. Scholz, 1998). The temperature range, where slow slip events occurred, is considered about 50^{o}C to 100^{o}C. The values of (*a*-*b*) on smectite-rich sediment is just small negative to neutral values under these temperature regime, which in agreement with the observed slow slip area. Furthermore, at the lowest temperature of 20^{o}C, velocity-weakening to strengthening transition also occurs, but with increasing slip velocity. This frictional property may thus inhibit further slip acceleration even if the slip and rupture propagation begin, and could associate with the upper limit of slow slip events at the shallow portion of the plate boundary.

3.5 Conclusions

I performed friction experiments on smectite-rich pelagic sediments retrieved from the plate-boundary thrust during IODP Expedition 343 to understand mechanisms of the slow slip events at the Japan Trench. The main results of my results are as follow.

1. At low temperatures of 20^{o}C, the value of parameter (*a*-*b*) depends significantly on slip velocities. The simulated gouges exhibit negative values of (*a*-*b*) at low velocities, while these values becomes positive as increasing velocity to 100 μm/s. This frictional property may prevent further slip acceleration even if the slip commences, and could thus represent the upper limit of slow slip events at the shallow portion of the plate boundary.
2. At temperatures of 50-100^{o}C, the gouges show nearly neutral or slightly negative values of (*a*-*b*). This frictional properties can yield slow slip events, which are considered to generate under the conditions where (*a*-*b*) is small negative values. The conditions met at temperatures of 50-100^{o}C in present

experiments, that is consistent with temperature conditions where the slow slip events occurs along the plate boundary.

3. At temperature of >150^{o}C those exhibit positive values of (a-b) under almost all velocity conditions tested. The transition in (a-b) value from neutral to positive occurs in the range between 100 to 150^{o}C. The downdip temperature limit of the slow slip events at Japan Trench seems to be at the same temperature range. Hence, frictional properties of the smectite-rich clay sediment could correspond to the observed downdip limit of the slow slip events.

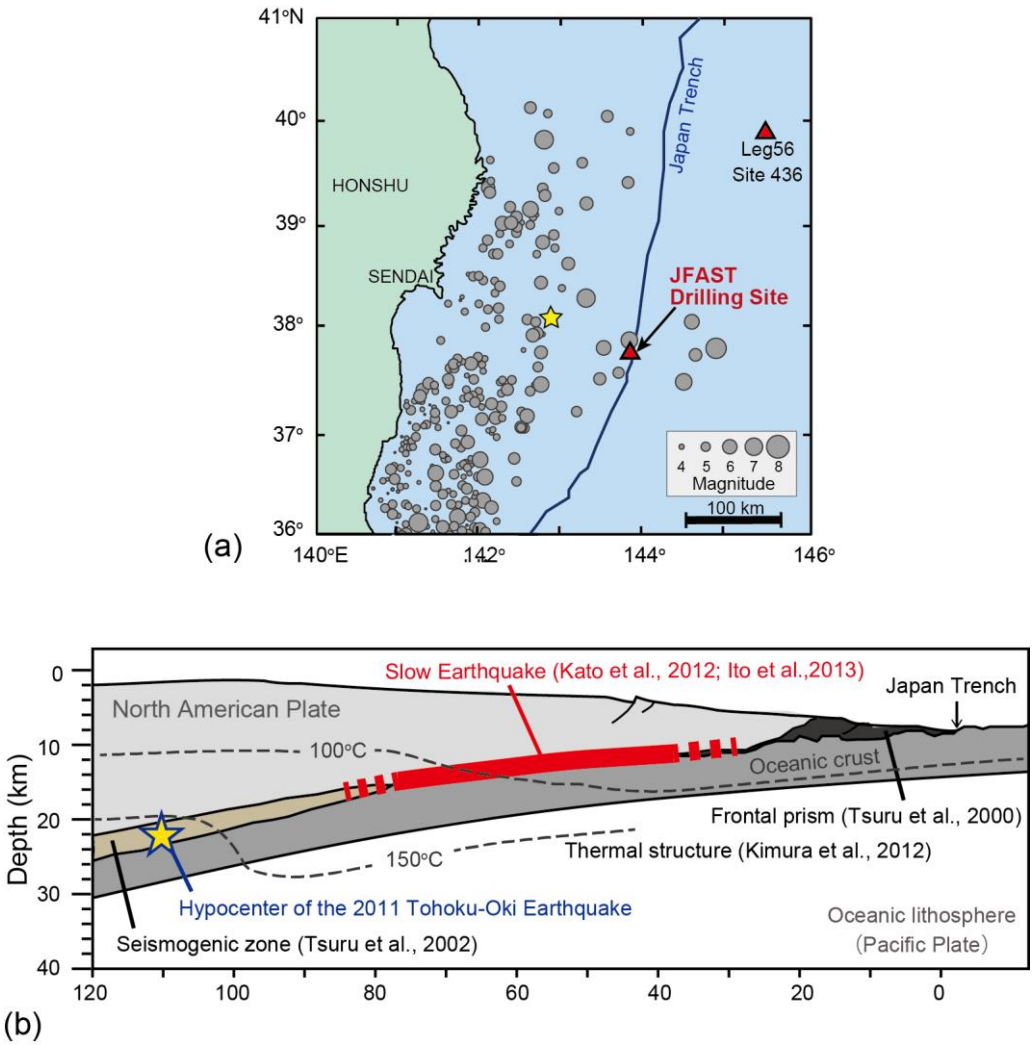

Figure 3.1.

(a) Locations of Site C0019 (IODP Expedition 343) (J-FAST) and Site 436 (DSDP Leg 56) (red triangles) (after Sawai et al., 2014). The yellow star denotes the epicenter of the mainshock, and gray circles are the aftershocks and the largest foreshock. The blue line shows the Japan Trench. (b) A schematic illustration of Tohoku subduction zone (modified from von Huene et al., 1982; Tsuru et al., 2000, 2002). Red line shows the area of slow earthquakes (Kato et al., 2012; Ito et al., 2013), yellow star indicate the hypocenter of the 2011 Tohoku-oki earthquake and black dashed-lines are the thermal structure (from Kimura et al., 2012).

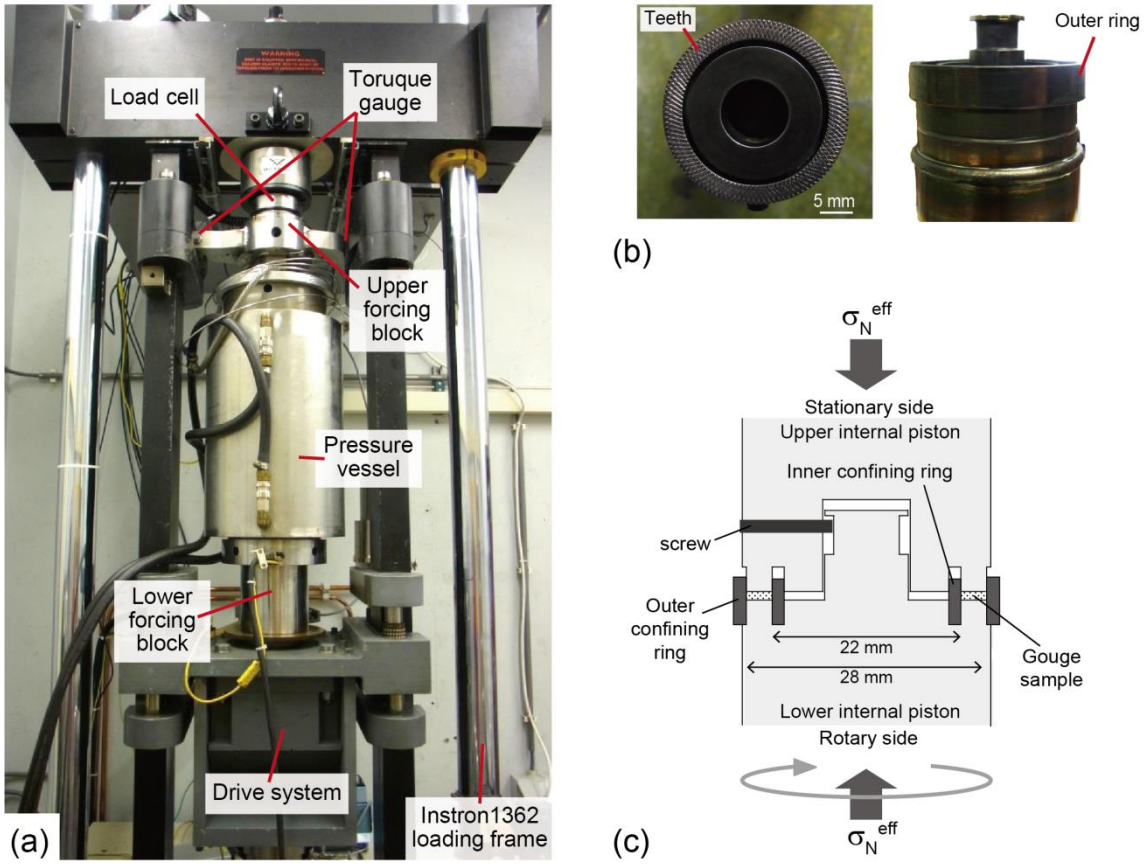

Figure 3.2

Photographs of (a) hydrothermal ring shear apparatus used in this study, and (b) the two internal pistons. (c) Schematic cross-sections of the sample assembly. σ_n^{eff} is the effective normal stress (after Niemeijer et al., 2008; den Hartog et al., 2012a).

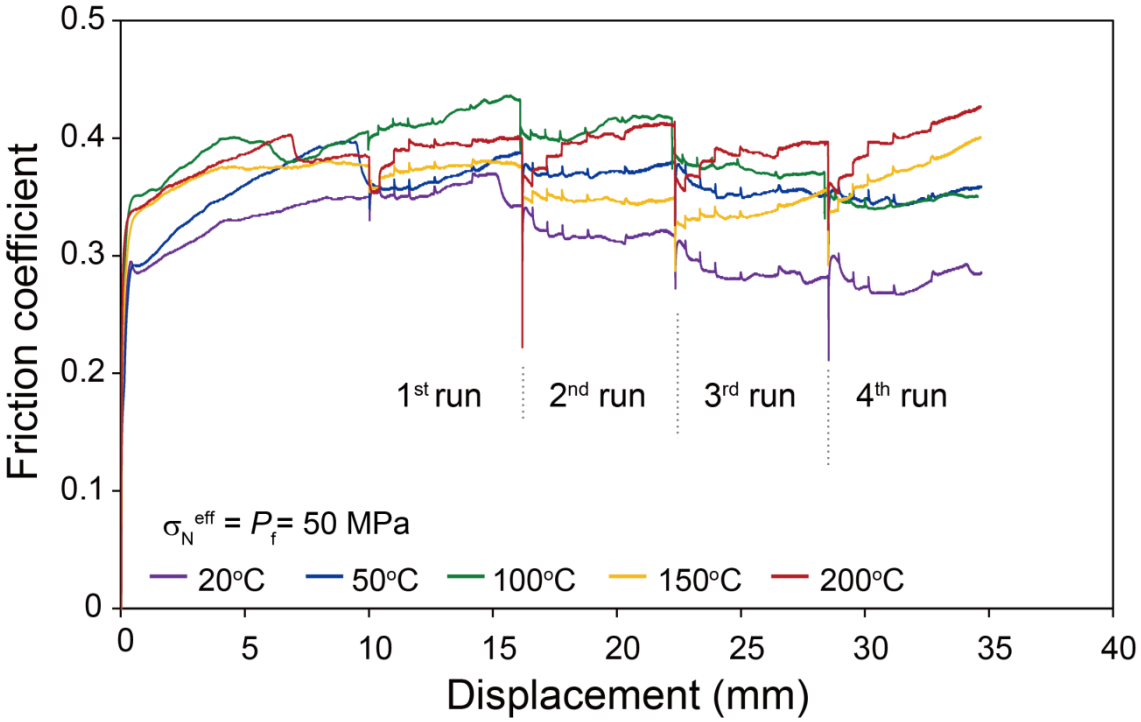

Figure 3.3

Friction data on smectite-rich clay sediment. Friction coefficient versus displacement curves at slip velocities of 0.3-100 μm/s under an effective normal stress and pore fluid pressure of 50 MPa. Velocity-stepping sequences were conducted four times during one experiment and I call them as 1st run, 2nd run, 3rd run and 4th run as shown in this figure.

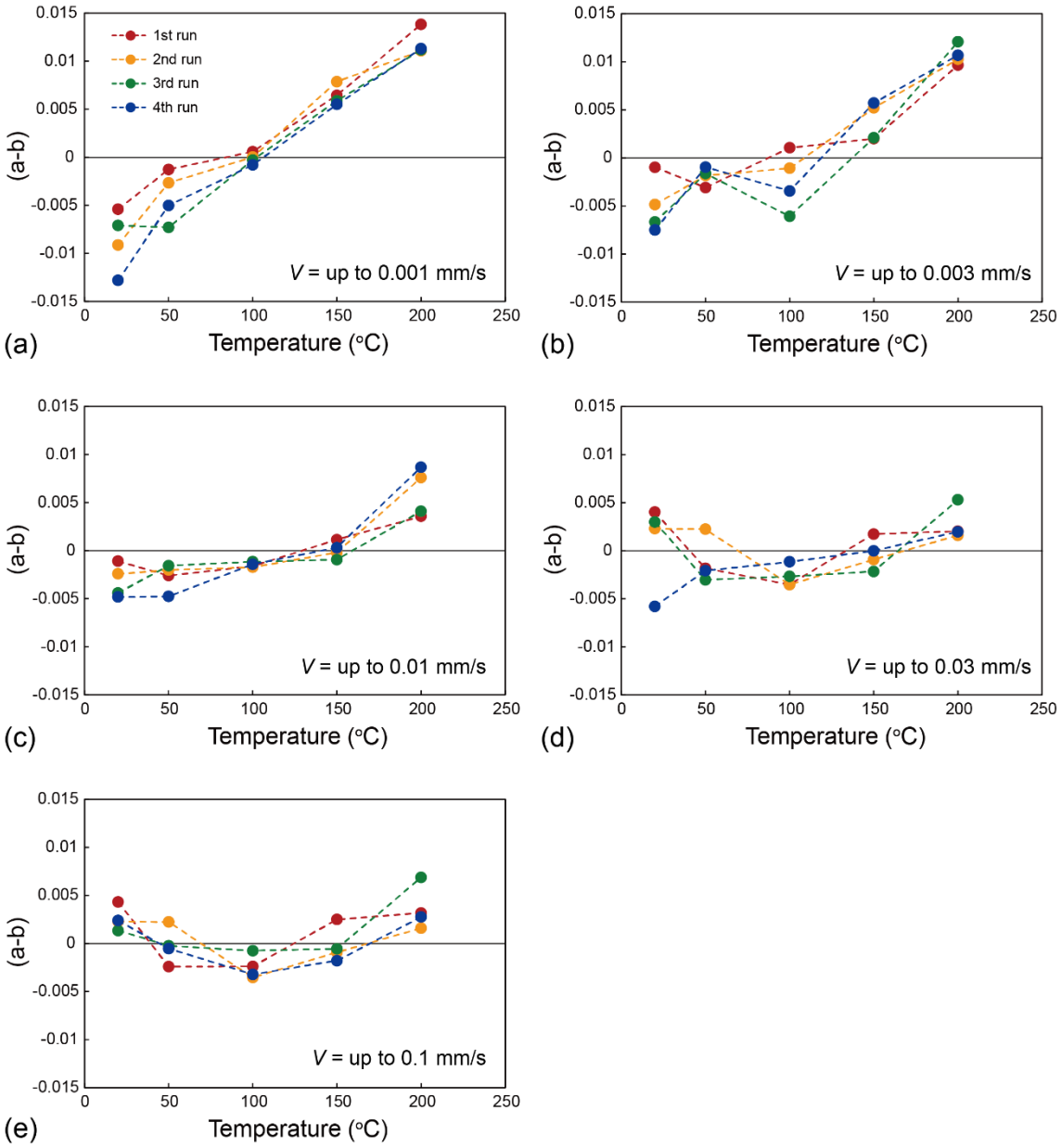

Figure 3.4

Frictional velocity dependence for smectite-rich clay sediment as a function of temperature under an effective normal stress and pore fluid pressure of 50 MPa. Each figure show the values at post-slip velocity of (a) 1.0 μm/s, (b) 3.0 μm/s, (c) 10 μm/s, (d) 30 μm/s and (e) 100 μm/s. Red symbols show the results of the 1st run, those of yellow are the 2nd run, green is the 3rd run and Blue ones are the results of the 4th run.

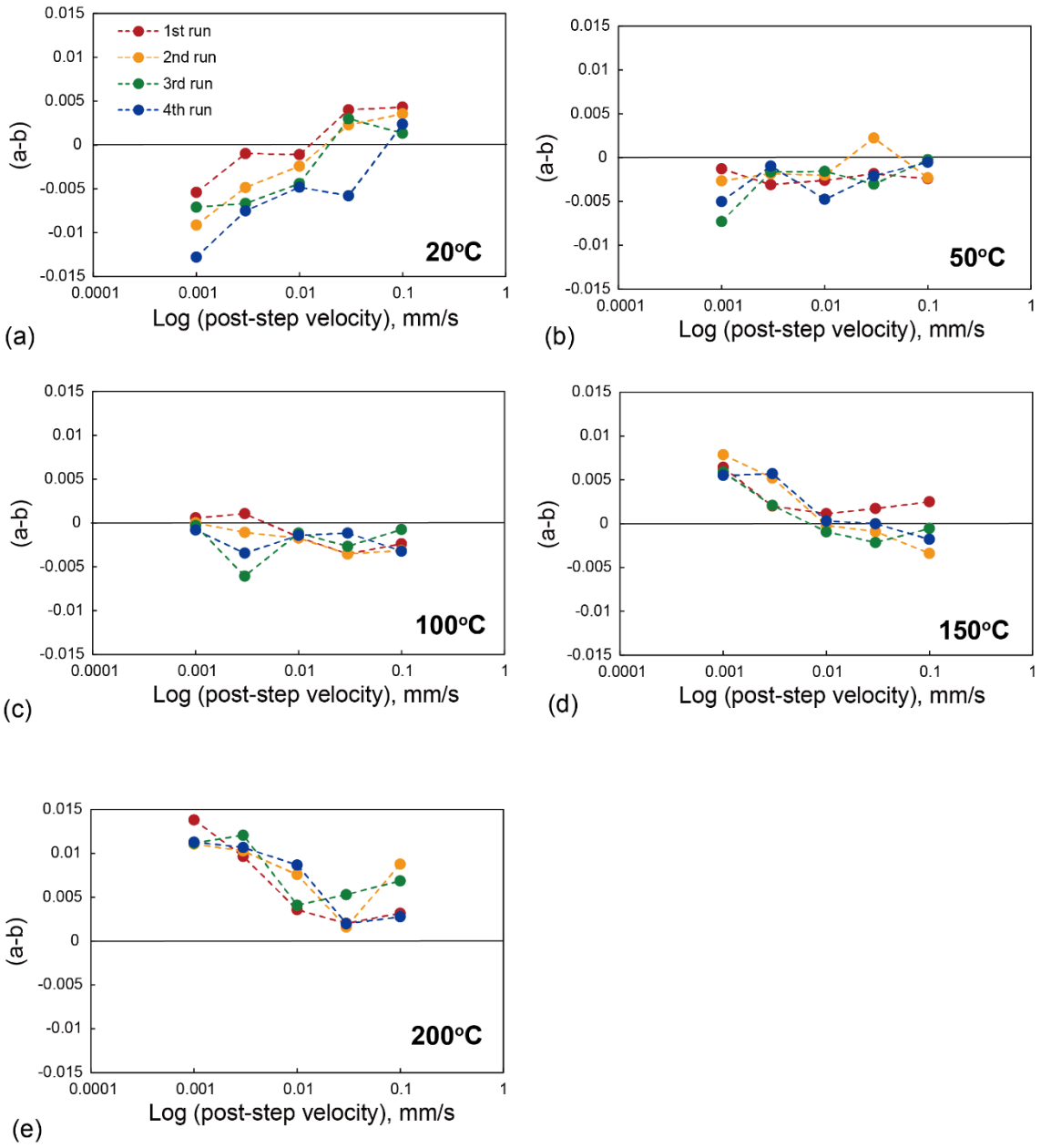

Figure 3.5

Values of the velocity dependence parameter (*a*-*b*) as a function of post-slip velocity under an effective normal stress and pore fluid pressure of 50 MPa. Each figure show the values at (a) 20°C, (b) 50°C, (c) 100°C, (d) 150°C and (e) 200°C. Red color show the result during the 1st run, yellow is those of the 2nd run, green is the 3rd run and blue is the 4th run.

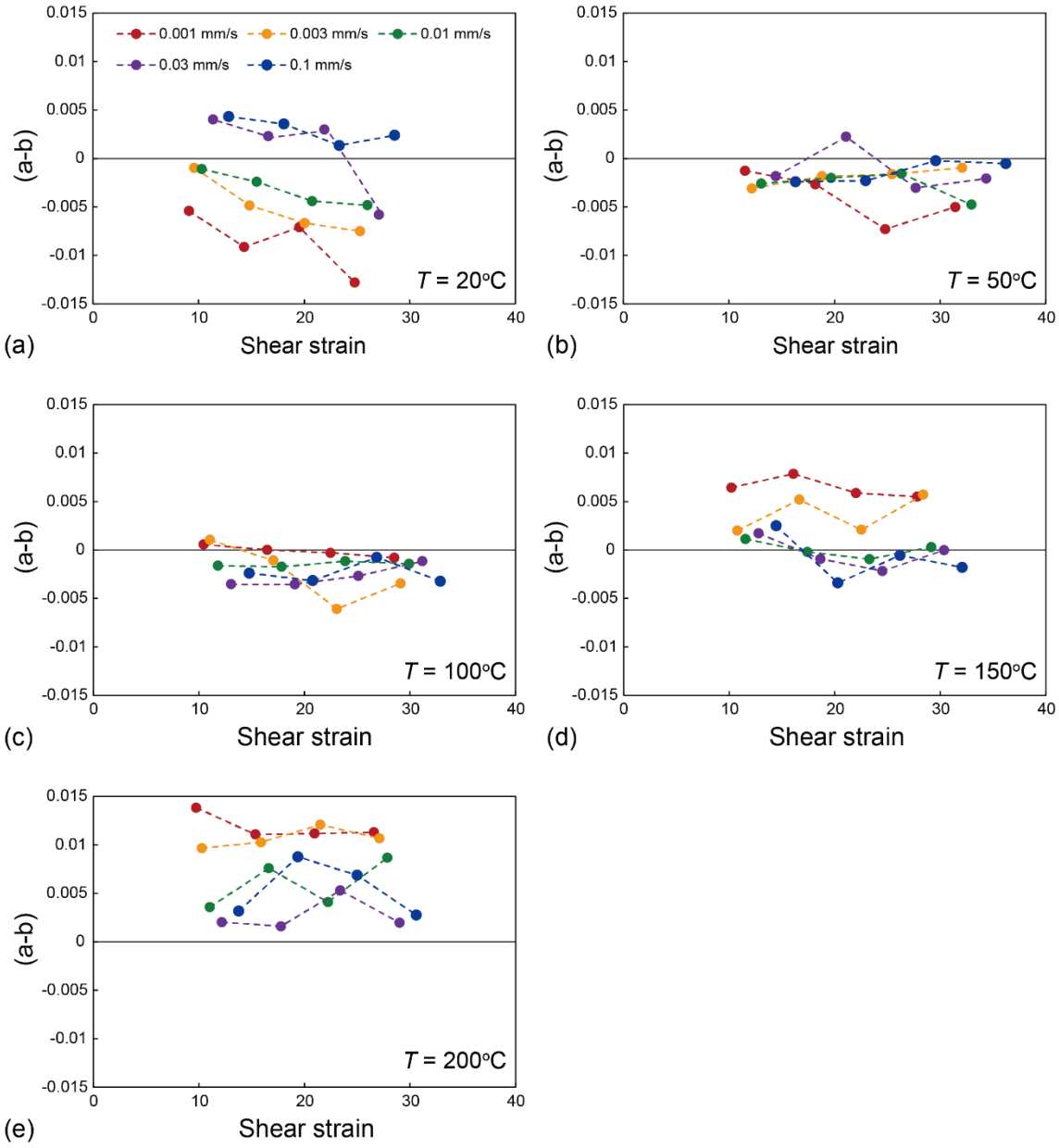

Figure 3.6

The friction parameter (*a*-*b*) under an effective normal stress and pore fluid pressure of 50 MPa plotted against shear strain Each figure show the values at (a) 20°C, (b) 50°C, (c) 100°C, (d) 150°C and (e) 200°C. Symbols in the figures indicate the post-slip velocity: Red = 1.0 μm/s, Yellow = 3.0 μm/s, Green = 10 μm/s, Purple = 30 μm/s and Blue = 100 μm/s.

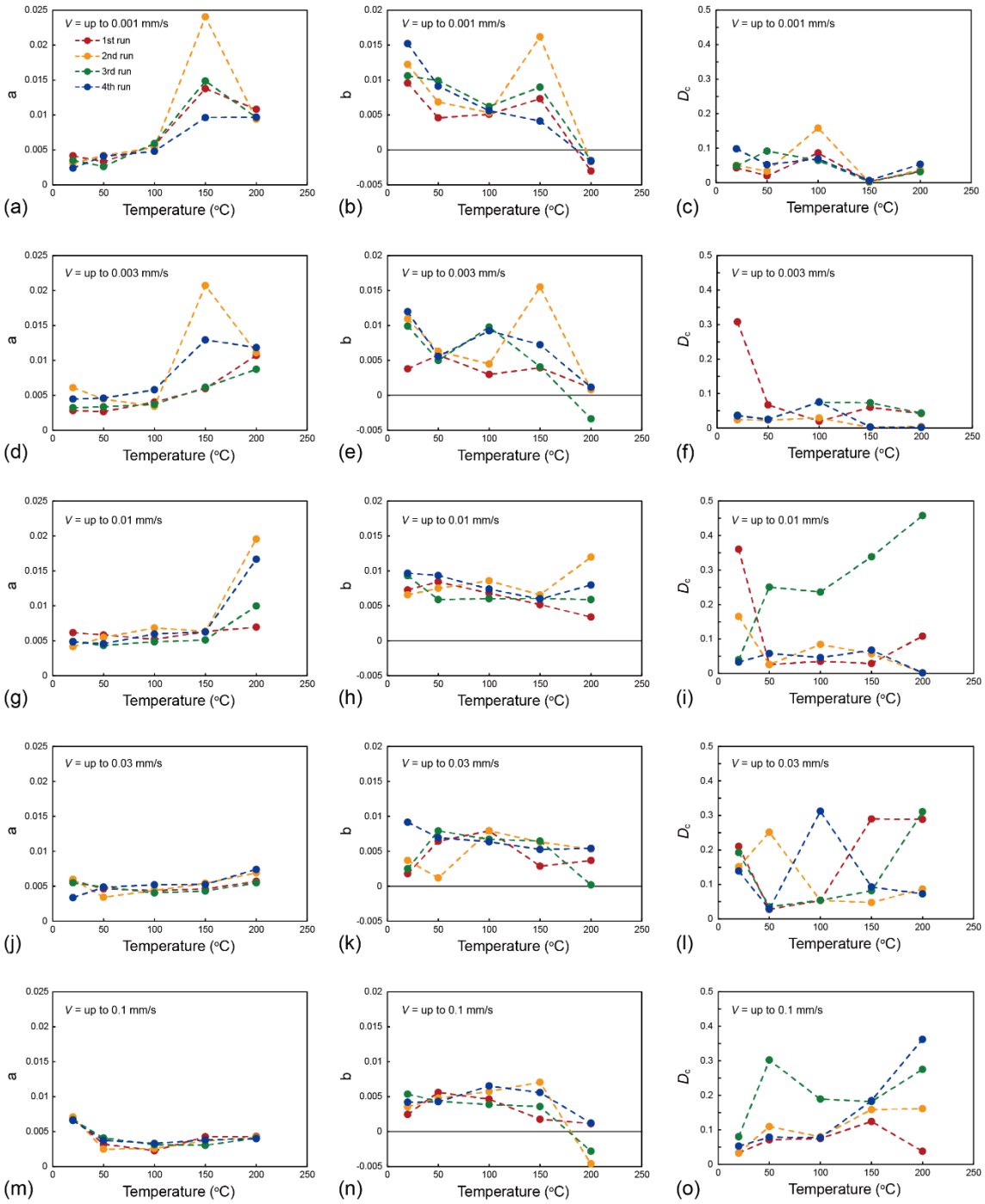

Figure 3.7

Rate and state friction parameters plotted against temperature. (a), (d), (g), (j) and (m) are parameter *a* at post-slip velocity of 1.0 μm/s, 3.0 μm/s, 10 μm/s, 30 μm/s and 100 μm/s, respectively. (b), (e), (h) (k) and (n) are parameter *b* at post-slip velocity of 1.0 μm/s, 3.0 μm/s, 10 μm/s, 30 μm/s and 100 μm/s, respectively. (c), (f), (i) (l) and (o) are

parameter D_c at post-slip velocity of 1.0 μm/s, 3.0 μm/s, 10 μm/s, 30 μm/s and 100 μm/s, respectively. Red symbols show the results of 1st run, yellow ones are those of the 2nd run, green ones shows data of the 3rd run and Blue data are from the 4th run. All data in these plots is under $\sigma_n^{eff} = P_f = 50$ MPa conditions.

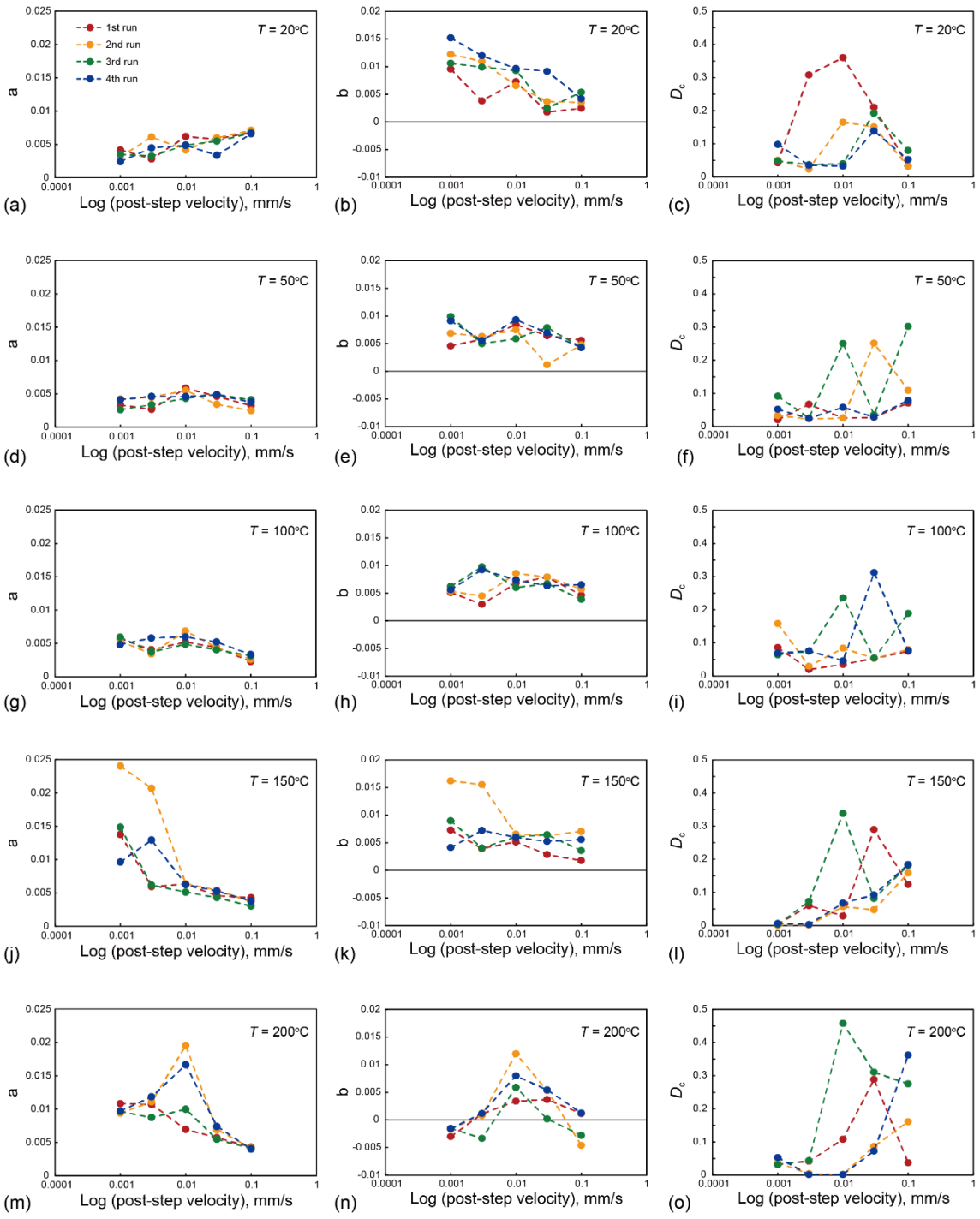

Figure 3.8

Constitutive parameters plotted against post-slip velocity. (a, d, g, j and m) parameter *a* at temperature of 20ºC, 50ºC, 100ºC, 150ºC and 200ºC, respectively. (b, e, h k and n) parameter *b* at temperature of 20ºC, 50ºC, 100ºC, 150ºC and 200ºC, respectively. (c, f, i l and o) parameter D_c at temperature of 20ºC, 50ºC, 100ºC, 150ºC and 200ºC,

respectively. All data in these plots is under $\sigma_n^{eff} = P_f = 50$ MPa conditions. Note that in all figures red symbols show the result during the 1st run, those of yellow are during the 2nd run, green is during the 3rd run, and red is the 4th run.

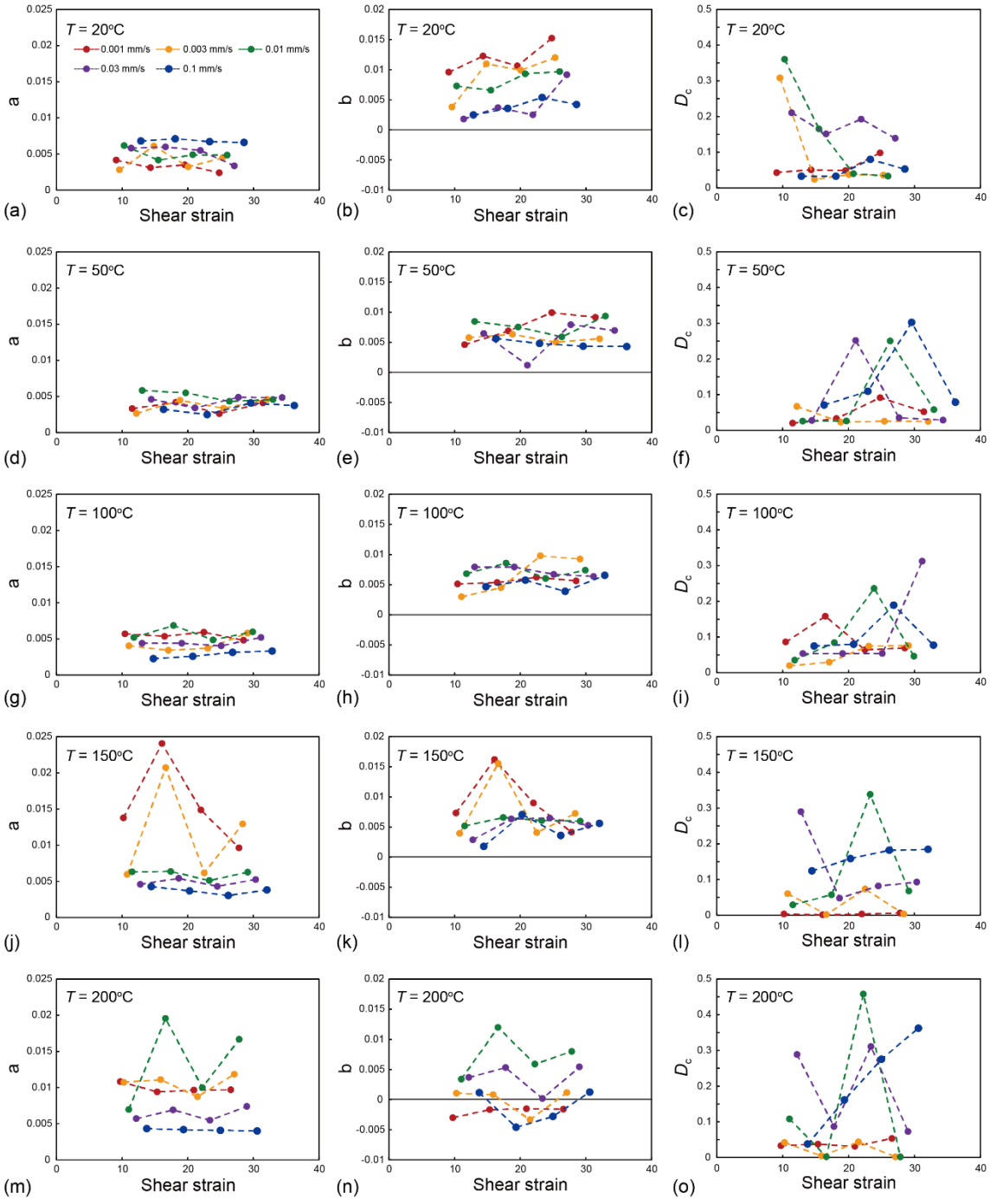

Figure 3.9

Constitutive parameters plotted against shear strain. (a, d, g, j and m) parameter *a* at temperature of 20°C, 50°C, 100°C, 150°C and 200°C, respectively. (b, e, h k and n) parameter *b* at temperature of 20°C, 50°C, 100°C, 150°C and 200°C, respectively. (c, f, i l and o) parameter D_c at temperature of 20°C, 50°C, 100°C, 150°C and 200°C,

respectively. All data in these plots is under $\sigma_n^{eff} = P_f = 50$ MPa conditions. Symbols in all figures indicate the post-slip velocity: Red = 1.0 μm/s, Yellow = 3.0 μm/s, Green = 10 μm/s, Purple = 30 μm/s and Blue = 100 μm/s.

Table 3.1 List of experimental conditions in this study.

Experimental number	Temperature (°C)	σ_n^{eff} (MPa)	P_f (MPa)	V-stepping sequence (μm/s)	Total shear displacement (mm)	Final gouge thickness (mm)
17R-03	100	50	50	10-0.3-1.0-3.0-10-30-100 -0.3-1.0-3.0-10-30-100 -0.3-1.0-3.0-10-30-100 -0.3-1.0-3.0-10-30-100	34.55	1.02
17R-04	20	50	50	10-0.3-1.0-3.0-10-30-100 -0.3-1.0-3.0-10-30-100 -0.3-1.0-3.0-10-30-100 -0.3-1.0-3.0-10-30-100	34.70	1.18
17R-05	200	50	50	10-0.3-1.0-3.0-10-30-100 -0.3-1.0-3.0-10-30-100 -0.3-1.0-3.0-10-30-100 -0.3-1.0-3.0-10-30-100	34.67	1.10
17R-06	50	50	50	10-0.3-1.0-3.0-10-30-100 -0.3-1.0-3.0-10-30-100 -0.3-1.0-3.0-10-30-100 -0.3-1.0-3.0-10-30-100	34.69	0.93
17R-07	150	50	50	10-0.3-1.0-3.0-10-30-100 -0.3-1.0-3.0-10-30-100 -0.3-1.0-3.0-10-30-100 -0.3-1.0-3.0-10-30-100	34.67	1.05

Note that σ_n^{eff} is the normal stress, P_f is pore fluid pressure and V is slip velocity.

Chapter 4

Relationship between effective normal stress and slow slip event: Insights from frictional behavior under high P-T conditions

Abstract

Slow slip events have occurred at shallow depth in the Tohoku subduction zone, and the area where it occurred overlapped with seismogenic zone. There is a possibility that pore pressure is one of significant factor to control the fault stability. I have thus investigated the frictional properties of blueschist, which probably distributed at the Tohoku subduction zone, using a rotary shear apparatus under the various pressure and temperature conditions. Friction experiments were conducted at temperatures of 22-300^{o}C, effective normal stresses of 25-200 MPa, pore fluid pressures of 25-200 MPa and sliding velocities of 0.1-100 μm/s. Blueschist showed an effective normal stress dependence: even at temperature conditions where (a-b) tends to be positive, (a-b) values are positive at high effective pressure and decrease to negative with decreasing effective normal stress. My results suggest that increasing pore pressure is a possible factor causing unstable slip, leading to slow slip events.

4.1 Introduction

Slow earthquakes (e.g., slow slip event, low frequency earthquakes, very low frequency earthquakes, and non-volcanic tremor) are one of the important factors in order to understand the various slip behavior in subduction zones. Diverse type of slow earthquakes occurred at shallow depths in a lot of subduction zones, such as the Japan Trench (Obara et al., 2004a, 2004b; Asano et al., 2008; Kato et al., 2012; Ito et al., 2013), the Nankai Trough (Obara and Ito, 2005; Ito and Obara, 2006), New Zealand (Wallace and Beavan, 2010) and Costa Rica (Brown et al., 2005). Recently, it was revealed that episodic slow slip events and seismicity migration toward the initial rupture point of the 2011 Tohoku-oki earthquake occurred just before the earthquake on

a shallow portion (about less than 20 km depth) in the subduction zone (Kato et al., 2012; Ito et al., 2013) (Figure 4.1a).

Some models have been explained slow slip events using rate and state friction law. Kato (2003), Shibazaki and Iio (2003), and Shibazaki and Shimamoto (2007) introduced a cutoff velocity in the friction laws, where friction changes from velocity weakening to velocity strengthening. Liu and Rice (2005) confirmed that slow slip events occur spontaneously near the downdip end of the seismogenic zone in their 3D model using the Dietrich-Ruina friction law. The models were considered the depth-dependent frictional properties of fault materials. However just a few frictional properties, e.g. on halite (Shimamoto, 1986) and on granite (Blanpied et al., 1991, 1995), have been used because there are few frictional data on rocks distributed at the subduction zone under in-situ PT conditions, except for that of serpentine (Takahashi et al., 2011) and clay minerals (den Hartog et al., 2012a, 2012b).

Segall et al. (2010) conducted another approach to demonstrate slow slip events. In their model, slow slip events is controlled by dilatant stabilization. Moreover there is a view that pore pressure is closely related to the slow slip events and key to the generation mechanism of them (Shelly et al., 2006). However there are a few data which showed the effect of pore pressure (He et al., 2007).

From the P-T phase diagram, the input materials imply the Japan Trench should be a blueschist in the area which downdip limit of the slow slip events were observed (Figure 4.1b). Then I investigate the frictional properties of the blueschist at in-situ PT conditions and discuss a possible generation mechanism of slow slip events in the Tohoku subduction zone based on its properties.

4.2 Experimental methods

Friction experiments on blueschist powders were performed using the hydrothermal ring shear apparatus at Utrecht University (described in detail by Niemeijer et al., 2008 and den Hartog et al., 2012) (Figure 4.2). I used a lawsonite-blueschist rock from Franciscan Belt, California. The blueschist was crushed by hand and sieved at <125 μm in order to prepare simulated gouges for the

experiments. XRD analysis and microstructure analysis showed the presence of Glaucophane, Lawsonite, Titanite, Pyrite, Garnet and Chlorite (Figure 4.3). Simulated fault gouges which thickness is between 0.6 and 1.0 mm were located between two roughened opposing superalloy pistons. The gouge sample is kept in place by inner and outer confining rings of stainless steel, with an inner diameter of 22 mm and an outer diameter of 28 mm. The confining rings were coated with Molykote spray to reduce wall friction and dried to remove volatiles at 150°C before assembly. The piston–sample assembly is located inside an internally heated pressure vessel filled with distilled water. Pressure vessel is positioned in an Instron 1362 loading frame and then moved upwards using the Instron ram. At first, an effective normal stress is applied, and then a pore fluid pressure is added. After that, a furnace was turned on in order to heat to a desired temperature and to gain a desired pore fluid pressure. The system was subsequently left to equilibrate and then start to be rotated by a servo-controlled motor and gearbox. Blueschist samples were sheared at temperatures (T) of 22-300°C, effective normal stresses (σ_n^{eff}) of 25-200 MPa and pore fluid pressures (P_f) of 25-200 MPa. I conducted pressure-stepping experiments at constant Temperature, with effective normal stress set equal to the pore fluid pressure ($\sigma_n^{eff} = P_f$, $\lambda = (P_f / \sigma_n) = 0.5$).

The velocity dependence of friction coefficient (μ) is described as (a-b). It is defined in rate and state dependent friction (RSF) model (Dieterich, 1978, 1979; Ruina, 1983) as:

$$(a - b) = \frac{\Delta \mu_{ss}}{\Delta \ln V}$$

where a is a direct effect, which is an instantaneous response with a positive proportionality coefficient to the change in magnitude of the velocity. b represents a decay in the friction to a new steady-state, called an evolutionary effect. $\Delta\mu_{ss}$ is the change in steady-state friction coefficient, V is the slip velocity (e.g. Marone, 1998). A positive (a-b) value means that a slip accelerates friction increases, so the fault shows a stable sliding, i.e. velocity-strengthening. On the other hand, at the negative value the

frictional behavior shows velocity-weakening and unstable slip can occur. I performed velocity-stepping sequences to determine this rate and state parameter (*a*-*b*) on the blueschist and investigated how this parameter changed with temperature and effective pressure.

4.3 Results

Each experimental conditions and mechanical data are listed in Table 4.1. Friction coefficient (μ) as a function of displacement is shown in Figure 4.4a ($\sigma_n^{eff} = P_f = 50$ MPa) for representative experiments. The friction versus displacement curve in each experiment was mostly similar, but in some cases the samples exhibit unstable stick-slip behavior only at 200ºC and 300ºC. The velocity dependence of μ is described as (*a*-*b*), is shown in Figure 4.4b and Figure 4.5. I can see the systematic influences of temperature (Figure 4.4b for representative condition at post-slip-velocity of 1.0 μm/s) and effective normal stress (Figure 4.5), as mentioned below.

At 22ºC, the gouges show a friction coefficient of ~ 0.75 and positive (*a*-*b*) values which decrease to become negative with increasing temperature. The velocity-strengthening to velocity-weakening transition is between 100 ºC and 200 ºC. Then at 200ºC, the behavior is velocity weakening and shows negative (*a*-*b*) values with a background friction of ~0.75. At 300ºC, friction is ~0.65 and slip shows larger (*a*-*b*) values than at 200 ºC and tends to become velocity-strengthening. In addition, it is also important to notice that there is effective normal stress dependence: (*a*-*b*) values are positive at high effective pressure and decreases to become negative with decreasing effective normal stress even at stable-temperature conditions such as 22 ºC, 100 ºC and 300 ºC, although I cannot see such a clear trend at 200 ºC. There is a velocity-strengthening to velocity-weakening transition between 25 MPa and 75 MPa.

4.4 Discussion

There are many numerical models to simulate the earthquake and slow slip events rupture nucleation and propagation (e.g. Kato, 2003: Shibazaki and Iio, 2003; Liu and Rice, 2005, 2007; Shibazaki and Shimamoto, 2007; Segall et al., 2010). In almost all

models, a large slip-weakening distance and low effective stress are common factors. And there is a view that a slow slip event occurs when (*a*-*b*) shows a very small negative value. In the present study, it is revealed that there is a dependence of effective normal stress: (*a*-*b*) value becomes negative with decreasing effective normal stress (Figure 4.5). In order to cause the slow slip events, (*a*-*b*) value has to across the (*a*-*b*) = 0 line, and its (a-b) values of this study show this velocity-strengthening to weakening transition at around 50-75 MPa with becoming low effective normal stress. This frictional property support the common features that previous numerical models have suggested: low effective stress play a key role for the generation mechanism of slow slip events.

In soil, effective normal stress equals total pressure minus pore pressure. It means that the area where the pore pressure is high become low effective pressure. Figure 4.4 shows the frictional properties at the Japan Trench based on this laboratory study under high and low effective normal stress conditions, which corresponded to low and high pore pressure. When effective normal stress is high, i.e. pore pressure is low, (*a*-*b*) shows neutral values at around 200^{o}C (Figure 4.6a and 4.6c). With decreasing effective normal stress, i.e. with increasing pore pressure, the neutral zones shift to the area where the temperature is less than 150^{o}C and more than 300^{o}C (Figure 4.6b and 4.6d). Ito et al (2013) showed that slow slip events occurred at about less than 20 km depth. According to the thermal structures at the Japan Trench, the temperature range of downdip limit of the slow slip events is between 100^{o}C to 150^{o}C. The transition in (a-b) value from neutral to positive at higher pore pressure, occurs at the same temperature range. Hence, the frictional properties at low effective normal stress (high pore pressure) could correspond to the observed downdip limit of the slow slip events, although I cannot see any observational evidence yet at deeper portion correspond to the temperature area of 300^{o}C.

Segall et al. (2010) have explored the effect of the dilatant stabilization to the slow slip events. As slip accelerates, dilatancy makes pore space and reduce pore pressure, resulting in the high effective normal stress. This process has limited to the slip and rupture in their models. My results indicate that a stable slip become to occur

with increasing the effective normal stress, which is in agreement with their model. Thus I confirmed the association of the effective normal stress (pore pressure) with slow slip events in the view point of laboratory work.

From the previous studies, slow slip events were detected just before the 2011 Tohoku-oki earthquake (Kato et al., 2012; Ito et al., 2013). There is a possibility that it was due to the changes of effective normal stress. In this study, (a-b) values are positive at high effective pressure and decrease to negative with decreasing effective normal stress at temperature conditions where (a-b) tends to be positive, i.e. positive (a-b) values shift to neutral with increasing pore pressure and subsequently to negative. This suggests that increasing pore pressure is a possible factor causing unstable slip, leading to slow slip events before the earthquakes.

4.5 Conclusions

A series of rotary shear friction experiments was conducted on the blueschist powder in order to understand the generation mechanisms of slow slip events within the Tohoku subduction zone. Simulated blueschist fault gouge become to show the velocity-weakening behavior when effective normal stress decreases. This behavior is a critical data which supported a lot of previous numerical simulations, demonstrating the mechanisms of slow slip events. The frictional properties at low effective normal stress can explain the observed slow slip events at shallow portion, particularly the downdip limit of the slow slip events. Such frictional behavior suggests that low effective normal stress, i.e. high pore pressure, is an important factor to the generation mechanism of slow slip events.

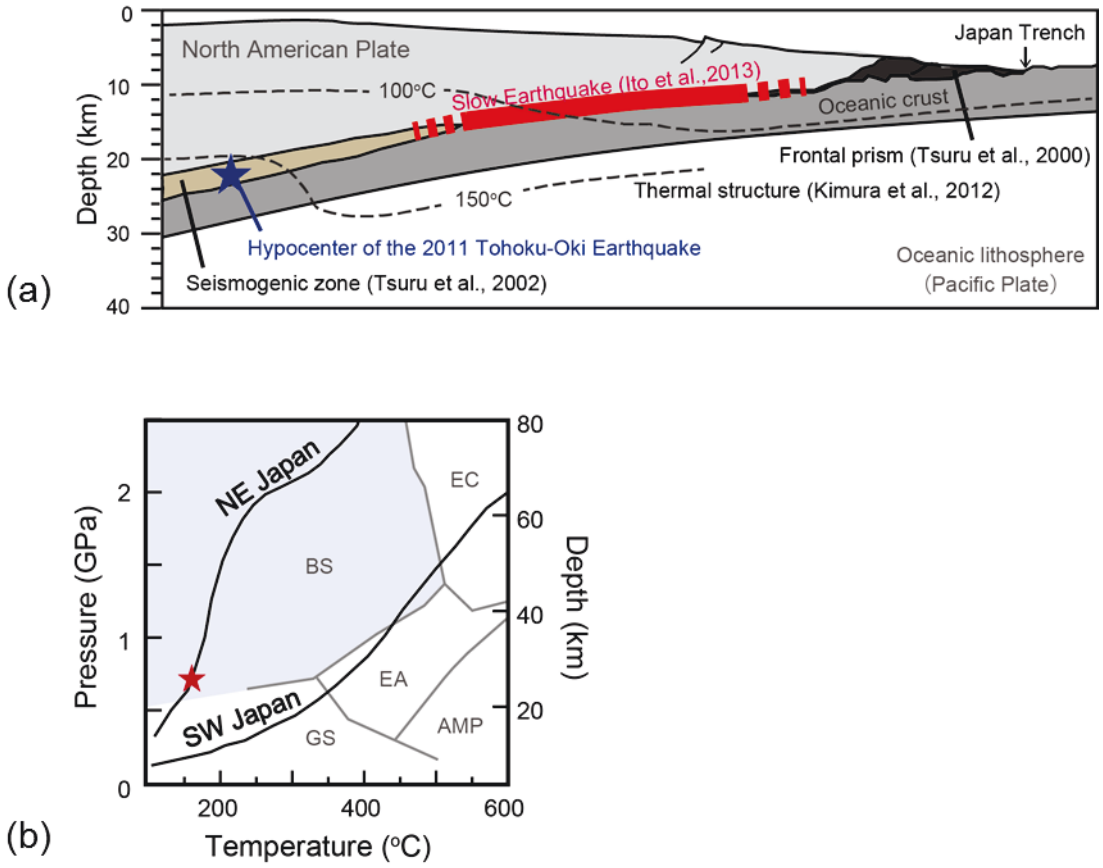

Figure 4.1

(a) A schematic illustration of Tohoku subduction zone (modified from von Huene et al., 1982; Tsuru et al., 2000, 2002). Red line shows the area of slow earthquakes (Kato et al., 2012; Ito et al., 2013), blue star indicate the hypocenter of the 2011 Tohoku-oki earthquake and black dashed-lines are the thermal structure (from Kimura et al., 2012) (after Chapter 3). (b) Metamorphic conditions in subducting oceanic crust (from Evans, 1990; Oh and Liou, 1998; Maruyama and Okamoto, 2007). Black lines indicate the geothermal gradients of the present subduction zone in NE Japan and that in SW Japan, respectively (Peacock and Wang, 1999). The hypocentral P-T conditions of the 2011 Tohoku-oki earthquake are plotted as a red star. BS = blueschist, EC = Eclogite, GS = greenschist, EA = epidote amphibolite, AMP = amphibolite

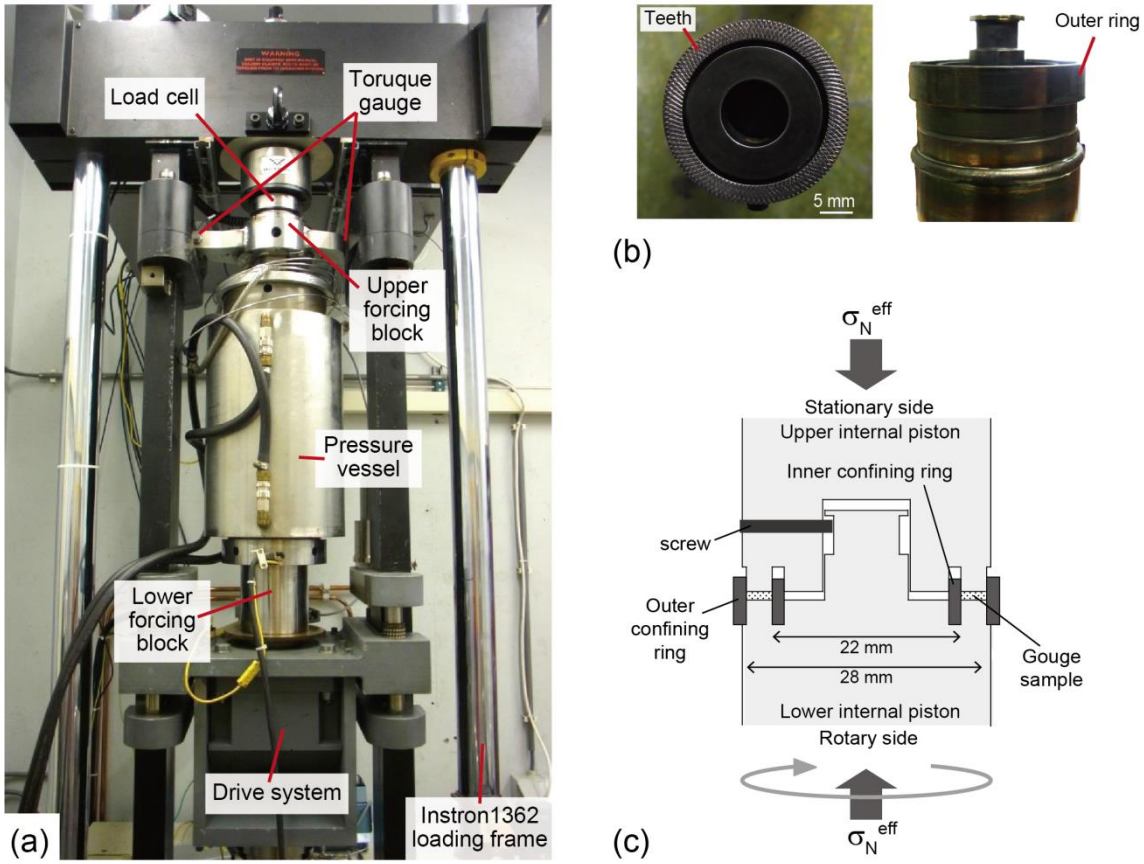

Figure 4.2

Photographs of (a) hydrothermal ring shear apparatus used in this study, and (b) the two internal pistons (after Chapter 3). (c) Schematic cross-sections of the sample assembly. σ_n^{eff} is the effective normal stress (after Niemeijer et al., 2008; den Hartog et al., 2012a).

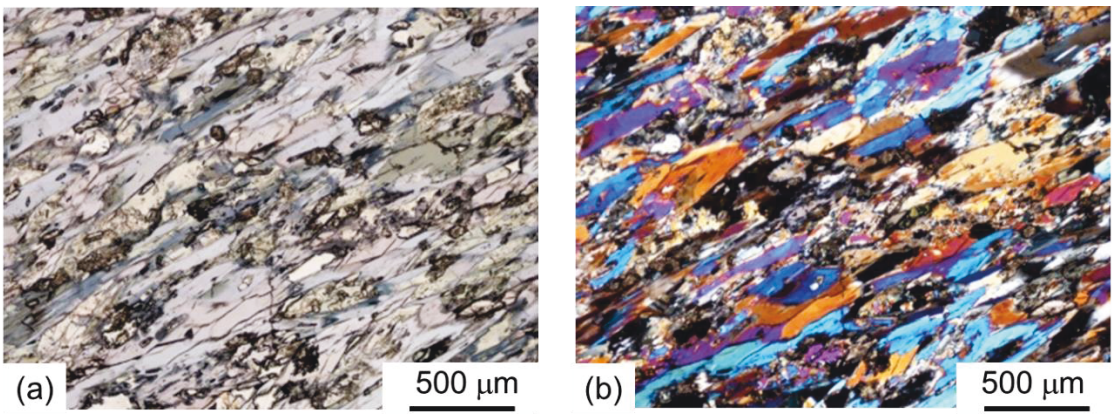

Figure 4.3

Photomicrographs of blueschist (a) under planepolarized light and (b) under cross-polarized light.

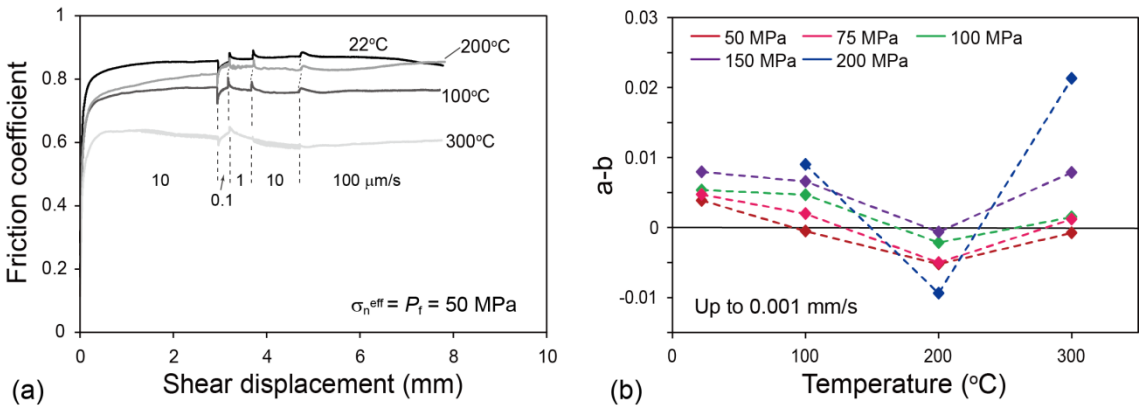

Figure 4.4

Representative frictional behavior of blueschist powder. (a) Friction coefficient versus displacement curves at slip velocities of 0.1-100 μm/s under an effective normal stress and pore fluid pressure of 50 MPa. (b) (*a*-*b*) at post-slip-velocity of 1.0 μm/s plotted against applied Temperatures. Each symbols indicate the condition of effective normal stress: red is 50 MPa, pink is 75 MPa, green is 100 MPa, purple is 150 MPa and blue is 200 MPa.

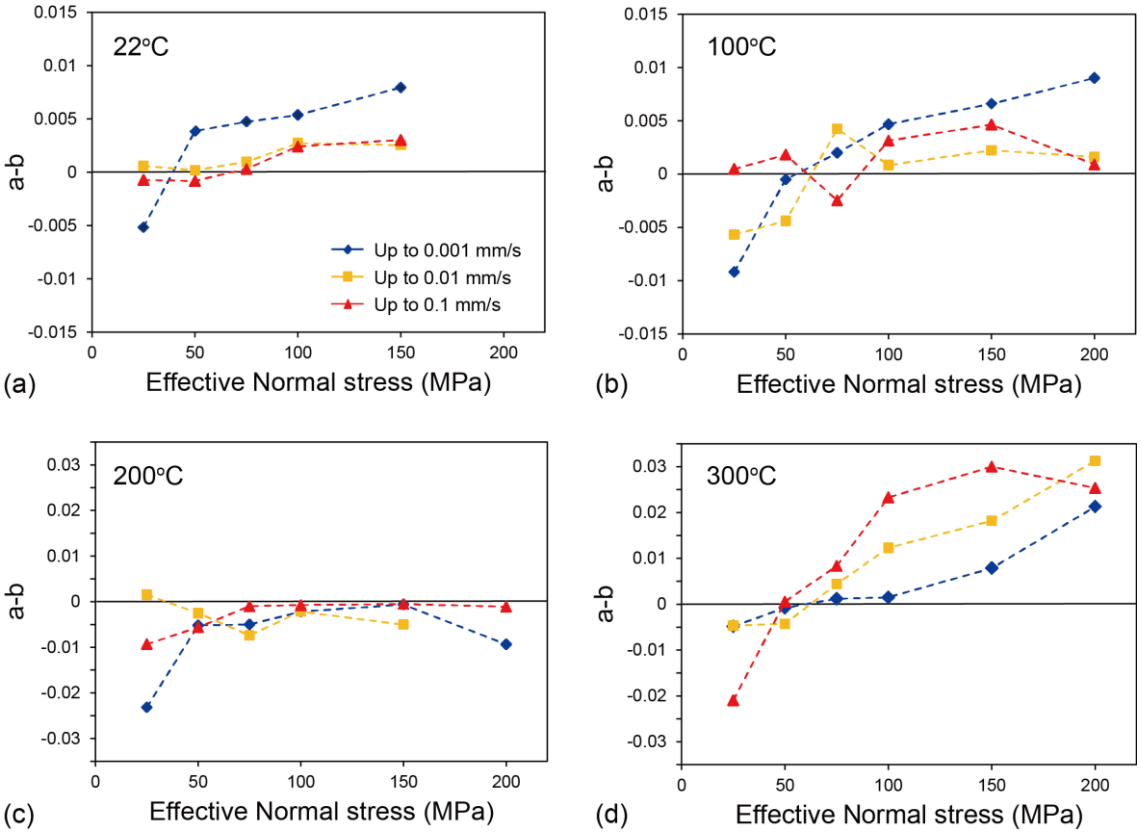

Figure 4.5

(*a-b*) at (a) 22°C, (b) 100 °C, (c) 200 °C and (d) 300 °C plotted against applied effective normal stress. Blue symbols are values at post-slip-velocity of 1.0 μm/s, yellow characters are those at post-slip-velocity of 10 μm/s, and those of red is at post-slip-velocity of 100 μm/s.

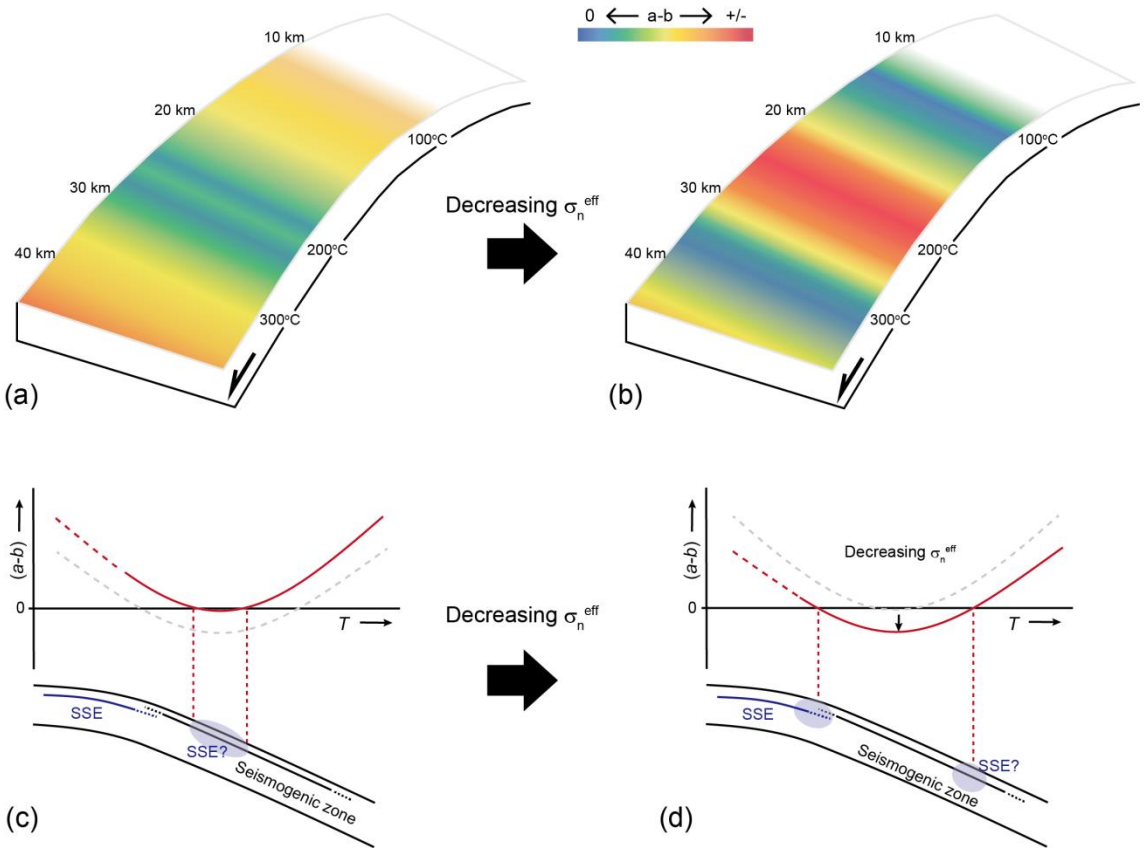

Figure 4.6

A schematic illustration of frictional properties under (a) high effective pressure and (b) low effective pressure at Tohoku subduction zone. (*a*-*b*) value showed the neutral value indicate blue. The blue color gradually changes to red as the value of (*a*-*b*) become positive or negative values. Schematic representation of the shift caused by effective normal stress (σ_n^{eff}) in (a-b) versus temperature (Red and grey line). (c) is under high effective normal stress and (d) is under low effective normal stress. Schematic cross section of the subduction zone in (c) and (d) show the Tohoku subduction zone. Blue line in the subducted crust represents the area where slow slip events occur and black line show the seismogenic zone.

Table 4.1 List of experimental conditions in this study.

Experimental number	Temperature (°C)	σ_n^{eff} stepping sequence (MPa)	P_f stepping sequence (MPa)	V-stepping sequence (μm/s)	Total shear displacement (mm)	Final gouge thickness (mm)	Occurrence of stick-slip or oscillation
BS 001	200	25-50-75	25-50-75	10-0.1-1.0-10-100	30.43	0.81	at (50MPa - 0.1, 1 μm/s), (75MPa – 1, 10 μm/s)
BS 002	300	25-50-75	25-50-75	10-0.1-1.0-10-100	30.07	0.83	at (25 MPa - 10 μm/s), (50 MPa - 10 μm/s), (75 MPa - 10 μm/s)
BS 003	100	25-50-75	25-50-75	10-0.1-1.0-10-100	30.05	0.63	–
BS 006	23	25-50-75	25-50-75	10-0.1-1.0-10-100	30.43	0.73	–
BS 010	22	100-150	100-150	10-0.1-1.0-10-100	22.22	0.68	–
BS 011	200	100-150-200	100-150-200	10-0.1-1.0-10-100	29.60	0.59	at (200 MPa - 1, 10 μm/s)
BS 013	100	100-150-200	100-150-200	10-0.1-1.0-10-100	29.87	0.66	–
BS 025	300	100-150-200	100-150-200	10-0.1-1.0-10-100	32.55	0.74	at (100 MPa - 10 μm/s), (150 MPa - 10 μm/s), (200 MPa - 10 μm/s)

Note that σ_n^{eff} is the effective normal stress, P_f is pore fluid pressure and V is slip velocity.

Chapter 5

Frictional properties of blueschist facies fault rocks expected at the hypocenter of the Tohoku-oki earthquake and implications for nucleation of the 2011 event

Abstract

The 2011 Tohoku-oki earthquake (Mw 9.0) nucleated at 24 km depth along the plate boundary. To understand the earthquake nucleation mechanisms, it is essential to reveal the frictional properties of metamorphic rocks, which are expected to be present at depth within the Tohoku subduction zone. I have thus investigated the frictional properties of glaucophane schist (blueschist) using a rotary shear apparatus. Friction experiments were conducted at temperatures of 22-400ºC, effective normal stresses of 25-200 MPa, pore fluid pressures of 25-200 MPa and sliding velocities of 0.1-100 μm/s. Blueschist showed a transition from velocity strengthening to velocity-weakening at around 100ºC, and its friction became velocity-strengthening again at around 300ºC. There is also effective normal stress dependence. The blueschist sample exhibited velocity-weakening at low effective pressure and changed to strengthening with increasing effective normal stress except those at 200ºC which remain negative under almost all pressure conditions. My results suggest that earthquakes can nucleate in blueschists at depths within a temperature range of 100-300ºC, which including the temperature of the hypocenter area of the 2011 Tohoku-oki earthquake, or/and at low effective pressure.

5.1 Introduction

Various and complicated slip behavior occurred during the 2011 Tohoku-Oki earthquake (e.g. Ammon et al., 2011; Ide et al., 2011; Lay et al., 2011). The rupture was composed of an initial phase, deep rupture, following propagation towards shallow portion and continuing deep rupture. And an unexpected large coseismic slip occurred on the shallow part of the megathrust fault, which the estimated displacement is more

than 50 m toward the trench, and resulted in destructive tsunamis (Fujiwara et al., 2011; Ito et al., 2011; Lay et al., 2011).

Frictional property of rocks composed of a subducting oceanic plate is one of factors for controlling the diverse slip behaviors from aseismic to seismogenic slip at the Japan Trench. Recently some studies have investigated the frictional properties on the clay-rich sediments collected from the Japan Trench under coseismic slip rate in order to understand the rupture processes and mechanism of large slip. From the previous studies, it revealed that the frictional strength of the clay-rich sediments at the Japan Trench is quite low over a wide range of slip rate (Ujiie et al., 2013; Sawai et al., 2014) and the fracture energy during coseismic slip is extremely low (Sawai et al., 2014). These studies provide information on the frictional property of plate boundary fault during the earthquake and critical data to discuss the possible mechanism of the huge slip. On the other hand, to understand a nucleation mechanism of the earthquakes, friction experiments under in-situ conditions using realistic metamorphic rocks in the Tohoku subduction zone are needed.

Frictional data of such a metamorphic/metapelitic rocks under high temperature and pressure conditions to model such subduction earthquakes are quite limited, except for that of serpentine (Moore et al., 1997; Takahashi et al., 2011) and clay minerals (den Hartog et al., 2012a, 2012b, 2013). In widely accepted earthquake models of a subduction zone (e.g. Scholz, 1998), a seismogenic zone defines as that the rate-depend parameter becomes negative value at a temperature range of 100-300ºC. However, this model is based on the experimental results on granite which does not exist at subduction zones (Blanpied et al., 1995). Frictional properties of gabbro (He et al., 2007) or halite (Shimamoto, 1986) are also widely used in a number of numerical simulations, although such materials are likely to be poorly representative of the rocks expected to be present in subduction zone. The hypocenter of the 2011 Tohoku-Oki earthquake is located on the subducting plate boundary at a depth of about 24 km (Figure 5.1a) and temperature of this area is estimated about 160ºC (Kimura et al., 2012). From the P-T phase diagram, these input materials imply there should be a blueschist in the hypocenter area (Figure 5.1b). In chapter 4, I presented preliminary data on the frictional behavior of blueschist

focused on the effective normal stress dependence. Here, I report experiments in detail including new data, it may be necessary to establish new initiation model of subduction earthquakes, and discuss a possible initiation mechanism of the 2011 Tohoku-oki earthquake based on its properties.

5.2 Experimental methods

5.2.1 Starting material

The sample tested in this study is a lawsonite-blueschist rock from Franciscan Belt, California. The blueschist was crushed by hand and sieved to a grain size below 125 μm in order to prepare simulated gouges for the experiments. XRD analysis and microstructure analysis showed the presence of glaucophane, lawsonite, titanite, pyrite, garnet and chlorite.

5.2.2 Friction experiments

Friction experiments were conducted using the hydrothermal ring shear machine at Utrecht University (described in detail by Niemeijer et al., 2008 and den Hartog et al., 2012a). 0.58 g of the simulated fault gouges were contained between two roughened opposing superalloy pistons, which thickness prior to loading is ~1.0 mm (Figure 5.2). Total shear displacement was approximately 30 mm and final thickness after the experiments became about 0.6-0.8 mm. The gouge sample is kept in place by inner and outer confining rings of stainless steel, with an inner radius of 11 mm and an outer radius of 14 mm. The confining rings were coated with Molykote spray to reduce wall friction before assembly. The piston–sample assembly is located inside an internally heated pressure vessel. Pressure vessel is positioned in an Instron 1362 loading frame and normal stress is given by the Instron loading ram. Fluid pressure is applied to the water in the pressure vessel using a manually driven pump. A servo-controlled motor and gearbox rotate the entire vessel and shear stress (τ) during a run is measured externally using the torque gauge couple mounted on the upper forcing block.

Blueschist samples were sheared at temperatures (T) of 22-400^{o}C, effective normal stresses (σ_n^{eff}) of 25-200 MPa and pore fluid pressures (P_f) of 25-200 MPa. I

conducted pressure-stepping experiments at constant Temperature, with effective normal stress set equal to the pore fluid pressure ($\sigma_n^{eff} = P_f$, $\lambda = (P_f / \sigma_n) = 0.5$). The apparent friction coefficient μ was calculated as $\mu = \tau / \sigma_n^{eff}$. The velocity ($V$) was increased stepwise by one order of magnitude in the range 0.1-100 μm/s.

I modeled data from present experiments using the rate and state dependent friction (RSF) model ("Dieterich law"; Dieterich, 1978, 1979; Ruina, 1983):

$$\mu = \mu_0 + aln\left(\frac{V}{V_0}\right) + bln\left(\frac{V_0\theta}{D_c}\right) \tag{4.1}$$

$$\frac{d\theta}{dt} = 1 - \frac{V\theta}{D_c} \tag{4.2}$$

where μ_0 is a reference friction coefficient at a reference velocity V_0. θ is a state variable and D_c is a characteristic distance. a is a direct effect, which represents an instantaneous response resulting from a stepwise change in velocity. b reflects the a decay in the friction to a new steady-state, called an evolutionary effect. I quantify the frictional stability using the parameter (a-b), which given by equation (4.1) and (4.2):

$$(a - b) = \frac{\Delta\mu_{ss}}{\Delta \ln(V/V_0)} \tag{4.3}$$

(e.g. Marone, 1998; Scholz, 1998). $\Delta\mu_{ss}$ is the change in steady-state friction coefficient when slip velocity changes from V_0 to V. Positive values of (a-b) mean that friction increases with increasing slip velocity, i.e. velocity-strengthening, and negative ones signify velocity-weakening. I conducted velocity-stepping sequences to determine the constitutive parameters (a-b), a, b and D_c, and investigated how this parameter changed with temperature and effective pressure.

5.3 Results

5.3.1 Mechanical data

Table 5.1 lists each experiment and the corresponding experimental conditions. The samples were first sheared through an initial displacement of approximately 10 mm or 3 mm before the velocity-stepping at each P-T condition. Friction coefficient (μ) as a function of displacement is shown in Figure 5.3 ($\sigma_n^{eff} = P_f$ = 50 MPa) and figure 5.4 ($\sigma_n^{eff} = P_f$ = 200 MPa) for representative experiments. The average of friction at each temperature is μ = 0.65-0.75. The samples exhibit unstable, oscillatory (stick-slip) behavior only at 200ºC and 300ºC (Figure 5.3d, e and Figure 5.4c, d). There may be a tendency that the level of friction become to decrease at 300-400ºC.

The velocity dependence of μ, described as (*a*-*b*), is shown in Figure 5.6, 5.7a-c and 4.8a-c, which illustrate the effect of temperature (Figure 5.6 and 5.7a-c) and effective normal stress (Figure 5.8a-c). I can see the systematic influences of temperature (Figure 5.6 and 5.7a-c). At 22ºC, the gouges show positive (*a*-*b*) values which decrease to become negative with increasing temperature. At 200ºC, the behavior is velocity-weakening and shows negative (*a*-*b*) values. At 300ºC, slip is velocity-weakening (negative (*a*-*b*) value) at low effective pressure but strengthening at high effective pressure, showing larger (*a*-*b*) values than at 200 ºC. (*a*-*b*) values slightly decrease at 400ºC. There is also effective normal stress dependence: (*a*-*b*) values are negative at low effective pressure and increase to positive with increasing effective normal stress, although the values of (*a*-*b*) at 200ºC remain negative under almost all pressure conditions.

Examples of frictional data and corresponding modeling results are shown in Figure 5.5. Rate and state friction law gives good fits to my experimental data. Friction parameters *a*, *b* and D_c are complex, which reflected the variation of temperature and effective normal stress. These values are plotted against temperature in Figure 5.7d-i. The parameter *a* seems to decrease with decreasing (*a*-*b*) and increase with increasing (*a*-*b*): *a* decrease with elevating temperature up to 200ºC, increase at 300ºC and decrease again at 400ºC. The values of b are roughly constant at low temperature (<200ºC), however at 300 ºC and 400 ºC, it becomes to be negative and to show an opposite trend to that of (*a*-*b*). D_c looks like it match the behavior of (*a*-*b*) for lower

up-step velocities (1 mm/s and 10 mm/s), although it show little effect of temperature.

Figure 5.8d-i show the same friction parameter a, b and D_c plotted against effective normal stress. Values of b decrease systematically with increasing the effective normal stress, while a and D_c is insensitive to effective normal stress.

5.3.2 Microstructual observations

Figure 5.9 shows an experimental sample after sheared at 200°C and constant velocity of 100 μm/s. At this temperature, (a-b) is negative. There is an extremely sharp localized boundary slip zone – or y-shear. The bulk gouge shows only a weak foliation and a granular cataclastic microstructure. The microstructure developed after shearing at 200°C shows a grain size reduction. On the other hand, the microstructure sheared at 300°C displays a quite different structure (Figure 5.10). The sample after deformation at 1 μm/s doesn't show strong reduction of grain size, occurring only at shear localized zone (Figure 5.10a-c). In the localized zone, lawsonite and pyrite grains are elongated strongly (Figure 5.10b, c) and glaucophane composed matrix area shows finer. In the microstructure tested at 300°C and 100 μm/s, the bulk gouge forms a foliation and lawsonite and titanite shows S-shaped structures (Figure 5.10d, e). R-shears in the samples sheared at 300°C are much more apparent than at lower temperature.

5.4 Discussion

5.4.1 Trends of the constitutive parameter

Comparison of the friction parameters on temperature and effective normal stress shows some relationship to the fault stability (a-b). First, for the temperature, the constitutive parameter a depends on temperature and parameter b also shows temperature dependence at high temperature regime. I can suggest that negative (a-b) at 200°C strongly reflect the values of a approaching ~0, while positive values of (a-b) at 300°C is attributed to not only the parameter a but also the negative values of b. For effective normal stress, constitutive parameter b decreases with increasing effective normal stress although the magnitude of a is approximately independent. It implies that the velocity dependence of (a-b) results from negative rate dependence of b. As a

function of both temperature and effective normal stress, the parameter D_c shows similar behavior of (a-b) at slip velocities < 0.01 μm/s, whereas for slip velocity 100 μm/s D_c is independent. It is very difficult to interpret, but at least there may be some relationship among temperature, effective normal stress and D_c.

5.4.2 Key minerals

Microstructures of blueschist samples sheared at 200°C and 300°C is quite different. The fracturing and grain size reduction are promoted in the sample deformed at 200°C, but grains still bigger a bit than that sheared at 200°C. There is a possibility that I get some more ductile deformation already at 300°C, which enough to stop grain breaking. In all textures, it is common that glaucophane has composed a matrix portion and other minerals have displayed unique structures (e.g. elongated shapes of pyrite, lawsonite and titanite). I considered two minerals as a key mineral, lawsonite and titanite, because pyrite has shown similar stretched structures at both temperature conditions. Lawsonite is a metamorphic mineral and commonly associated with glaucophane. It is a hydrous mineral, including a H_2O content of approximately 11.5 wt.%. Newton and Kennedy (1963) determined the equilibrium curve experimentally and indicated that an invariant point involving the phase lawsonite-zoisite-anorthite-sillimanite-quartz-vapor is at 540 MPa and 410°C. This property may contribute to the behavior of the friction parameter (a-b) at 400°C. Newton and Kennedy (1963) also mentioned that lawsonite is likely to be replaced by a zeolite at pressure < 300 MPa and temperature <350°C. I cannot deny the possibility that this feature results in the frictional behavior at 300°C, although I cannot detect any of reactions in the microstructures. The second considerable mineral, titanite, is an accessory mineral in igneous rocks and common in schists. In comparison to lawsonite, it is less content of H2O (approximately 1 wt.%) and doesn't react under the experimental conditions. Thus lawsonite probably play a key role in the frictional properties of blueschist.

5.4.3 Implications for nucleation of the 2011 Tohoku-oki earthquake

Subduction megathrust faults generate earthquakes at limited depth range where the temperature reaches between ~100-150°C and ~350°C (Hyndman et al., 1997). As already indicated, blueschist gouge shows temperature dependence: it shows velocity-weakening or potentially unstable at depths within a temperature range of 100-300ºC. Similar frictional behavior has reported on granite (Blanpied et al., 1991; 1995; 1998), gabbro (He et al., 2007), San Andreas Fault gouge which composed of illite-smectite-quartz gouge (Tembe et al., 2009) and illite-quartz and musucovite-quartz gouge (Den Hartog 2012a, 2013). The temperature range of velocity-weakening of blueschist is roughly the same temperature regime for granite (100-350ºC) and gabbro (200-300ºC), but shifted towards lower temperature compared with that of San Andreas Fault gouge (250-350ºC), illite-quartz gouge (250-400ºC) and musucovite-quartz gouge (350-500ºC). The temperature at the hypocenter of the 2011 Tohoku-oki earthquake is estimated at about 160ºC (Kimura et al., 2012), which is in agreement with my experimental results: blueschist shows unstable slip at this temperature. Thus the property of simulated blueschist fault rock may be a possible factor causing the 2011 Tohoku-oki earthquake. In addition, (*a*-*b*) also has a tendency to become negative with decreasing effective pressure even at stable-temperature conditions. This implies that earthquakes can nucleate in blueschist at low effective pressure (less than about 75 MPa) because of the high pore fluid pressure.

The down-dip seismogenic limit at ~350°C is widely believed to be corresponded to the transition from brittle to ductile behavior with increasing temperature (e.g. Hyndman and Wang, 1993; Hyndman et al., 1997; Scholz, 1998). Tohoku subduction zone is cold and old one, and the fore-arc mantle is reached by the thrust shallower than the 350°C temperature and probably aseismic. Some studies have explained this by stable-sliding of serpentinite produced by the dehydration of the hydrous minerals in the crust (e.g. Hyndman et al., 1997; Hyndman and Peacock, 2003). However blueschist may also be able to explain this situation because it shows velocity-strengthening around 300ºC (i.e., less than 350ºC).

5.5 Conclusions

A series of rotary shear friction experiments was conducted on the blueschist powder in order to understand the earthquake nucleation mechanisms within the Tohoku subduction zone. The main results of my study are as follows:

1. Simulated blueschist fault gouge shows the potential for unstable slip at around 200ºC. This frictional behavior depended on temperature results from the changes in friction parameter *a* and negative *b* at high temperature. It suggests that earthquakes can nucleate in blueschists at depths within a temperature range of 100-300ºC, including the hypocentral temperature regime of the 2011 Tohoku-oki earthquake.
2. Simulated blueschist fault gouge shows essentially unstable slip at low effective normal stress even at stable temperature conditions. This property corresponds to negative rate dependence of constitutive parameter *b*. It suggests that low effective pressure is a possible factor causing the earthquake or nucleation of earthquakes ceases at high effective pressure area.
3. SEM observations of the experimental samples revealed the key minerals during the deformations. Blueschist sample is characterized by the elongated or/and S-shaped structures of lawsonite, titanite and pyrite at 200ºC and 300ºC. Lawsonite is probably critical mineral attributed to the frictional properties of blueschist because of its high content of water and the P-T conditions allowed to occur some reactions.

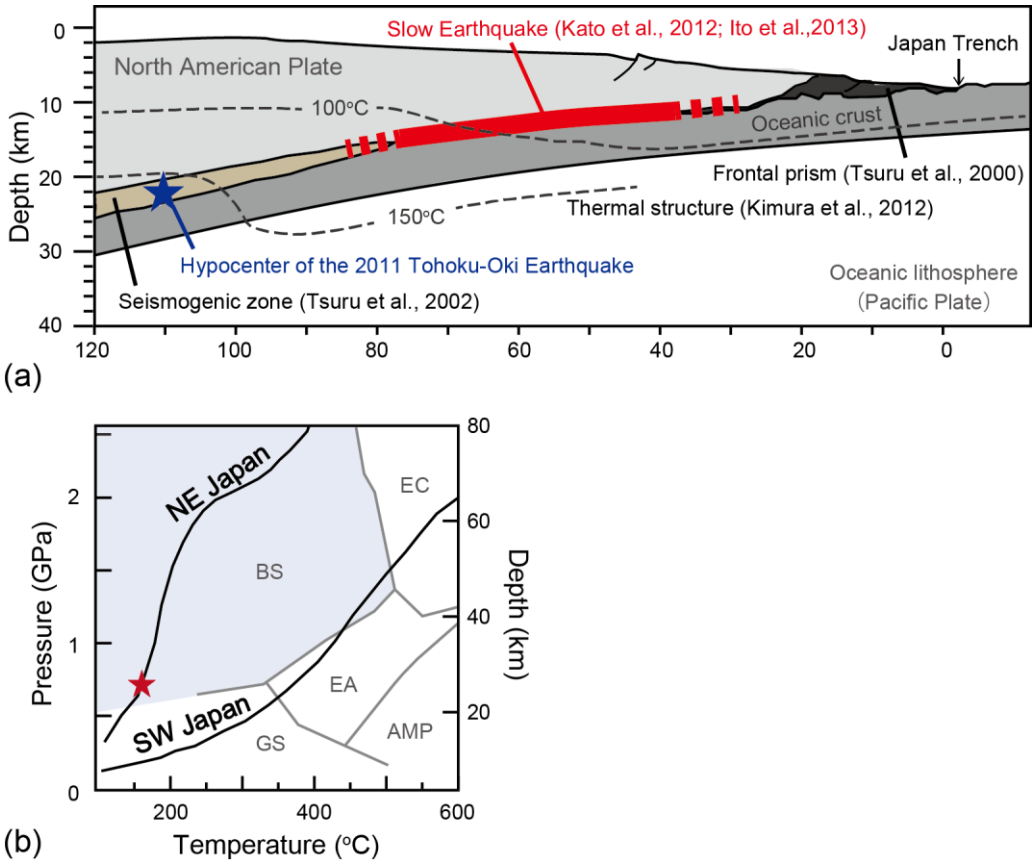

Figure 5.1

(a) A schematic illustration of Tohoku subduction zone (modified from von Huene et al., 1982; Tsuru et al., 2000, 2002) and the thermal structure (from Kimura et al., 2012) (after Chapter 3). Blue star indicate the hypocenter of the 2011 Tohoku-oki earthquake. (b) Metamorphic conditions in subducting oceanic crust (from Evans, 1990; Oh and Liou, 1998; Maruyama and Okamoto, 2007) (after Chapter 4). Black lines indicate the geothermal gradients of the present subduction zone in NE Japan and that in SW Japan, respectively (Peacock and Wang, 1999). The hypocentral P-T conditions of the 2011 Tohoku-oki earthquake are plotted as a red star. BS = blueschist, EC = Eclogite, GS = greenschist, EA = epidote amphibolite, AMP = amphibolite, GR = Granulite

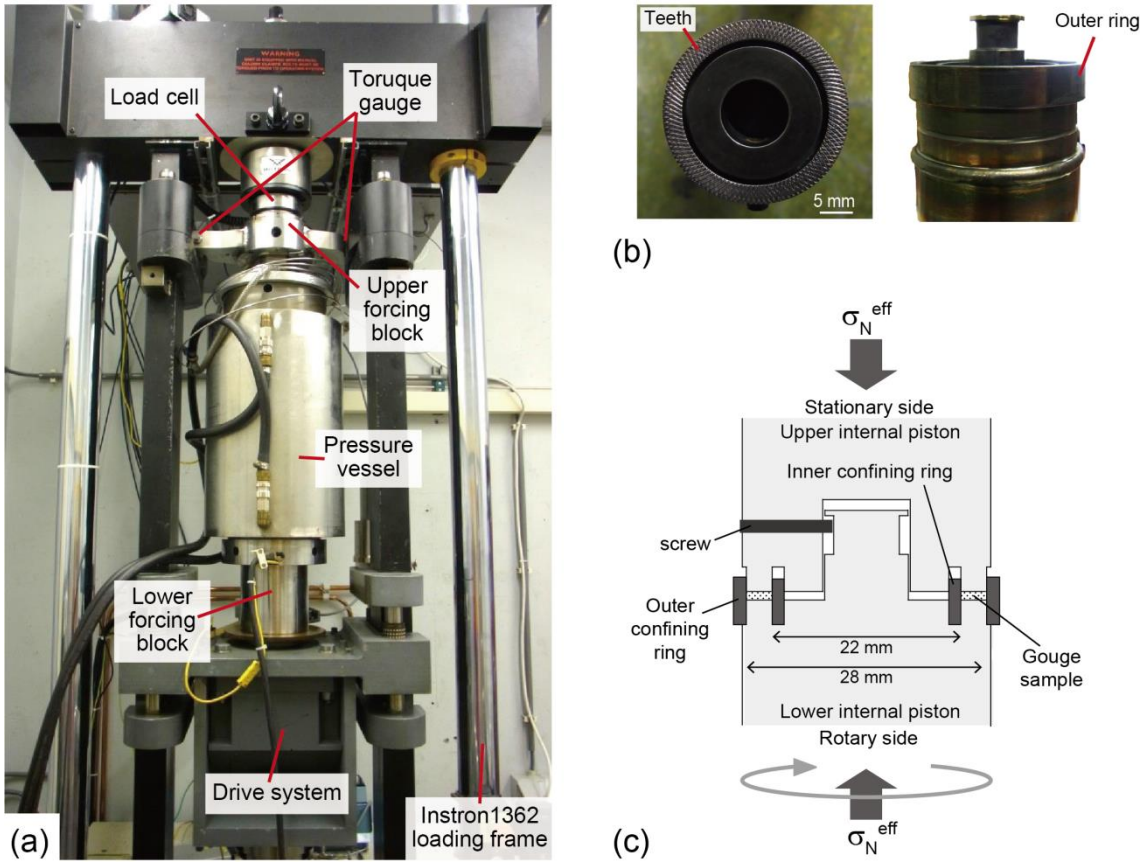

Figure 5.2

Photographs of (a) hydrothermal ring shear apparatus used in this study, and (b) the two internal pistons (after Chapter 3). (c) Schematic cross-sections of the sample assembly. σ_n^{eff} is the effective normal stress (after Niemeijer et al., 2008; den Hartog et al., 2012a).

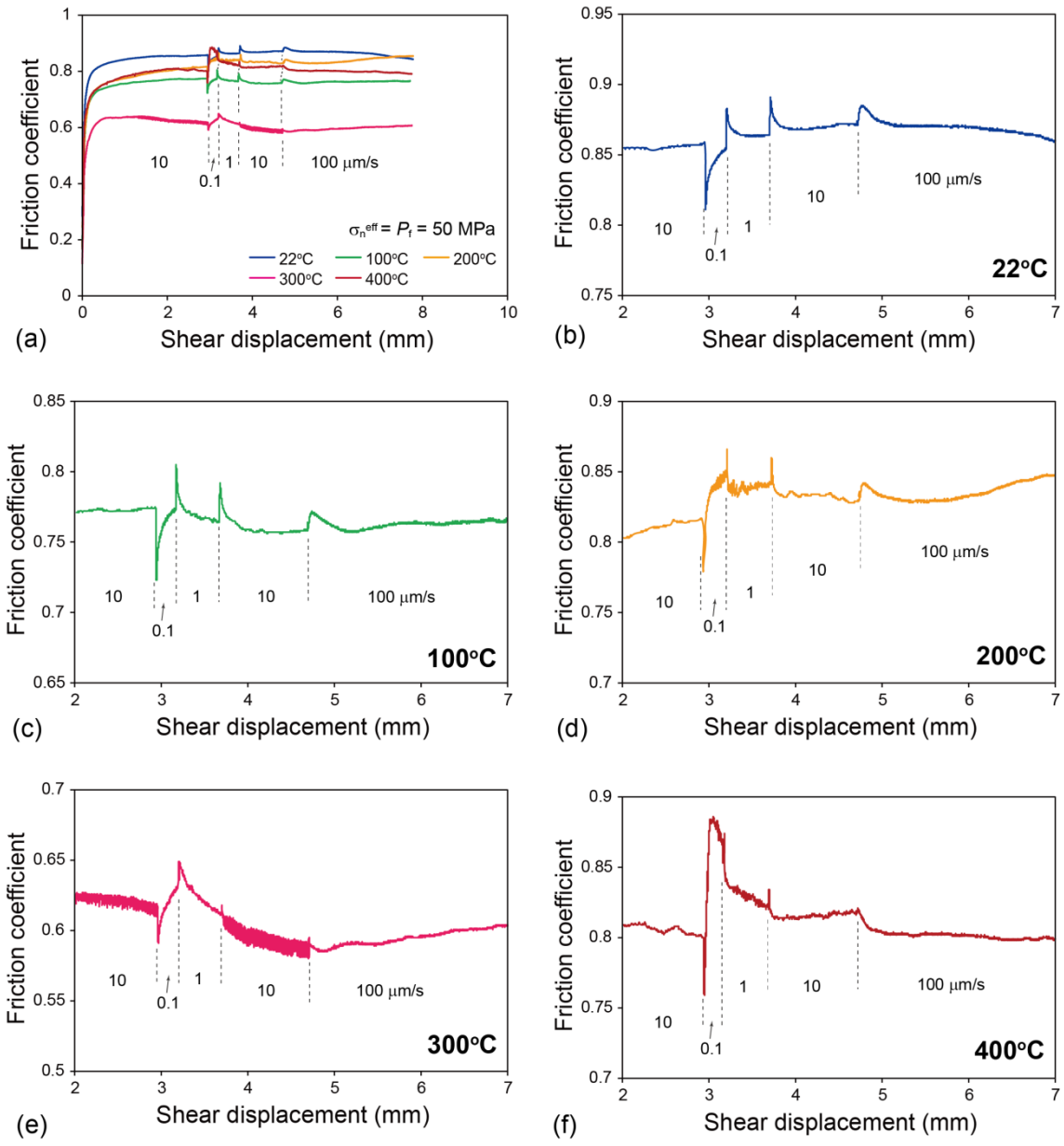

Figure 5.3

Representative frictional behavior of blueschist powder under a constant effective normal stress and pore fluid pressure of 50 MPa. (a) Friction coefficient versus displacement curves at slip velocities of 0.1-100 μm/s, (b-f) Enlarged figures of velocity steps at each temperature. All velocity steps are shown in μm/s. Friction curves of (b-f) are plotted at the same scale. Blue = 22ºC, Green = 100 ºC, Yellow = 200 ºC, Pink = 300 ºC, Red = 400 ºC

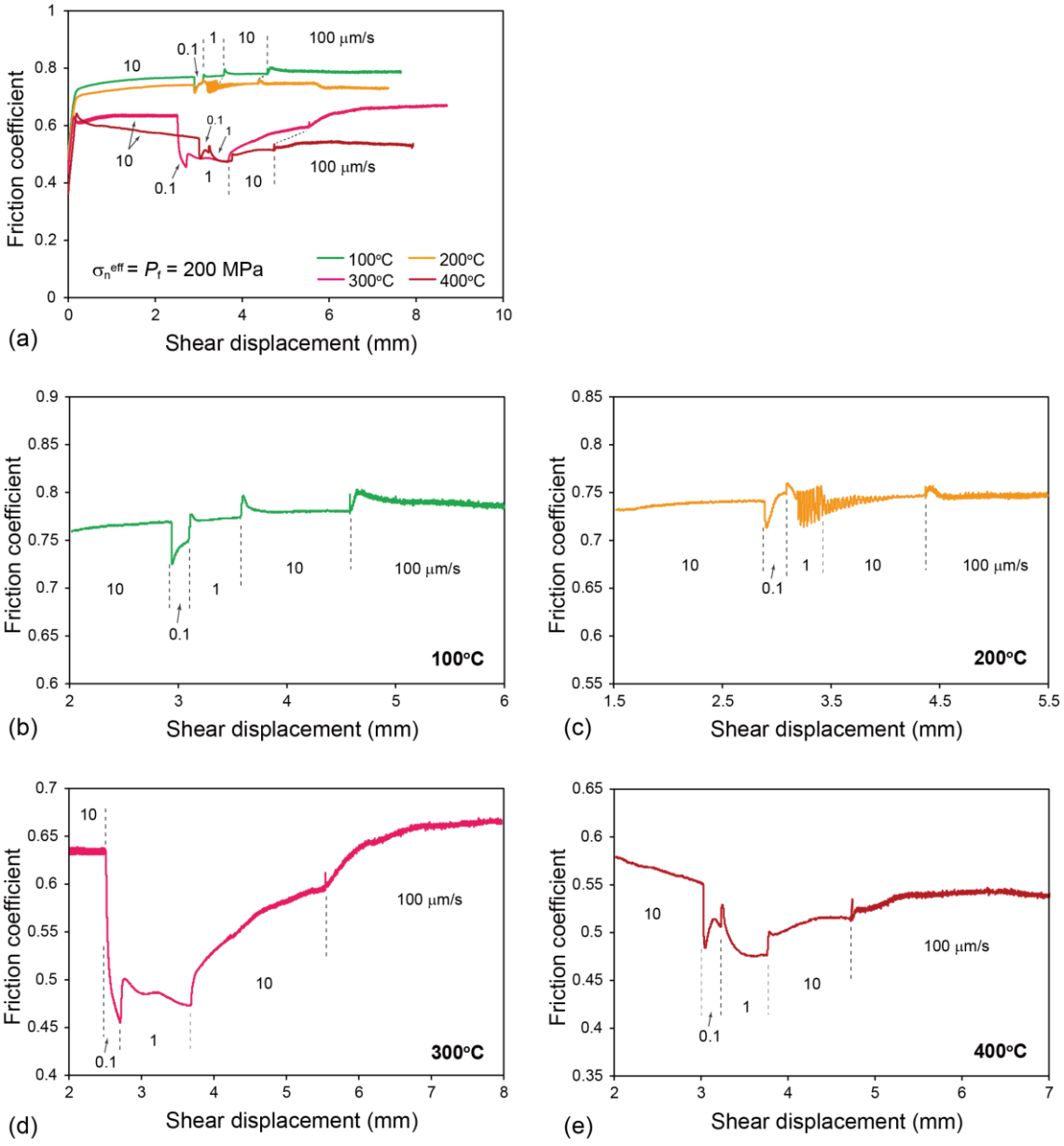

Figure 5.4

Typical evolution of friction coefficient with shear displacement under a constant effective normal stress and pore fluid pressure of 200 MPa. (a) Effect of temperature on friction coefficient, (b-e) Detailed view of velocity steps at each temperature. Scales of y-axis in (b-e) are the same. Blue = 22ºC, Green = 100 ºC, Yellow = 200 ºC, Pink = 300 ºC, Red = 400 ºC

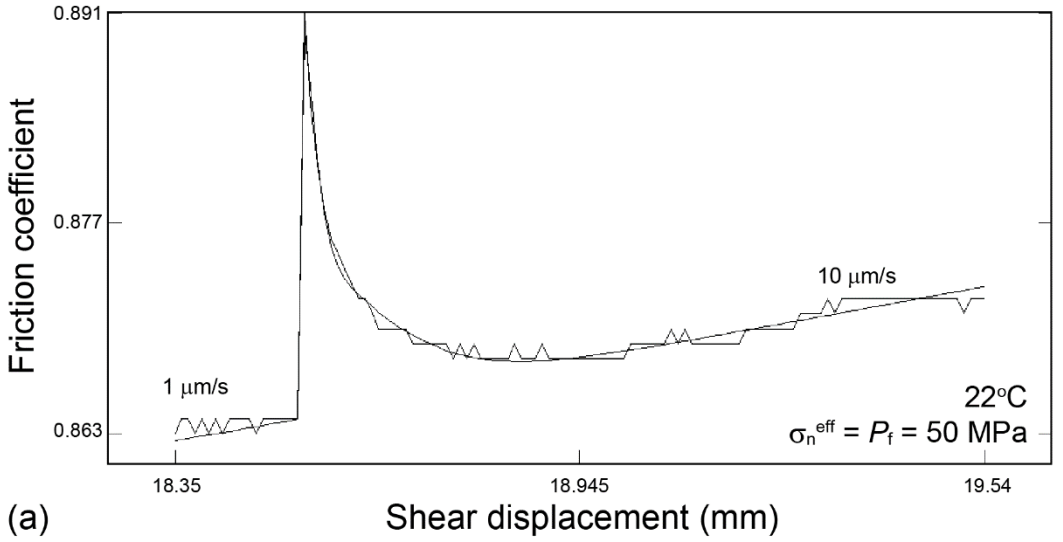

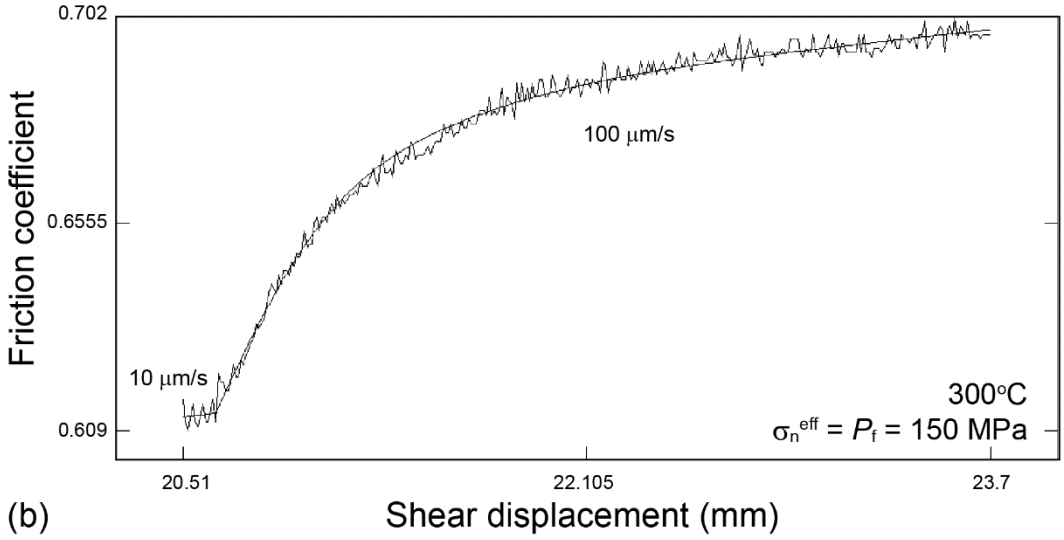

Figure 5.5

Examples of modeling results for constitutive parameter in this study.

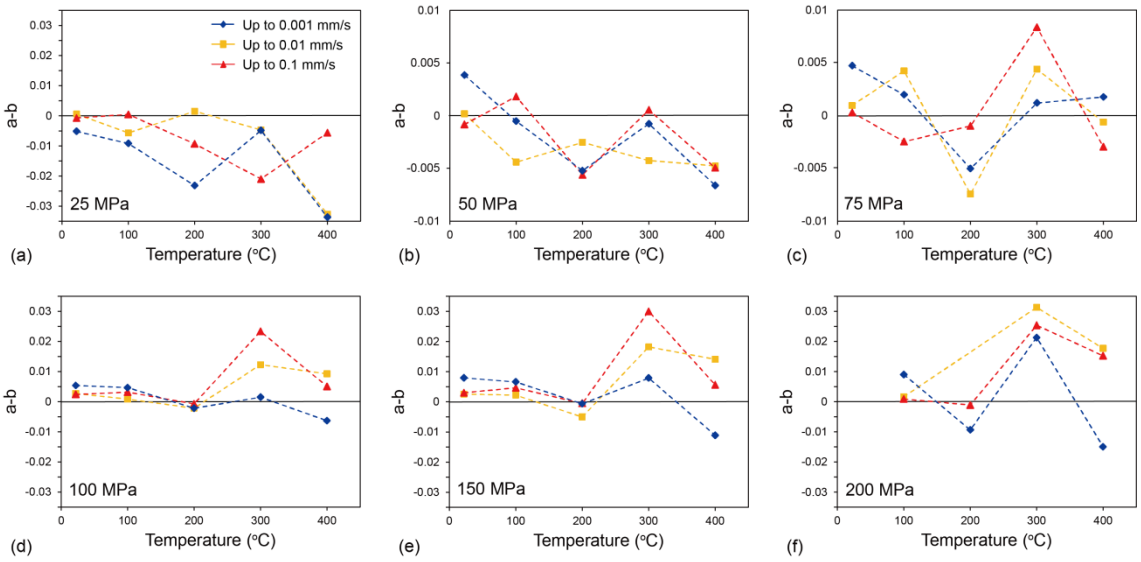

Figure 5.6

Frictional velocity dependence for blueschist as a function of temperature; $\sigma_n^{eff} = P_f =$ (a) 25 MPa, (b) 50 MPa, (c) 75 MPa, (d) 100 MPa, (e) 150 MPa and (f) 200 MPa. Note that σ_n^{eff} is the effective normal stress, P_f is pore fluid pressure

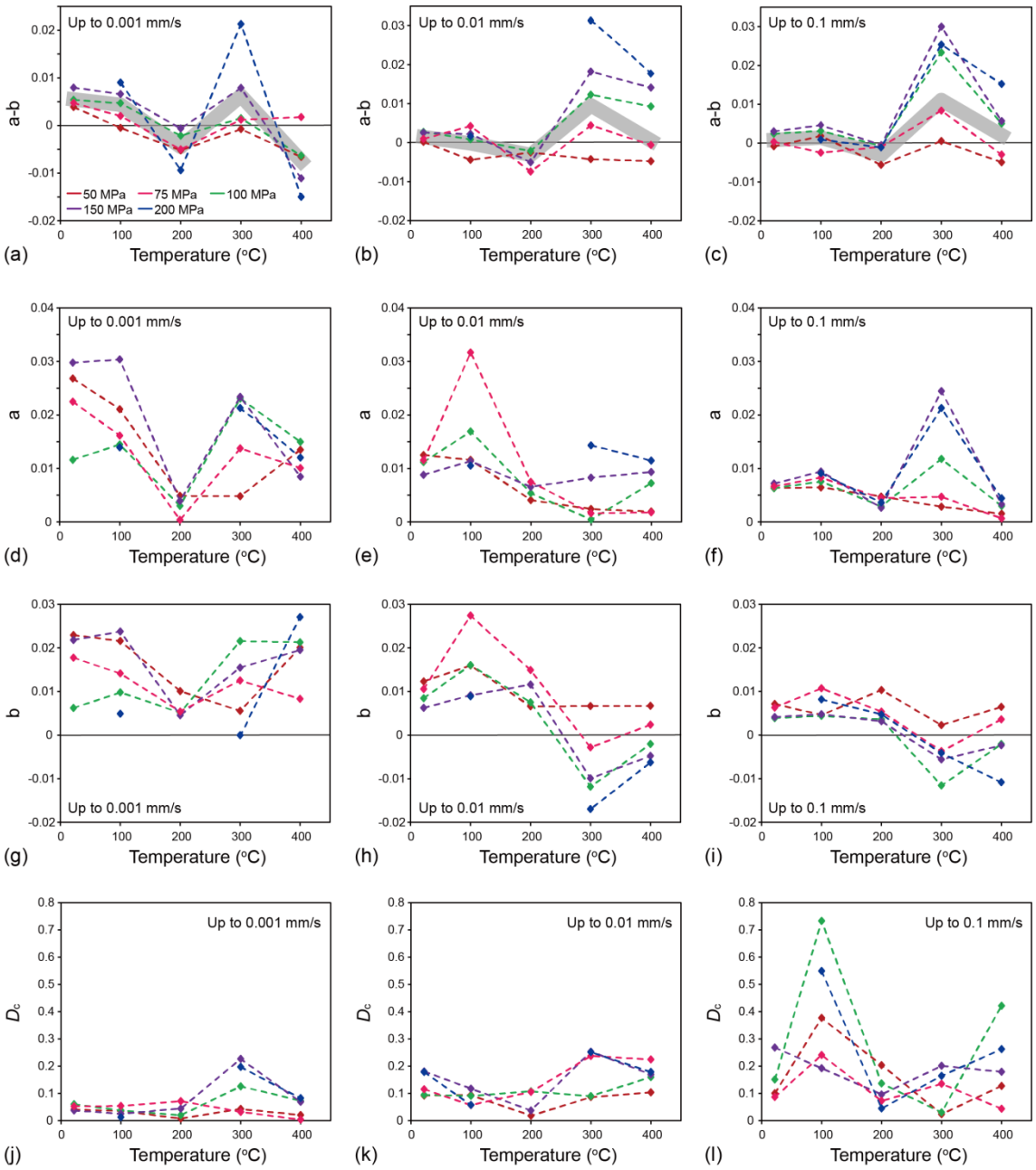

Figure 5.7

Rate and state friction parameters plotted against temperature. (a), (d), (g) and (j) are parameter (*a*-*b*), *a*, *b* and D_c, respectively, at post-slip-velocity of 1.0 μm/s. (b), (e), (h) and (k) are parameter (*a*-*b*), *a*, *b* and D_c, respectively, at post-slip velocity of 10 μm/s. (c), (f), (i) and (l) are parameter (*a*-*b*), *a*, *b* and D_c, respectively, at post-slip velocity of 100 μm/s. Gray line in (a-c) show the mean data values for each temperature condition. All data in these plots is under $\sigma_n^{eff} = P_f$ conditions; Red is at 50 MPa, Pink is at 75 MPa,

Green is at 100 MPa, Purple is at 150 MPa, and Blue is at 200 MPa. Note that σ_n^{eff} is the effective normal stress, P_f is pore fluid pressure.

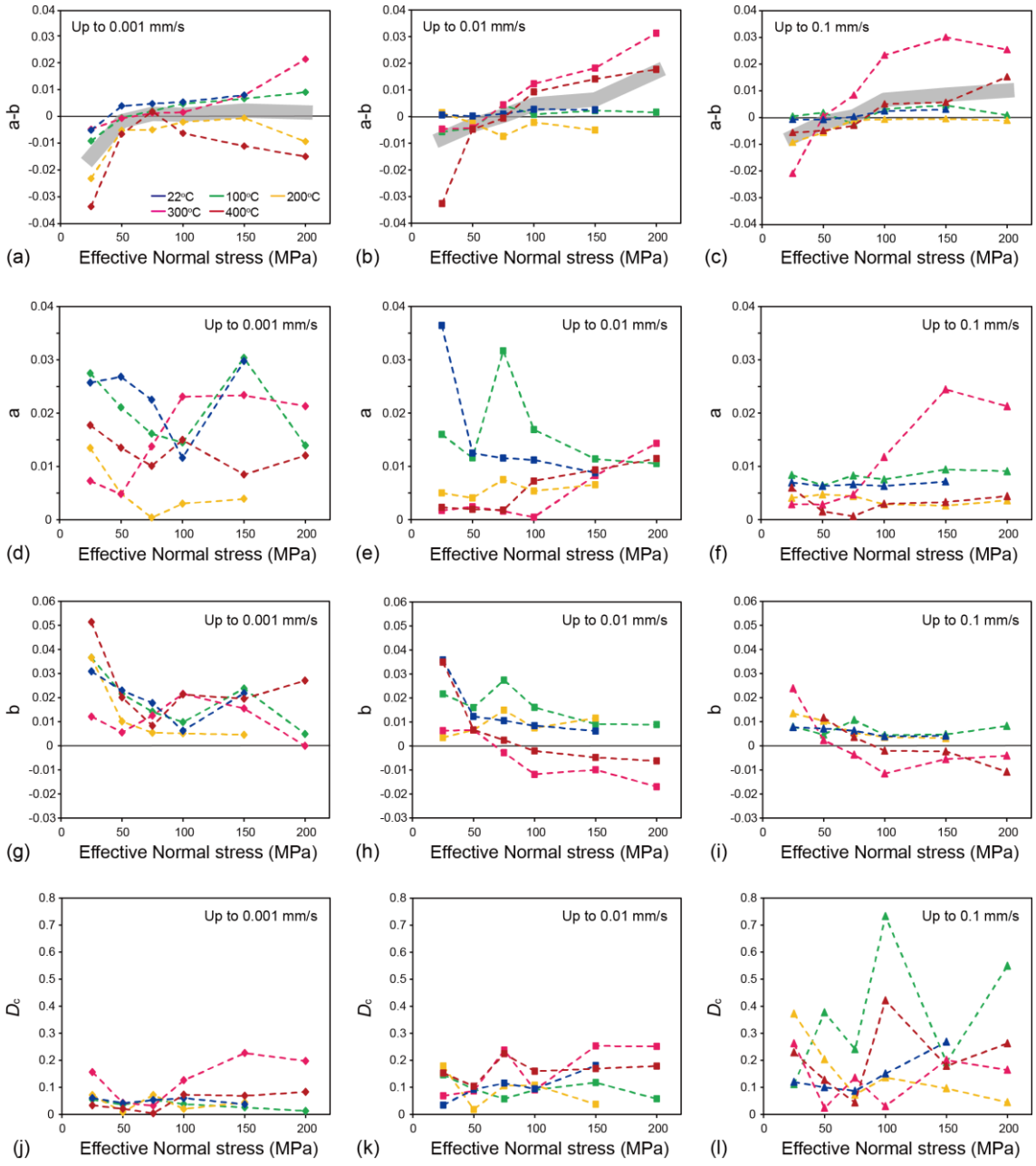

Figure 5.8

Constitutive parameters plotted against effective normal stress (σ_n^{eff}). Gray line in (a-c) designate the avarage values of (a-b) at each σ_n^{eff} condition. (a, b, c) (a-b) at post-slip-velocity of 1.0, 10 and 100 μm/s, respectively. (d, e, f) a at post-slip-velocity of 1.0, 10, 100 μm/s, respectively. (g, h, i) b at post-slip-velocity of 0.1, 10, 100 μm/s, respectively. (j, k, l) D_c at post-slip-velocity of 1.0, 10, 100 μm/s, respectively. Note that in all figures blue symbols and line show the result at 22°C, those of green are at 100°C,

yellow is at 200ºC, pink is at 300ºC and red is 400ºC.

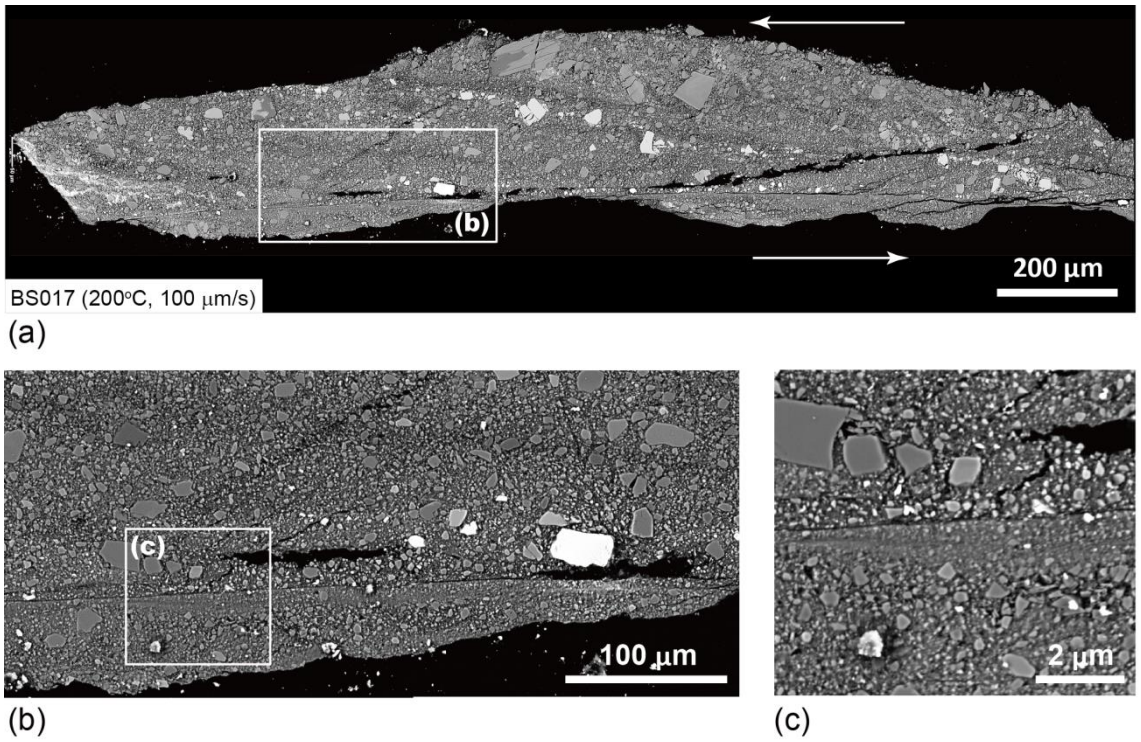

Figure 5.9

SEM photomicrographs of experimental samples after sheared at T = 200°C, V= 100 μm/s and $\sigma_n^{eff} = P_f$ = 75MPa. (a) Microstructure of blueschist after experiment. (b) and (c) are close-up of the frame portion in (a) and (b), respectively.

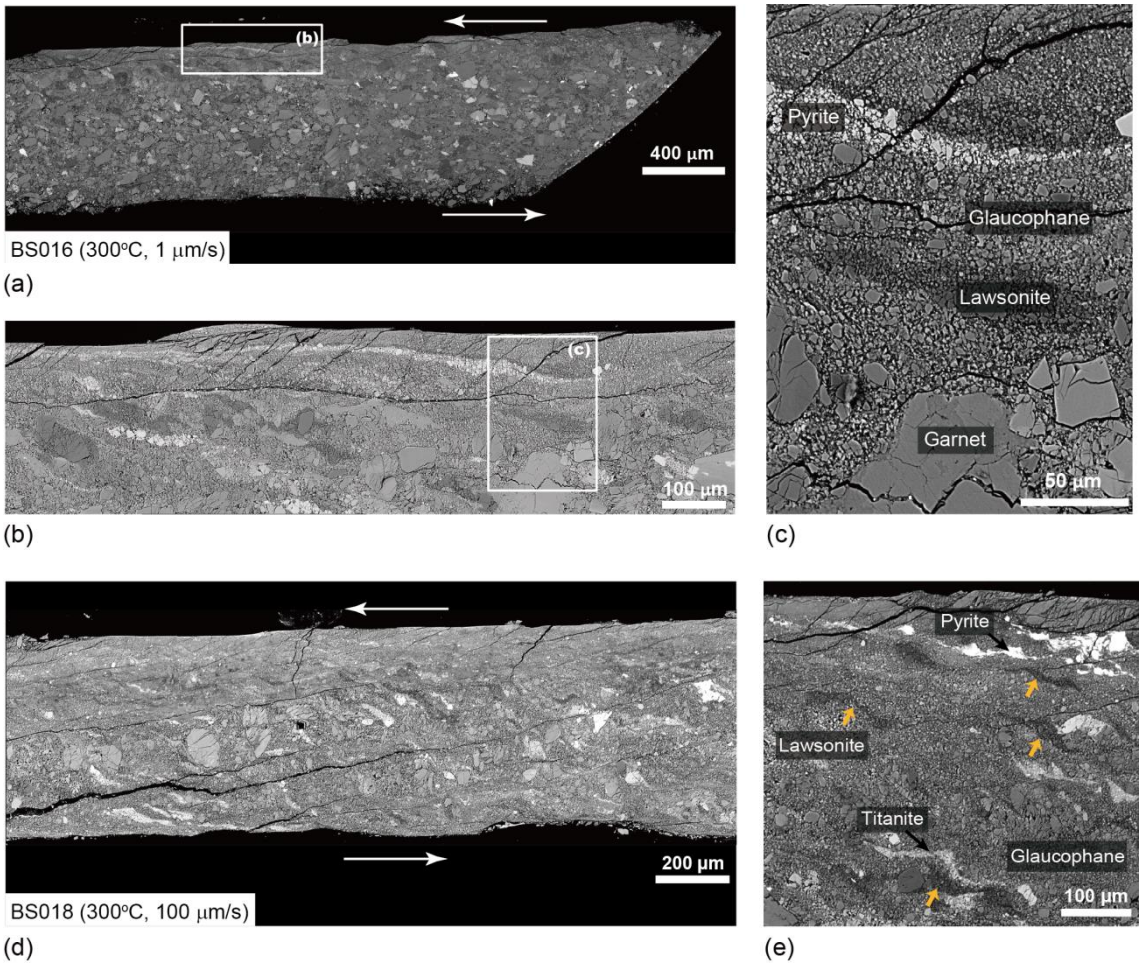

Figure 5.10

Blueschist samples deformed at T = 300°C, $\sigma_n^{eff} = P_f$ = 75MPa. (a-c) Sheared at V = 1 μm/s. (b) and (c) are close-up of the frame portion in (a) and (b), respectively. (d,e) Sheared at V = 100 μm/s. The unique features described in the manuscript are highlighted with yellow allow in (e).

Table 5.1 List of experimental conditions in this study.

Experimental number	Temperature (°C)	σ_n^{eff} stepping sequence (MPa)	P_f stepping sequence (MPa)	V-stepping sequence (μm/s)	Total shear displacement (mm)	Final gouge thickness (mm)	Occurrence of stick-slip or oscillation
BS 001	200	25-50-75	25-50-75	10-0.1-1.0-10-100	30.43	0.81	at (50MPa - 0.1, 1 μm/s), (75MPa – 1, 10 μm/s)
BS 002	300	25-50-75	25-50-75	10-0.1-1.0-10-100	30.07	0.83	at (25 MPa - 10 μm/s), (50 MPa - 10 μm/s), (75 MPa - 10 μm/s)
BS 003	100	25-50-75	25-50-75	10-0.1-1.0-10-100	30.05	0.63	–
BS 004	400	25-50-75	25-50-75	10-0.1-1.0-10-100	30.18	0.68	–
BS 006	23	25-50-75	25-50-75	10-0.1-1.0-10-100	30.43	0.73	–
BS 010	22	100-150	100-150	10-0.1-1.0-10-100	22.22	0.68	–
BS 011	200	100-150-200	100-150-200	10-0.1-1.0-10-100	29.60	0.59	at (200 MPa - 1, 10 μm/s)
BS 013	100	100-150-200	100-150-200	10-0.1-1.0-10-100	29.87	0.66	–
BS 015	400	100-150-200	100-150-200	10-0.1-1.0-10-100	30.59	0.73	–
BS 016	300	75	75	1	14.39	0.89	–
BS 017	200	75	75	100	14.75	0.64	–
BS 018	300	75	75	100	14.83	0.57	–
BS 025	300	100-150-200	100-150-200	10-0.1-1.0-10-100	32.55	0.74	at (100 MPa - 10 μm/s), (150 MPa - 10 μm/s), (200 MPa - 10 μm/s)

Note that σ_n^{eff} is the effective normal stress, P_f is pore fluid pressure and V is slip velocity.

Chapter 6

Conclusions

Subduction megathrust earthquakes generate when unstable slip is nucleated in the seismogenic zone, and sometimes result in tsunami. Moreover slow earthquakes (e.g. slow slip events; low frequency earthquakes) occur near upper and lower limit of seismogenic zone. Indeed, in the Japan Trench the 2011 Tohoku-oki earthquake nucleated at 24 km depth along the plate boundary and produced huge slip on the shallow part of the megathrust fault, resulting in destructive tsunamis. Also episodic tremor and slow slip events occurred just before the 2011 Tohoku-oki earthquake at the depth less than 20 km in the Tohoku subduction zone. Frictional property of rocks composed of a subducting oceanic plate is one of factors for controlling the diverse slip behavior from aseismic to seismogenic slip at the Japan Trench. Many previous studies have focused on the frictional behavior of fault rocks to understand the stability of frictional sliding. However, almost all experiments have been conducted under limited experimental conditions (e.g. limit of temperature, pressure, and shear displacements) and almost no experiments have been performed on compositionally realistic materials under relevant in-situ conditions. I have believed that it is essential to reveal the frictional properties of such a realistic rocks to understand the mechanism of diverse seismic activities. In this thesis, I have reported the results of an experimental study aimed at determining the frictional behavior of materials expected to present in the Tohoku subduction zone under near in-situ P-T conditions, addressing low sliding velocities relevant to earthquake nucleation and slow slip events and high slip velocities associated with the rupture propagation during the earthquakes. The main conclusions of this thesis are summarized as follows:

1) A series of rotary shear friction experiments was performed on the pelagic sediments entering the Japan Trench in order to understand the rupture processes that caused the large slip during the Tohoku earthquake. My results indicated that incoming pelagic

sediments on the Pacific Plate collected from Site 436 of DSDP Leg 56 (Cores 38 and 40) show slip weakening behavior at coseismic slip velocities. However, at low velocities, there is a significant difference in the friction coefficient between the two cores. The steady-state friction coefficient of Core 38 has high values of approximately 0.5 at low velocities, but decreases to <0.1 as seismic slip velocity increases to 1.3 m/s. In contrast, the steady-state friction coefficient of Core 40 is remarkably low (<0.2) over a wide range of velocities (0.25 mm/s to 1.31 m/s).

SEM observations of the samples revealed different deformation processes in the fault zone. Core 40 is characterized by the preferred orientation of clay particles along distributed shear planes, resulting in the development of a scaly fabric, similar to that from the Tohoku plate boundary fault documented by IODP Expedition 343. In contrast, fracturing and subsequent shear-enhanced compaction appear to be the dominant deformation processes in Core 38. The difference in frictional properties between the two sediments can be attributed to a difference in smectite content that potentially controls deformation processes during fault zone shearing.

The specific fracture energy of the sediments during slip weakening at coseismic slip velocity ranges from 0.001 to 0.121 MJ/m^2. These values are lower by more than 2 orders of magnitude than those of previous experiments conducted under similar conditions on disaggregated sediments. These results suggest that the incoming pelagic sediments make it energetically easy for earthquake ruptures to propagate up-dip along the plate boundary and therefore led to the large near-trench slip during the Tohoku earthquake.

2) Rotary shear friction experiments was conducted on the blueschist powder in order to understand the generation mechanisms of slow slip events within the Tohoku subduction zone, especially to reveal the relationship between slow slip events and effective pressure. Simulated blueschist fault gouge become to show the velocity-weakening behavior when effective normal stress decreases. This behavior is

a critical data which supported a lot of previous numerical simulations, demonstrating the mechanisms of slow slip events. The frictional properties at low effective normal stress can explain the observed slow slip events at shallow portion, particularly the downdip limit of the slow slip events. Such frictional behavior suggests that low effective normal stress, i.e. high pore pressure, is an important factor to the generation mechanism of slow slip events.

3) Frictional properties on the blueschist powder were investigated systematically in order to understand the earthquake nucleation mechanisms within the Tohoku subduction zone. Simulated blueschist fault gouge shows the potential for unstable slip at around 200°C. This frictional behavior depended on temperature results from the changes in friction parameter *a* and negative *b* at high temperature. It suggests that earthquakes can nucleate in blueschists at depths within a temperature range of 100-300°C, including the hypocentral temperature regime of the 2011 Tohoku-oki earthquake. In addition, simulated blueschist fault gouge shows essentially unstable slip at low effective normal stress even at stable temperature conditions. This property corresponds to negative rate dependence of constitutive parameter *b*. It suggests that low effective pressure is a possible factor causing the earthquake or nucleation of earthquakes ceases at high effective pressure area.

SEM observations of the experimental samples revealed the key minerals during the deformations. Blueschist sample is characterized by the elongated or/and S-shaped structures of lawsonite, titanite and pyrite at 200°C and 300°C. Lawsonite is probably critical mineral attributed to the frictional properties of blueschist because of its high content of water and the P-T conditions allowed to occur some reactions.

4) To understand mechanisms of the slow slip events at the Japan Trench, frictional behavior on smectite-rich pelagic sediments retrieved from the plate-boundary thrust during IODP Expedition 343 was investigated using a rotary shear apparatus. At low temperatures of 20°C, the simulated gouges exhibit negative values of (*a*-*b*) at low

velocities, while these values becomes positive as increasing velocity to 100 μm/s. This frictional property may prevent further slip acceleration even if the slip begins, and could thus represent the upper limit of slow slip events at the shallow portion of the plate boundary. At temperatures of 50-100^{o}C, the gouges show nearly neutral or slightly negative values of (*a*-*b*). This frictional properties can yield slow slip events, which are considered to generate under the conditions where (*a*-*b*) is small negative values. The conditions met at temperatures of 50-100^{o}C in present experiments, that is consistent with temperature conditions where the slow slip events occurs along the plate boundary. At temperature of >150^{o}C those exhibit positive values of (*a*-*b*) under almost all velocity conditions tested. The transition in (*a*-*b*) value from neutral to positive occurs in the range between 100 to 150^{o}C. The downdip temperature limit of the slow slip events at Japan Trench seems to be at the same temperature range. Hence, frictional properties of the smectite-rich clay sediment could correspond to the observed downdip limit of the slow slip events.

Thus, the frictional properties on the pelagic sediments explain well the observed distributions of slow slip events along the plate boundary fault in the Tohoku subduction zone.

5) In almost all numerical models, a large slip-weakening distance and low effective stress are common factors to reproduce the slow slip events. I have reported the experimental results on smectite-rich pelagic sediments and blueschist, which exist at the Japan Trench. By comparing and combing the present results, I can extend the insight into the frictional properties of plate-boundary fault systematically. Summary of the friction I investigated under low effective pressure conditions agree very well with the observed slow slip events, reported by Ito et al. (2013), more than that under the high effective pressure conditions (Figure 6.1). My experimental results import that effective normal stress probably plays a key role in not only the nucleation mechanism of the earthquake but also that of slow slip events, which support the previous numerical models and observed events, and suggest the possibility that there are some slow slip events at deeper portion in the Tohoku subduction zone.

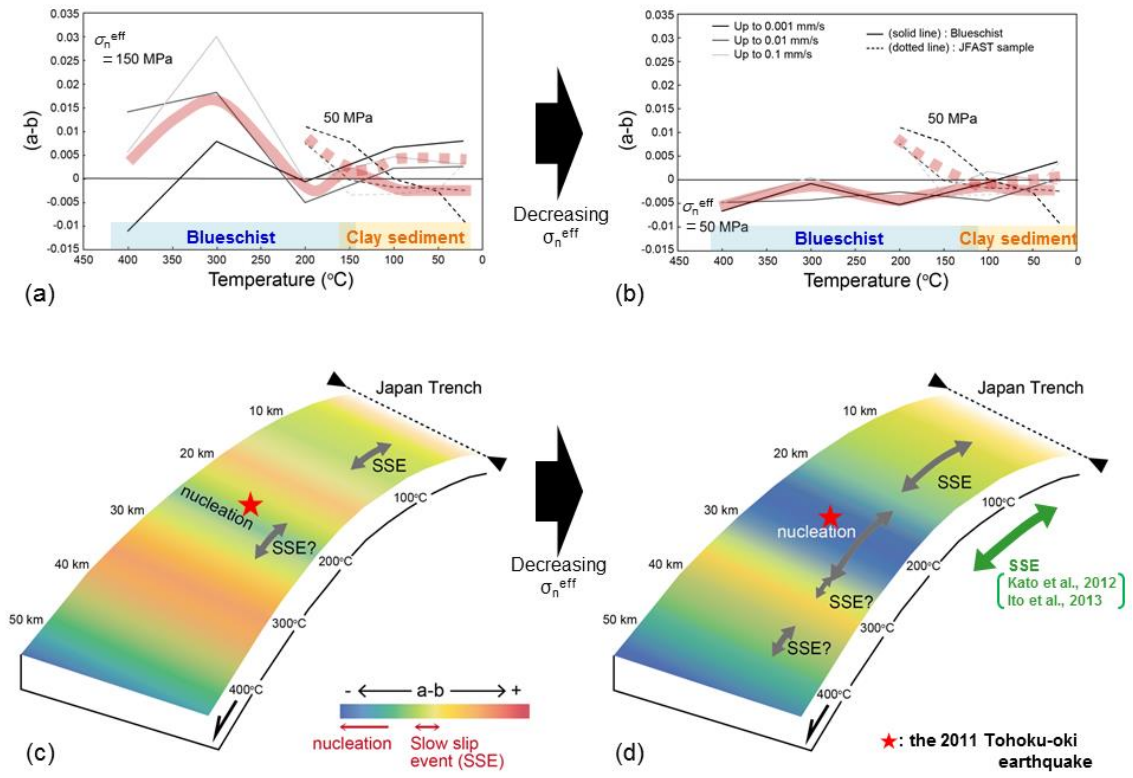

Figure 6.1

Summary of velocity dependence of friction at Tohoku subduction zone obtained in this thesis under (a, c) high effective pressure and (b, d) low effective pressure. (*a*-*b*) value showed the negative value indicate blue. The blue color gradually changes to red as the value of (*a*-*b*) become positive values. Slow slip events (SSE) occur at yellowish green area.

Acknowledgements

A lot of people have helped me to make this thesis. I would like to thank them for that.

I would like to express my sincere thanks to my promotor, Takehiro Hirose. It has been a pleasure to learn much from you and be supported by you. Discussions with you have been always useful and encourage me. You have also slowed me down when my enthusiasm made me overlook some points. Takehiro, thank you for that.

Another important person during the 3 years of my PhD is Chris Spiers. Chris, thank you very much for giving me the opportunity to spend 1 year in the great group of the HPT laboratory at Utrecht University. You have always encourage me and your words have made me happy and positive. I hope to visit you and work with you again.

I also want to express special thanks to André Niemeijer for being a main buddy of the experiments, discussion partner on the ring shear machine and a critical co-author. I have learned a lot from you about the apparatus, the experiments, how to use a software and so on. I could promote my PhD project with your help. Oliver Plümper helped me with the microstructural work of chapter 5 and would be co-author of one of my papers, which I highly appreciate. Sabine den Hartog taught me how to use the ring shear machine and how to analyze the data. I could start my stay and study smoothly at Utrecht because your kind guidance. Andre, Oliver and Sabine, it was enjoyable working with you.

XRD analyses on the samples using in chapter 2 were performed by Jun Kameda, also co-author of one of my papers. Thank you for your detail analyses.

I appreciate the advice and help of Colin Peach when using the Utrecht ring shear machine. Hans de Bresser has always been helpful and encouraging. The experimental work using the ring shear apparatus have been supported by the technicians of HPT lab, Thony van der Gon Netscher, Gert Kastelein and Eimert de Graaff. I also thank to Peter van Krieken for his help in conducting XRD analyses.

I would like to thank to Toshihiko Shimamoto for continued guidance and encouragements. You have always inspired me when I was depressed or had negative

attitude toward the research since I was undergraduate student. Toshi, I am happy to have learned a lot of things from you.

In Geological Survey of Japan, AIST, Miki Takahashi taught me how to use a gas-medium, high PT deformation triaxial apparatus. Hiroko Kitajima also helped my experiments using the gas apparatus and has always encouraged me. Although I did not include the experimental results in this thesis, I hope to publish them in the future.

At Kochi Institute for Core Sample Research, JAMSTEC, Hideki Mukoyoshi taught me how to use a high-velocity rotary shear friction apparatus and prepared the thin sections of chapter 2. Osamu Tadai performed the XRD analysis and I learned from Kentaro Hatakeda on the use of a scanning electron microscope (SEM). I express my gratitude to you.

I want to thank two anonymous reviewers for their careful revision and suggestions of Chapter 2 during its review as a paper. The following people have contributed to my understanding of faults, its frictional properties and seismic activities during discussions at conferences and during visits: Hiroyuki Noda, Bunichiro Shibazaki, Yoshihiro Ito, Takanori Matsuzawa, Tom Mitchell, Masataka Kinoshita, Changrong He, Weiren Lin, Shin-ichi Uehara, Kazuo Mizoguchi, Wataru Tanikawa, Ken-ichi Hirauchi.

I gratefully acknowledge the following professors at Hiroshima University for constructive and valuable suggestions and advices to me and for examination of this thesis: Hiroshi Hidaka, Toshimori Sekine, Naoki Suda, Ikuo Katayama. And I specifically acknowledge Jun-ichi Ando and Ken-ichi Hoshino for useful discussions and encouragements.

Magda Mathot-Martens took care of administration concerned with my visit, my stay and my work at Utrecht. Magda, thank you very much. Noriko Miyoshi, Chikako Kobayashi and Akiko Ito have taken care of all administration on my work. I can just focus on my work because of your continued help. Thank you for that. Manami Kitamura have always supported me and helped me on miscellaneous matters. Thank you, Manami.

Data analysis was performed using the XLook program developed at

Pennsylvania State University. In the research of chapter 2 and 3, I used samples and data provided by the Deep Sea Drilling Project (DSDP) and Integrated Ocean Drilling Program (IODP). This PhD project was supported by a Grant-in-Aid for JSPS Fellows awarded by the Japan Society for the Promotion of Science (to MS, 24-7181).

My research life at Hiroshima University has been fun and very satisfying because of my colleagues. In the Netherlands, I had a very fulfilling life with members of HPT laboratory. I hope to express my gratitude to all colleagues for many useful advices, collaborations and encouragements.

Finally I am thankful to my father, mother, younger brother, pet dog and late grandmother for their strong financial support and warm encouragements.（私の長年の学生生活を経済的かつ精神的に支えてくれた両親，弟，愛犬，そして亡き祖母に心から感謝する.）

References

Ammon, C.J., Lay, T., Kanamori, H., and Cleveland, M., 2011, A rupture model of the 2011 off the Pacific coast of Tohoku Earthquake, Earth Planets and Space, 63, 693–696.

Asano, Y., Obara, K., and Ito, Y., 2008, Spatiotemporal distribution of very-low frequency earthquakes in Tokachi-oki near the junction of the Kuril and Japan trenches revealed by using array signal processing. Earth Planets Space, v. 60, p. 871–875.

Behnsen, J, Faulkner, D.R., 2013, Permeability and frictional strength of cation-exchanged montmorillonite, Journal of Geophysical Research Solid Earth, v. 118, doi:10.1002/jgrb.50226.

Blanpied, M.L., Lockner, D.A., and Byerlee, J.D., 1991, Fault stability inferred from granite sliding experiments at hydrothermal conditions, Geophysical Research Letters, v. 18 (4), p. 609–612.

Blanpied, M.L., Lockner, D.A., and Byerlee, J.D., 1995, Frictional slip of granite at hydrothermal conditions. Journal of Geophysical Research, v. 100 (B7), p. 13045–13064.

Blanpied, M.L., Marone, C.J., Lockner, D.A., Byerlee, J.D., and King, D.P., 1998, Quantitative measure of the variation in fault rheology due to fluid-rock interactions, Journal of Geophysical Research, v. 103, p. 9691– 9712.

Boutareaud, S., Hirose, T., Andréani, M., Pec, M., Calugaru, D-G., Boullier, A-M., Doan, M-L., 2012, On the role of phyllosilicates on fault lubrication: insight from micro- and nanostructural investigations on talc friction experiments, Journal of Geophysical Research, v. 117 (B08408), doi:10.1029/2011JB009006.

Brantut, N., Schubnel, A., Rouzaud, J.N., Brunet, F., Shimamoto, T., 2008, High-velocity frictional properties of a clay-bearing fault gouge and implications for earthquake mechanics, Journal of Geophysical Research, v. 113 (B10401), doi:10.1029/2007JB005551.

Brown, K.M., Tryon, M.D., DeShon, H.R., Dorman, L.M., and Schwartz, S.Y., 2005,

Correlated transient fluid pulsing and seismic tremor in the Costa Rica subduction zone. Earth and Planetary Science Letters, 238(1), p.189–203, doi: 10.1016/j.epsl.2005.06.055.

Chester, F.M., Mori, J.J., Toczko, S., Eguchi, N., and the Expedition 343/343T Scientists, 2012, Japan Trench Fast Drilling Project (JFAST): Integrated Ocean Drilling Program Preliminary report, Volume 343: Tokyo, Integrated Ocean Drilling Program Management International, Inc., doi:10.2204/iodp.pr.343343T.

Chester, F.M., Rowe, C., Ujiie, K., Kirkpatrick, J., Regalla, C., Remitti, F., Moore, J.C., Toy, V., Wolfson-Schwehr, M., Bose, S., Kameda, J., Mori, J.J., Brodsky, E.E., Eguchi, N., Toczko, S., and Expedition 343 and 343T Scientists, 2013, Structure and composition of the plate-boundary slip zone for the 2011 Tohoku-Oki Earthquake, Science, v. 342, p. 1208–1211, doi:10.1126/science.1243719.

Cocco, M., Spudich, P., Tinti, E., 2006, On the mechanical work absorbed on faults during earthquake ruptures, In: Abercrombie, R.E., Mc Garr, A., Kanamori, H., Di Toro, G., (eds) Earthquakes: radiated energy and the physics of faulting, AGU Monograph Series, v. 170, AGU, Washington, DC, pp 237–254

Den Hartog, S.A.M., Niemeijer, A.R., and Spiers, C.J., 2012a, New constraints on megathrust slip stability under subduction zone P–T conditions. Earth and Planetary Science Letters, v. 353–354, p. 240–252.

Den Hartog, S.A.M., Niemeijer, A.R., and Spiers, C.J., 2013, Friction on subduction megathrust faults: Beyond the illite–muscovite transition, Earth and Planetary Science Letters, v. 373, p. 8-19.

Den Hartog, S.A.M., Peach, C.J., Matthijs de Winter, D.A., Spiers, C.J., and Shimamoto, T., 2012b, Frictional properties of megathrust fault gouges at low sliding velocities: New data on effects of normal stress and temperature, Journal of Structural Geology, v. 38, p. 156–171, doi:10.1016/j.jsg.2011.12.001.

Dieterich, J.H., 1978, Time-dependent friction and the mechanics of stick-slip, Pure and Applied Geophysics, v. 116, p. 790–806.

Dieterich, J.H., 1979, Modeling of rock friction 1. Experimental results and constitutive equations, Journal of Geophysical Research, v. 84 (B5), p. 2161–2168.

Di Toro, G., Han, R., Hirose, T., De Paola, N., Nielsen, S., Mizoguchi, K., Ferri, F., Cocco, M., Shimamoto, T., 2011, Fault lubrication during earthquakes, Nature, v. 471 (7339), p. 494–498.

Evans, B.W., 1990, Phase relations of epidote-blueschists, Lithos, 25(1), 3-23.

Expedition 316 Scientists, 2009a, Expedition 316 Site C0004. In: Kinoshita, M., Tobin, H., Ashi, J., Kimura, G., Lallemant, S., Screaton, E.J., Curewitz, D., Masago, H., Moe, K.T., the Expedition 314/315/316 Scientists, Proc Integr Ocean Drill Program, 314/315/316. doi:10.2204/iodp.proc.314315316.123.2009.

Expedition 316 Scientists, 2009b, Expedition 316 Site C0007. In: Kinoshita, M., Tobin, H., Ashi, J., Kimura, G., Lallemant, S., Screaton, E.J., Curewitz, D., Masago, H., Moe, K.T., the Expedition 314/315/316 Scientists, Proc Integr Ocean Drill Program, 314/315/316. doi:10.2204/iodp.proc.314315316.123.2009.

Faulkner, D.R., Mitchell, T.M., Behnsen, J., Hirose, T., and Shimamoto, T., 2011, Stuck in the mud? Earthquake nucleation and propagation through accretionary forearcs, Geophysical Research Letters, v. 38 (L18303), doi:10.1029/2011GL048552.

Ferri, F., Di Toro, G., Hirose, T., Han, R., Noda, H., Shimamoto, T., Quaresimin, M., de Rossi, N., 2011, Low‐to high‐velocity frictional properties of the clay‐rich gouges from the slipping zone of the 1963 Vaiont slide, northern Italy, Journal of Geophysical Research, v. 116 (B09208), doi:10.1029/2011JB008338.

Fujiwara, T., Kodaira, S., No, T., Kaiho, Y., Takahashi, N., and Kaneda, Y., 2011, The 2011 Tohoku-Oki earthquake: displacement reaching the trench axis, Science, v. 334, p. 1240.

Fulton, P.M., Brodsky, E.E., Kano, Y., Mori, J., Chester, F., Ishikawa, T., Harris, R.N., Lin, W., Eguchi, N., Toczko, S., Expedition 343, 343T, and KR13-08 Scientists, 2013, Low coseismic friction on the Tohoku-Oki fault determined from temperature measurements, Science, v. 342, p. 1214–1217, doi:10.1126/science.1243641.

He, C., Wang, Z., and Yao, W., 2007, Frictional sliding of gabbro gouge under hydrothermal conditions, Tectonophysics, 445(3), 353-362, doi: 10.1016/j.tecto.2007.09.008.

Hirose, T., and Shimamoto, T., 2005, Growth of molten zone as a mechanism of slip weakening of simulated faults in gabbro during frictional melting, Journal of Geophysical Research, v. 110 (B05202), doi:10.1029/2004JB003207.

Hirose, T., Tanikawa, W., Sakaguchi, M., Tadai, O., Lin, W., and Scientific Party., 2008, High-velocity frictional behavior of clay-rich sediments from IODP Expedition 316, Nankai Trough, offshore Japan, American Geophysical Union 2008 Fall Meeting, T31A-1980, San Francisco, USA, 17/12/2008.

Hirose, T., Tanikawa, W., Mukoyoshi, H., Tadai, O., Lin, W., and Expedition 343 Scientific Party., 2013, Extreme low friction of the Tohoku plate boundary as a possible factor for seismic slip propagation toward the trench, Japan Geoscience Union Meeting 2013, SSS01–05 Chiba, Japan, 19/05/2013.

Hyndman, R.D., and Peacock, S.M., 2003, Serpentinization of the forearc mantle, Earth and Planetary Science Letters, v. 212 (3–4), p. 417-432.

Hyndman, R.D., and Wang, K., 1993, Thermal constraints on the zone of major thrust earthquake failure: the Cascadia subduction zone, Journal of Geophysical Research, v. 98 (B2), p. 2039-2060.

Hyndman, R.D., Yamano, M., and Oleskevich, D.A., 1997, The seismogenic zone of subduction thrust faults, The Island Arc, v. 6 (3), p. 244–260.

Ide, S., Baltay, A., and Beroza, G.C., 2011, Shallow Dynamic Overshoot and Energetic Deep Rupture in the 2011 Mw 9.0 Tohoku-Oki Earthquake, Science, v. 332, p. 1426–1429, doi:10.1126/science.1207020.

Ikari, M.J., Kameda, J., Saffer, D.M., and Kopf, A.J., 2015, Strength characteristics of Japan Trench borehole samples in the high-slip region of the 2011 Tohoku-Oki earthquake, Earth and Planetary Science Letters, v. 412, p. 35-41.

Ikari, M.J., Saffer, D.M., and Marone, C., 2007, Effect of hydration state on the frictional properties of montmorillonite-based fault gouge, Journal of Geophysical Research, v. 112 (B06423), doi:10.1029/2006JB004748.

Ikari, M.J., Saffer, D.M., and Marone, C., 2009, Frictional and hydrologic properties of clay-rich fault gouge, Journal of Geophysical Research, v. 114 (B05409), doi:10.1029/2008JB006089.

Ito, Y., and Obara, K., 2006a, Dynamic deformation of the accretionary prism excites very low frequency earthquakes, Geophysical Research Letters, v. 33, L02311, doi:10.1029/2005GL025270.

Ito, Y., and Obara, K., 2006b, Very low frequency earthquakes within accretionary prisms are very low stressdrop earthquakes. Geophysical Research Letters, v. 33 (L09302), doi:10.1029/2006GL025883.

Ito, Y., Hino, R., Kido, M., Fujimoto, H., Osada, Y., Inazu, D., Ohta, Y., Iinuma, T., Ohzono, M., Miura, S., Mishina, M., Suzuki, K., Tsuji, T., and Ashi, J., 2013, Episodic slow slip events in the Japan subduction zone before the 2011 Tohoku-Oki earthquake, Tectonophysics, v. 600, p. 14–26.

Ito, Y., Tsuji, T., Osada, Y., Kido, M., Inazu, D., Hayashi, Y., Tsushima, H., Hino, R., and Fujimoto, H., 2011, Frontal wedge deformation near the source region of the 2011 Tohoku-oki earthquake, Geophysical Research Letters, v. 38 (L00G05), doi:10.1029/2011GL048355.

Kameda, J., Shimizu, M., Ujiie, K., Hirose, T., Ikari, M., Mori, J., Oohashi, K., and Kimura, G., 2015, Pelagic smectite as an important factor in tsunamigenic slip along the Japan Trench, Geology, G35948-1, doi: 10.1130/G35948.1.

Kato, A., Obara, K., Igarashi, T., Tsuruoka, H., Nakagawa, S., and Hirata, N., 2012, Propagation of slow slip leading up to the 2011 Mw 9.0 Tohoku-Oki Earthquake, Science, v. 335, p. 705–708.

Kato, N., 2003, A possible model for large preseismic slip on a deeper extension of a seismic rupture plane, Earth and Planetary Science Letters, V. 216, p. 17–25.

Kimura, G., Hina, S., Hamada, Y., Kameda, J., Tsuji, T., Kinoshita, M., and Yamaguchi, A., 2012, Runaway slip to the trench due to rupture of highly pressurized megathrust beneath the middle trench slope: The tsunamigenesis of the 2011 Tohoku earthquake off the east coast of northern Japan, Earth and Planetary Science Letters, v. 339–340, p. 32-45, doi:10.1016/j.epsl.2012.04.002.

Lay, T., Ammon, C.J., Kanamori, H., Xue, L., and Kim, M.J., 2011, Possible large near-trench slip during the great 2011 Tohoku (Mw 9.0) earthquake, Earth Planets Space, v. 63(7), p. 687–692.

Lay, T., Kanamori, H., Ammon, C.J., Nettles, M., Ward, S.N., Aster, R.C., Beck, S.L., Bilek, S.L., Brudzinski, M.R., Butler, R., DeShon, H.R., Ekström, G., Satake, K., and Sipkin, S., 2005, The great Sumatra-Andaman earthquake of 26 december 2004, Science, v. 308(5725), p. 1127-1133.

Liu, Y., and Rice, J.R., 2005, Aseismic slip transients emerge spontaneously in three‐dimensional rate and state modeling of subduction earthquake sequences, Journal of Geophysical Research, v. 110 (B08307), doi:10.1029/2004JB003424.

Liu, Y., and Rice, J.R., 2007, Spontaneous and triggered aseismic deformation transients in a subduction fault model, Journal of Geophysical Research, v. 112 (B09404), doi:10.1029/2007JB004930.

Logan, J.M., and Rauenzahn, K.A., 1987, Frictional dependence of gouge mixtures of quartz and montmorillonite on velocity, composition, and fabric, Tectonophysics, v. 144, p. 87– 108.

Marone, C., and Cox, S.J.D., 1994, Scaling of rock friction constitutive parameters: The effects of surface roughness and cumulative offset on friction of gabbro, pure and applied geophysics, v. 143(1-3), p. 359-385.

Marone, C., 1998, Laboratory-derived friction laws and their application to seismic faulting, Annual Review of Earth and Planetary Sciences, v. 26, p. 643–696.

Maruyama, S., and Okamoto, K., 2007, Water transportation from the subducting slab into the mantle transition zone. Gondwana Research, v. 11(1), p. 148–165.

Mitsui, Y., Iio, Y., and Fukahata, Y., 2012, A scenario for the generation process of the 2011 Tohoku earthquake based on dynamic rupture simulation: role of stress concentration and thermal fluid pressurization, Earth Planets Space, v. 64(12), p. 1177–1187.

Mizoguchi, K., Hirose, T., Shimamoto, T., and Fukuyama, E., 2007, Reconstruction of seismic faulting by high-velocity friction experiments: an example of the 1995 Kobe earthquake, Geophysical Research Letters, v. 34 (L01308), doi:10.1029/2006GL027931.

Moore, D.E., and Lockner, D.A., 2004, Crystallographic controls on the frictional behavior of dry and water-saturated sheet structure minerals, Journal of Geophysical Research, v. 109 (B03401), doi:10.1029/2003JB002582.

Moore, D.E., Lockner, D.A., Shengli, M., Summers, R., and Byerlee, J., 1997, Strengths of serpentinite gouges at elevated temperatures, Journal of Geophysical Research, v. 102 (B7), p. 14787–14801, doi:10.1029/97JB00995.

Newton, R.C., and Kennedy, G.C., 1963, Some equilibrium reactions in the join $CaAl_2Si_2O_8$ - H_2O, Journal of Geophysical Research, v. 68(10), p. 2967-2983.

Niemeijer, A.R., Spiers, C.J., and Peach, C.J., 2008, Frictional behaviour of simulated quartz fault gouges under hydrothermal conditions: Results from ultra-high strain rotary shear experiments, Tectonophysics, v. 460, p. 288–303, doi:10.1016/j.tecto.2008.09.003.

Obara, K., Haryu, Y., Ito, Y., and Shiomi, K., 2004a, Low frequency events occurred during the sequence of aftershock activity of the 2003 Tokachi-Oki earthquake; a dynamic process of the tectonic erosion by subducted seamount, Earth Planets Space, v. 56, p. 347–351.

Obara, K., Hirose, H., Yamamizu, F., and Kasahara, K., 2004b, Episodic slow slip events accompanied by non-volcanic tremors in southwest Japan subduction zone, Geophysical Research Letters, v. 31, http://dx.doi.org/10.1029/2004GL020848.

Obara, K., and Ito, Y., 2005, Very low frequency earthquake excited by the 2004 off the Kii peninsula earthquake: a dynamic deformation process in the large accretionary prism. Earth Planets Space, v. 57, p. 321–326.

Oh, C.W., and Liou, J.G., 1998, A petrogenetic grid for eclogite and related facies under high-pressure metamorphism, Island Arc, v. 7 (1-2), p. 36–51.

Ozawa, S., Nishimura, T., Suito, H., Kobayashi, T., Tobita, M., and Imakiire, T., 2011, Coseismic and postseismic slip of the 2011 magnitude-9 Tohoku-Oki earthquake, Nature, v. 475, p. 373–376. doi:10.1038/nature10227.

Peacock, S.M., and Wang, K., 1999, Seismic consequences of warm versus cool subduction metamorphism: Examples from southwest and northeast Japan, Science, v. 286 (5441), p. 937–939, doi: 10.1126/science.286.5441.937.

Plafker, G., and Savage, J.C., 1970, Mechanism of the Chilean Earthquakes of May 21 and 22, 1960, Geological Society of America Bulletin, V. 81 (4), p. 1001-1030.

Ruina, A., 1983, Slip instability and state variable friction laws, Journal of Geophysical Research, v. 88 (B12), p. 10359–10370.

Rogers, G., and Dragert, H., 2003, Episodic tremor and slip on the Cascadia subduction zone: The chatter of silent slip, Science, v. 300(5627), p. 1942-1943.

Saffer, D. M., Frye, K.M., Marone, C., and Mair, K., 2001, Laboratory results indicating complex and potentially unstable frictional behavior of smectite clay, Geophysical Research Letters, 28(12), 2297–2300, doi:10.1029/2001GL012869.

Saffer, D.M., and Marone, C., 2003, Comparison of smectite- and illiterich gouge frictional properties: Application to the updidp limit of the seismogenic zone along subduction megathrusts, Earth and Planetary Science Letters, v. 215, p. 219– 235.

Sawai, M., Hirose, T., and Kameda, J., 2014, Frictional properties of incoming pelagic sediments at the Japan Trench: implications for large slip at a shallow plate boundary during the 2011 Tohoku earthquake, Earth, Planets and Space, v. 66 (1), 1-8.

Sawai, M., Shimamoto, T., and Togo, T., 2012, Reduction in BET surface area of Nojima fault gouge with seismic slip and its implication for the fracture energy of earthquakes, Journal of Structural Geology, v. 38, p. 117–138.

Scholz, C.H., 1998, Earthquakes and friction laws. Nature, v. 391(6662), 37–42, doi:10.1038/34097.

Scholz, C.H., 2002, The mechanics of earthquakes and faulting, 2nd ed., Cambridge university press, New York.

Segall, P., Rubin, A.M., Bradley, A.M., and Rice, J.R., 2010, Dilatant strengthening as a mechanism for slow slip events, Journal of Geophysical Research, v. 115 (B12305), doi:10.1029/2010JB007449.

Shelly, D.R., Beroza, G.C., Ide, S., and Nakamula, S., 2006, Low-frequency earthquakes in Shikoku, Japan, and their relationship to episodic tremor and slip, Nature, 442 (7099), 188-191.

Shibazaki, B., and Iio, Y., 2003, On the physical mechanism of silent slip events along the deeper part of the seismogenic zone, Geophysical Research Letters, v. 30, doi:10.1029/2003GL017047.

Shibazaki, B., and Shimamoto, T., 2007, Modeling of short-interval silent slip events in deeper subduction interfaces considering the frictional properties at the unstable–stable transition regime, Geophys. J. Int. v. 171:191–205.

Shimamoto, T., 1986, Transition between frictional slip and ductile flow for halite shear zones at room temperature, Science, v. 231, p. 711–714, doi:10.1126/science.231.4739.711.

Shimamoto, T., and Tsutsumi, A., 1994, A new rotary-shear high-velocity friction testing machine: its basic design and scope of research. Structural Geology, v. 39, p. 65–78 (in Japanese with English abstract).

Shipboard Scientific Party, 1980, Site 436: Japan Trench outer rise, Leg 56, Initial Report Deep Sea Drilling Project, v. 56, 57(1), p. 399–446.

Simons, M., Minson, S.E., Sladen, A., Ortega, F., Jiang, J., Owen, S.E., Meng, L., Ampuero, J.-P., Wei, S., Chu, R., Helmberger, D.V., Kanamori, H., Hetland, E., Moore, A.W., and Webb, F.H., 2011, The 2011 magnitude 9.0 Tohoku-Oki earthquake: Mosaicking the megathrust from seconds to centuries, Science, v. 332(6036), p. 1421-1425.

Takahashi, M., Uehara, S.-I., Mizoguchi, K., Shimizu, I., Okazaki, K., and Masuda, K., 2011, On the transient response of serpentine (antigorite) gouge to stepwise changes in slip velocity under high-temperature conditions, Journal of Geophysical Research, v. 116, B10405, doi:10.1029/2010JB008062.

Tembe, S., Lockner, D., and Wong, T.F., 2009, Constraints on the stress state of the San Andreas Fault with analysis based on core and cuttings from San Andreas Fault Observatory at Depth (SAFOD) drilling phases 1 and 2, Journal of Geophysical Research, v. 114 (B11401), doi:10.1029/2008JB005883.

Tembe, S., Lockner, D.A., and Wong, T.F., 2010, Effect of clay content and mineralogy on frictional sliding behavior of simulated gouges: Binary and ternary mixtures of quartz, illite, and montmorillonite, Journal of Geophysical Research, 115

(B03416), doi:10.1029/2009JB006383.

Tinti, E., Spudich, P., and Cocco, M., 2005, Earthquake fracture energy inferred from kinematic rupture models on extended faults, Journal of Geophysical Research, v. 110 (B12303), doi:10.1029/2005JB003644.

Togo, T., Shimamoto, T., Ma, S., and Hirose, T., 2011, High-velocity frictional behavior of Longmenshan fault gouge from Hongkou outcrop and its implications for dynamic weakening of fault during the 2008 Wenchuan earthquake, Earthquake Science, v. 24, p. 267–281, doi:10.1007/s11589-011-0790-6.

Tse, S.T., and Rice, J.R., 1986, Crustal earthquake instability in relation to the depth variation of frictional slip properties, Journal of Geophysical Research: Solid Earth (1978–2012), v. 91(B9), p. 9452-9472.

Tsuru, T., Park, J.-O., Takahashi, N., Kodaira, S., Kido, Y., Kaneda, Y., and Kono, Y., 2000, Tectonic features of the Japan Trench convergent margin off Sanriku, northeastern Japan, revealed by multichannel seismic reflection data, Journal of Geophysical Research, v. 105 (B7), p. 16,403–16,413, doi:10.1029/2000JB900132.

Tsuru, T., Park, J.-O., Miura, S., Kodaira, S., Kido, Y., and Hayashi, T., 2002, Along-arc structural variation of the plate boundary at the Japan Trench margin: Implication of interplate coupling, Journal of Geophysical Research, v. 107(B12), 2357, doi:10.1029/2001JB001664.

Tsutsumi, A., Fabbri, O., Karpoff, A.M., Ujiie, K., and Tsujimoto, A., 2011, Friction velocity dependence of clay-rich fault material along a megasplay fault in the Nankai subduction zone at intermediate to high velocities, Geophysical Research Letters, v. 38 (L19301), doi:10.1029/2011GL049314.

Ujiie, K., Tsutsumi, A., 2010, High-velocity frictional properties of clay-rich fault gouge in a megasplay fault zone, Nankai subduction zone, Geophysical Research Letters, v. 37 (L24310), doi:10.1029/2010GL046002.

Ujiie, K., Tanaka, H., Saito, T., Tsutsumi, A., Mori, J.J., Kameda, J., Brodsky, E.E., Chester, F.M., Eguchi, N., Toczko, S., Expedition 343 and 343T Scientists., 2013, Low coseismic shear stress on the Tohoku-Oki megathrust determined from

laboratory experiments, v. Science 342, p. 1211–1214, doi:10.1126/science.1243485.

von Huene, R., Langseth, M., Nasu, Y., Okada, H., 1982, A summary of Cenozoictectonic history along the IPOD Japan Trench transect, Bull.Geol.Soc.Am, v. 93, p. 829–846.

Wallace, L.M., and Beavan, J., 2010, Diverse slow slip behavior at the Hikurangi subduction margin, New Zealand, Journal of Geophysical Research, v. 115, B12402, doi:10.1029/2010JB007717.

公表論文

(1) Sawai, M., Hirose, T. and Kameda, J., 2014. Frictional properties of incoming pelagic sediments at the Japan Trench: implications for large slip at a shallow plate boundary during the 2011 Tohoku earthquake. Earth, Planets and Space, 66(1), 1-8, DOI 10.1186/1880-5981-66-65.

(2) Sawai, M., Katayama, I. Hamada, A., Maeda, M. and Nakashima, S., 2013. Dehydration kinetics of antigorite using in situ high-temperature infrared microspectroscopy. Physics and Chemistry of Minerals 40, 319–330, DOI 10.1007/s00269-013-0573-9.

(3) Sawai, M., Shimamoto, T. and Togo, T., 2012. Reduction in BET surface area of Nojima fault gouge with seismic slip and its implication for the fracture energy of earthquakes. Journal of Structural Geology 38, 117-138, doi: 10.1016/j.jsg.2012.01.002.